Understanding and Attenuating Simulator Sickness when Driving in Urban Environments

Final Thesis

M. Hogerbrug

Delft University of Technology

TU Delft

Understanding and Attenuating Simulator Sickness when Driving in Urban Environments

Final Thesis

by

M. Hogerbrug

to obtain the degree of Master of Science
at the Delft University of Technology,
to be defended publicly on Thursday November 28, 2019 at 14:00 PM.

Student number:	4548523	
Project duration:	January 7, 2018 – November 28, 2019	
Thesis committee:	prof. dr. ir. M. Mulder,	TU Delft, Chair
	dr. ir. D. M. Pool,	TU Delft, Responsible Thesis Supervisor
	dr. ir. J. Venrooij,	BMW Group, Supervisor
	dr. J. Hartcher-O'Brien,	TU Delft, Examiner

This thesis is confidential and cannot be made public until December 31, 2019.

TU Delft Delft University of Technology

Delft University of Technology
Department of Control and Operations, Section Control and Simulation
Delft, The Netherlands

The undersigned hereby certify that they have read, and recommend to the Faculty of Aerospace Engineering at Delft University of Technology for acceptance, a thesis entitled: **Understanding and Attenuating Simulator Sickness when driving in Urban Environments**, submitted by **M. Hogerbrug**, in partial fulfillment of the requirements for the degree of **Master of Science**.

Dated: _____

Readers:

_____
prof. dr. ir. M. Mulder

_____
dr. ir. D. M. Pool

_____
dr. ir. J. Venrooij

_____
dr. J. Hartcher-O'Brien

Acknowledgments

Before you lies my final thesis: Understanding and Attenuating Simulator Sickness when Driving in Urban Environments. It has been written to obtain the Master of Science (MSc) degree in Aerospace Engineering at the Delft University of Technology. I started this thesis in January 2019 after completing my internship at the BMW Group in Munich, which I much enjoyed. The theme of my graduation work was initiated during this period. Therefore, I would first like to thank the BMW Group, department Driving Simulation for assisting in setting up this research project and the ability to perform my experiments at your facilities. In particular, I want to thank dr. ir. Joost Venrooij for his help in starting up the research project and his supervision. Joost, I had a great time working with you. Your insightful comments helped me a lot along the way and you helped me in having a great and successful time in Munich.

Secondly, I would like to thank my daily supervisor dr. ir. Daan Pool for the time he spent on providing me feedback, helping me with the framework of the project and setting up clear research goals. Daan, your quick response to my emails and our regular meetings helped me a lot with finishing my research work efficiently, which I really appreciate. Thirdly, prof. dr. ir. Max Mulder arranged not only my internship at the BMW Group, but also the cooperation with the BMW Group during my thesis work. Max, for this and your advice in person, I am very grateful.

Two other persons that I would like to thank for their contribution to this thesis work are Jesse Eppink and Rowenna Wijlens. Jesse helped me during the preparation and execution of the experiment. We had a limited amount of time for the experiment, but together we were able to efficiently set it up while having a great time in Munich. Rowenna extensively read my paper voluntarily and the amount of feedback she provided was overwhelming. Your feedback was both accurate and enlightening and is much appreciated.

Furthermore, I spent ten months in the Control and Simulation Upper House graduation room. Sven, Simon, Peter, Michiel, Stephan, Joeri, Jesse, thank you for the assist when I needed it, the magnificently decorated room, the insightful memes, sticker wars, the coffee breaks, but foremost, the great time.

Finally, I would like to thank my family and friends for their support and encouragement. In particular, my roommates from Het Kraaiennest, who made my time in Delft including the graduation period a lot more fun. But also my parents, who were always there for me and made the 7 years of studying possible.

M. Hogerbrug
Delft, November 2019

Contents

List of Figures

List of Tables

Nomenclature

Abbreviations

CoF	Center of Gravity
DOF	Degrees of Freedom
DS	Disorientation score
FOV	Field of View
GIF	Gravito Inertial Force
MIMO	Multi Input Multi Output
MISC	Misery Scale
MS	Motion Sickness
MSHQ	Motion Sickness History Questionnaire
MSI	Motion Sickness Incidence
NS	Nausea score
OKN	Optokinetic Nystagmus
OS	Occulumotor score
OTO	Otoliths
OVAR	Off Vertical Axis Rotation
PMI	Perceived Motion Incongruence
SC	Sensory conflict
SCC	Semi Circular Canals
SQ	Sub-question
SS	Simulator Sickness
SSI	Simulator Sickness Incidence
SSQ	Simulator Sickness Questionnaire
SVC	Subjective Vertical Conflict
TS	Total score
VOR	Vestibular Occular Reflex

Latin Symbols

Symbol	Description	Unit
$\vec{a}$	Linear motion acceleration	$\frac{m}{s^2}$
A	Body and sense organ differential equations coefficient matrix	-
$\hat{A}$	Internal estimate of A	-
b	Fitting parameter Hill function	-
B	The mass and inertia coefficients matrix	-
$\hat{B}$	Internal estimate of B	-
$\vec{c}$	Conflict vector of expected and measured afferent signal	-
C	Control strategy matrix	-
$\vec{d}$	Conflict vector of expected and sensed vertical	-
e_a	Error between actual and expected acceleration (Sensory conflict model Merfeld)	-
e_f	GIF rotation error (Sensory conflict model Merfeld)	-
e_ω	Error between actual and expected SCC signals (Sensory conflict model Merfeld)	-
$\vec{f}$	Specific force or GIF	g's
$\vec{f}_h$	Head specific force transfer function	g's
$\vec{f}_{OTO}$	Otolith specific force transfer function	g's
$\vec{g}$	Linear gravitational acceleration	g's
$\vec{g}_e$	Linear gravitational acceleration with respect to earth	g's
g_{exp}	Subjective or expected vertical	g's
$\vec{g}_h$	Linear gravitational acceleration with respect to the head	g's
g_{sens}	Sensed vertical	g's
$\vec{g}_{tot}$	Resulting vertical	g's
$\vec{g}_{vis}$	Visual linear gravitational acceleration	g's
k_a	Feedback gain (Sensory conflict model Merfeld)	-
K_{ac}	Acceleration conflict gain	-
$K_{\omega c}$	Angular velocity conflict gain	-
k_f	Feedback gain (Sensory conflict model Merfeld)	-
K_{gc}	Gravitational conflict gain	-
k_ω	Feedback gain (Sensory conflict model Merfeld)	-
$k_{f\omega}$	Feedback gain (Sensory conflict model Merfeld)	-
$\vec{m}$	Input forces from the muscular system	-
$\vec{n}_a$	Sensor noise	-
$\vec{n}_e$	Disturbance noise	-

n_h	Parameter that accounts for the steepness of the hill function	-
P	Maximum amount of participants that get sick under the given circumstances	%
$\hat{S}$	Internal estimate of S	-
S	Sensory organs coefficient matrix	-
$\vec{u}$	Forcing vector	-
$\vec{v}$	Velocity	$\frac{m}{s}$
$\vec{v}_e$	Velocity with respect to earth	$\frac{m}{s}$
$\vec{v}_{VIS}$	Velocity as perceived by visual sysem	$\frac{m}{s}$
w	Weight factor in linear weighting addition	-
w_a	Vestibular velocity weighting vector	-
w_f	Visual vertical weighting vector	-
w_g	Visual vertical weighting vector	-
w_i	Idiotropic vertical weighting vector	-
w_v	Visual velocity weighting vector	-
$\vec{x}$	Actual state vector	-
$\vec{x}_d$	Desired state vector	-
$\hat{\vec{x}}$	Estimated state vector	-
$\vec{y}$	Afferent signals	-
$\hat{\vec{y}}$	Expected afferent signals	-
$\hat{\vec{y}}$	Expected afferent signal from internal observer	-
$\vec{y}_f$	Afferent GIF signal	-
$\hat{\vec{y}}_f$	Expected afferent GIF signal	-
$\vec{y}$	Measured afferent signal from human sense organs	-

Greek Symbols

Symbol	Description	Unit
μ	Time constant leaky integrator	s
τ	Time delay	s
τ_a	Adaptation time constant	s
τ_{av}	Time delay high-pass filter velocity perception vestibular system	s
τ_c	Time constant SCC	s
τ_d	Dominant time constant	s
τ_g	Time constant low-pass filter gravity perception visual system	s

τ_v	Time constant low-pass filter linear velocity perception visual system	s
ω	Angular velocity	rad/s
ω_c	SCC angular velocity	rad/s
ω_h	Head angular velocity	rad/s
ω_{vest}	Vestibular angular velocity	rad/s
ω_{vis}	Visual angular velocity	rad/s

Subscripts

0	Initial or static term

1 Introduction

1.1. Background

Car manufacturers are operating in a highly dynamic market where innovation plays a key role. At this moment a transition is being made from manually-driven to autonomously-driven cars. This innovation requires testing of take-over behavior, cooperative strategies and the use of automation [2]. Testing within urban environments requires dealing with major amounts of traffic causing traffic jams and safety issues. However, simulator testing provides numerous advantages over real-life testing, such as reduced crash risks [3], controlled weather, topography and vehicle characteristics [4], reduced costs as well as being less harmful for the environment. The increasing potential of computer technology will lead to even more applications of driving simulation in areas such as driver assessment, driver training, research and entertainment [5]. However, performing simulator testing comes at a price: simulator sickness (SS), which is a form of motion sickness (MS). Basically, everyone with a properly functioning vestibular system can be made sick if the provocative stimuli are large enough [6]. The main symptom of MS is nausea and the main signs are palor, sweating and vomiting [7]. Humans have been struggling with MS for thousands of years and still do not understand what the exact cause is.

Extensive research has been done on MS [8–16], but this phenomenon is still barely understood. MS can be described as the discomforting feeling when encountering an unexpected actual or apparent movement [17]. The most effective remedy against MS, including SS, is adaptation [18]. Prolonged exposure to any type of provocative stimulus leads to an attenuation and eventual disappearance of the signs and symptoms for most humans. Furthermore, there is no drug that reduces the severity of sickness for everyone and the existing drugs always have side effects [18–20].

Sensation of the above mentioned actual or apparent movement is detected by our senses for spatial orientation perception. They integrate and interpret the afferent or sensory information to estimate orientation and self-movement [21]. Human perception mechanisms are often incorporated in theories and mathematical models that try to explain and predict MS. Two main theoretical approaches of models that try to explain MS are the Sensory Conflict (SC) theory and the Subjective Vertical Conflict (SVC) theory [17]. The SC theory suggests that MS is primarily provoked by two conflicts. First, the conflict between the signals coming from the human sense organs. Second, the conflict between the sensed signals and the expected signals based on prior experience [8, 20]. As for the SVC theory, it is just the mismatch between the sensed vertical and the expected or subjective vertical based on prior experience that provokes MS [11].

Adding motion cueing to a simulator could be a way to reduce the SC or SVC and thereby theoretically attenuate SS. However, it is disputable if providing a motion base to a simulator always has the desired effects. On the one hand, Sharkey and McCauley [22] noted that adding a motion base to a simulator did not have the predicted effect of reducing SS and could even make it worse due to false cues. Furthermore, Klüver [23] found that SS is only marginally less in motion-base simulators compared to fixed-base simulators. On the other hand, Blana [24] states that one of the primary advantages

of a motion base is the attenuation of SS. Additionally, Stoner, Fisher, and Mollenhauer [25] showed several other examples that give positive results on attenuating SS when adding motion cueing.

1.2. Problem statement

Several scientists have attempted to quantitatively predict and explain the severity of MS using a model that incorporates the SC and SCV theories [8, 9, 11, 12, 14]. However, these models often lack a mathematical basis, are only implemented for one dimension and, above all, lack an implementation of the visual system. Implementing the visual system in MS models might enhance the predictive power of the currently available mathematical models and add the ability to predict simulator sickness [11]. Furthermore, implementation of the visual system would enable investigating the effects of the driver's head movement on the incidence of MS in more detail, which could help in designing more comfortable motions in vehicles and simulators [26].

Experience has shown that urban driving environments are associated with an increased occurrence of SS. Mourant et al. [27] showed that subjects reported significantly lower MS scores when driving on straight roads in the country and sub-urban environments compared to driving in city environments. These city or urban environments require a lot of 90-degree turns during which the optic flow rate perceived by the driver is very high and also the textures associated with optic flow rate seem to be distorted [27]. So, it should be investigated if adding a pure yaw movement to a simulator without that is congruent with the simulated vehicle motion could attenuate SS.

The objective of this Final Thesis is to better understand and explain SS by first identifying and verifying a mathematical model to predict SS. Secondly, the goal is to investigate the effects of adding scaled and veridical yaw motion to a simulator on SS while urban driving scenarios are simulated.

The research objective can be divided into several sub-goals, which are visually presented in Fig. 1.1:

a. Perform an in-depth literature study on the cause, the prediction, and modeling of SS.
b. Implement and test existing human perception models and MS models obtained from literature to identify the required subsystems to be used in the proposed model. The implementation of the visual system in the perception models has been considered here as well.
b. Propose a conceptual mathematical model, which can predict SS when simulating urban scenarios.
b. Verify this model by comparing its dynamic motion outputs to experimental data of vestibular motion, visual sensory and visual-vestibular sensory paradigms obtained from literature and by comparing the SS prediction results to experimentally obtained MS data.
c. State several hypotheses regarding the effects of adding yaw motion to a simulator on the occurrence and severity of SS.
d. Investigate in a simulator experiment the actual effects of adding motion to simulator simulating an urban environment through a simulator experiment.
e. Validate the SS prediction model using the experimental results.
f. Finally, draw conclusions on the effects of the addition of motion on SS together with the usefulness of the developed SS prediction model. Recommendations are made about how to use this model in the future, its limitations and possible adaptations to improve it.

The objectives are divided over two main parts:

1. *Paper* - First, the scope of the paper is to explain the developed SS prediction model and its contribution to the hypothesis of the experiment. Secondly, the paper provides the setup and the results of the simulator experiment that investigated the effects of adding congruent yaw motion to a simulator on SS. This part considers objectives **d, e, f** in Figure 1.1.
2. *Preliminary Research Report* - The scope of the preliminary research report is to give a state-of-the-art literature review on MS, theories that try to explain the cause of MS and SS and MS

modeling. Furthermore, the identification, verification and results of the first iteration of the developed SS prediction model are explained in detail. Finally, the experimental design for the final experiment is given. This part considers objectives **a, b, c** in Figure 1.1.

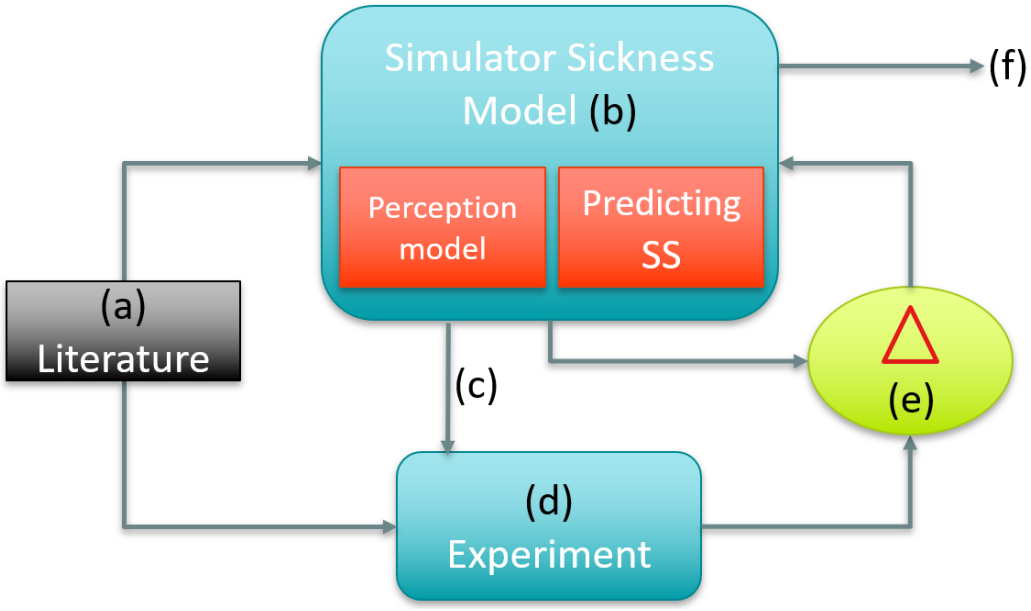

Figure 1.1: Theoretical Framework

1.3. Methodology

A SS prediction model was developed based on observer theory, by implementing human spatial orientation perception mechanisms and mechanisms that model the development of sickness symptoms. Subsequently, theories on MS and SS together with the predictions of the SS prediction model were used to formulate several hypotheses for the experiment. This experiment consisted of three cases, where Case 1 considered no-motion, Case 2 considered scaled yaw cueing, and Case 3 considered the same yaw cueing together with the full vehicle pitch and roll motions. The effect of motion on SS was investigated using the misery scale (MISC) [28] and the simulator sickness questionnaire (SSQ) [29]. Then, the experimental results were used to validate the developed model.

Furthermore, two additional measurements were the perceived motion incongruence (PMI) and head movements. The PMI may be used to quantify a part of the SC theory, which is a qualitative description to explain the cause of MS. However, as the SSQ and MISC measurements are quantitative; it is hard to match the theory with the experimental results. This is also suggested by Stoffregen and Riccio [30], because they argued that the SC is not a measurable variable meaning that it cannot even be falsified. However, a reliable and validated method has been developed by Cleij et al. [31] to measure the PMI. The PMI describes the mismatch between the visual and inertial motion as perceived in a simulator by a human participant [31], which is similar to the visual-vestibular rearrangement as used in the SC theory by Reason [8]. This PMI could be a way to make the SC theory quantifiable, which will substantiate the hypotheses about the sensory rearrangement theory by Reason [8] and help in better understanding MS characteristics. The PMI was rated by the participants using a rotary knob on the center console inside the motion cabin of the simulator. Their output was visualized by a scale bar on the projection screen.

Head movement strategies might attenuate SS. It has been found that activity and anticipation are both effects that can reduce SS [26, 32]. So, when participants move their head more actively in the direction of the curve, as drivers also do during car driving, they get a clearer picture of the road geometry. This enables the participants to better anticipate their future motion [32, 33]. Therefore, it was investigated if head movements may have a consistent effect on SS. Head movements were

measured by a gyroscope and accelerometer inside glasses that participants put on.

1.4. Outline

This Final Thesis is structured as follows. Part I presents the research paper describing the final SS prediction model and the results of the experiment that investigated the effects of adding yaw motion to a simulator on SS. Part II is the Preliminary Research Report including Chapters 2 to 7, which starts with a state-of-the-art literature study considering MS and SS in Chapter 2. Then, Chapter 3 elaborates on the literature study with a detailed description of theories describing the etiology of MS and SS. Some of these theories are used in mathematical models that try to explain or predict MS and these models are described in Chapter 4. Subsequently, the first iteration of the SS prediction model is presented in Chapter 5 together with its initial verification and simulation results. The experimental set-up of the final experiment is given in Chapter 6. Chapter 7 concludes the Preliminary Research Report. Part III incorporates the appendices of the Preliminary Research Report, which include, among others, some implemented human spatial orientation perception and MS models. Finally, the appendices of this Final Thesis are given in Part IV.

I

Scientific Paper

To be graded as part of AE5310 - Thesis Control and Operations

Understanding and Attenuating Simulator Sickness when driving in Urban Environments

M. Hogerbrug

Understanding and Attenuating Simulator Sickness when Driving in Urban Environments

M. Hogerbrug
Supervisors: D. M. Pool, M. Mulder, J. Venrooij

***Abstract*—A necessity in driving simulation testing is to understand and attenuate simulator sickness in urban environments to reduce the number of undesired drop-outs. This paper explains a 6 degree-of-freedom simulator sickness prediction model based on observer theory including the visual system. The model incorporates state-of-the-art knowledge of human spatial orientation perception and qualitative theories that try to explain motion sickness. Predictions are made regarding the simulator sickness incidence and expected rotary and translational motions for different motion and sensory paradigms. A between-subjects experiment was conducted to verify the model. Furthermore, the effect of adding scaled, but veridical, yaw motion to a simulator on the sickness incidence and severity while driving in urban environments was investigated. Participants were required to indicate a misery scale score every minute and to fill in the simulator sickness questionnaire prior to and after the experiment. Additionally, the perceived motion incongruence was measured together with head movements. Three cases were considered; a no-motion case, a case with a scaled yaw movement and a case with a scaled yaw movement together with pitch and roll motions. A significant relationship has been found between the simulator sickness prediction model outputs and the experimental outputs. Therefore, the model with the implemented visual system could be used to better understand and predict simulator sickness. A significant relationship has also been found between the measured perceived motion incongruence and the simulator sickness incidence. This perceived motion incongruence can be used to quantify a part of the qualitative sensory rearrangement theory. Furthermore, humans that indicated lower sickness scores, moved their head significantly more along with the direction of the curve. Head movement strategies can be taught to participants of simulator studies to attenuate simulator sickness symptoms. Finally, significantly less participants dropped out in the cases that included simulator motion when driving in urban environments. The findings in this paper could assist in attenuating the number of drop-outs during driving simulation testing in urban scenarios.**

***Index Terms*—Simulator Sickness, Human Spatial Orientation Perception, Modeling, Sensory Rearrangement.**

I. Introduction

CAR manufacturers are operating in a highly dynamic market where innovation plays a key role. At this moment a transition is being made from manually-driven to autonomously-driven cars. This innovation requires testing of take-over behavior, cooperative strategies and the use of automation [1]. Testing within urban environments requires dealing with major amounts of traffic causing traffic jams and safety issues. However, simulator testing provides numerous advantages over real-life testing, such as reduced crash risks [2], controlled weather, topography and vehicle characteristics [3], reduced costs as well as being less harmful for the environment. The increasing potential of computer technology will lead to even more applications of driving simulation in areas such as driver assessment, driver training, research and entertainment [4]. However, performing simulator testing comes at a price: simulator sickness (SS), which is a form of motion sickness (MS). Basically, everyone with a properly functioning vestibular system can be made sick if the provocative stimuli are strong enough [5]. The main symptom is nausea and the main signs are palor, sweating and vomiting [6]. Documents considering MS date back from the ancient Greeks. Back then, MS was provoked by transportation over sea. Humans have been struggling with MS for thousands of years and still do not understand what the exact cause is.

Extensive research has been done on MS [7]–[15], but this phenomenon is still barely understood. MS can be described as the discomforting feeling when encountering an unexpected actual or apparent movement [16]. The most effective remedy against MS, including SS, is adaptation [17]. Prolonged exposure to any type of provocative stimulus leads to an attenuation and eventual disappearance of the signs and symptoms for most humans. Furthermore, there is no drug that reduces the severity of sickness for everyone and the existing drugs always have side effects [17]–[19].

Sensation of the above mentioned actual or apparent movement is detected by our senses for spatial orientation perception. They integrate and interpret the afferent or sensory information to estimate orientation and self-movement [20]. Human perception mechanisms are often incorporated in theories and mathematical models that try to explain and predict MS. Two main theoretical approaches of models that try to explain MS are the Sensory Conflict (SC) theory and the Subjective Vertical Conflict (SVC) theory [16]. The SC theory suggests that MS is primarily provoked by two conflicts. First, the conflict between the signals coming from the human sense organs. Second, the conflict between the sensed signals and the expected signals based on prior experience [7], [19]. As for the SVC theory, it is just the mismatch between the sensed vertical and the expected or subjective vertical based on prior

Submitted on 18-10-2019 for review. This work was supported in part by the Control and Simulation section of Delft University of Technology and the simulation department of the BMW Group.

M. Hogerbrug is with the Delft University of Technology, Delft, 2629 HS Netherlands (e-mail: m.hogerbrug@student.tudelft.nl).

D. M. Pool is with the Delft University of Technology, Delft, 2629 HS Netherlands (e-mail: d.m.pool@tudelft.nl).

M. Mulder is with the Delft University of Technology, Delft, 2629 HS Netherlands (e-mail: m.mulder@tudelft.nl).

J. Venrooij is with the BMW Group, Munich, 80788 Germany (e-mail: joost.venrooij@bmw.de).

experience that provokes MS [10].

Several scientists have attempted to quantitatively predict and explain the severity of MS using a model that incorporates the SC and SCV theories [7], [8], [10], [11], [13]. However, these models often lack a mathematical basis, are only implemented for one dimension and, above all, lack an implementation of the visual system. Implementing the visual system in MS models might enhance the predictive power of the currently available mathematical models and add the ability to predict simulator sickness [10]. Furthermore, implementation of the visual system would enable investigating the effects of the driver's head movement on the incidence of MS in more detail, which could help in designing more comfortable motions in vehicles and simulators [21].

Besides more comfortable motions, adding motion cueing to a simulator could be a way to reduce the SC or SVC and thereby theoretically attenuate SS. However, it is disputable if providing a motion base to a simulator always has the desired effects. On the one hand, Sharkey and McCauley [22] noted that adding a motion base to a simulator did not have the predicted effect of reducing SS and could even make it worse due to false cues. Furthermore, Klüver [23] found that SS is only marginally less in motion-base simulators compared to fixed-base simulators. On the other hand, Blana [24] states that one of the primary advantages of a motion base is the attenuation of SS. Additionally, Stoner, Fisher, and Mollenhauer [25] showed several other examples that give positive results on attenuating SS when adding motion cueing.

Experience has shown that urban driving environments are associated with an increased occurrence of SS. Mourant et al. [26] showed that subjects reported significantly lower MS scores when driving on straight roads in the country and suburban environments compared to driving in city environments. These city or urban environments require a lot of 90-degree turns during which the optic flow rate perceived by the driver is very high and also the textures associated with optic flow rate seem to be distorted [26]. So, an experiment is performed in which a pure yaw movement is added to a simulator without false cues. The addition of this yaw movement could be a way to attenuate the sensory conflict and in turn reduce the occurrence and severity of SS.

The objective of this paper is to better understand and predict SS by explaining a identified and verified mathematical SS prediction model. Secondly, the goal is to investigate the effect of adding scaled, veridical yaw motion to a simulator simulating urban driving scenarios on SS. A SS prediction model was developed based on observer theory, by implementing human spatial orientation perception mechanisms and mechanisms that model the development of sickness symptoms. Subsequently, theories on MS and SS together with the predictions of the SS prediction model were used to formulate several hypotheses for the experiment. This experiment consisted of three cases, where Case 1 considered no-motion, Case 2 considered scaled yaw cueing, and Case 3 considered the same yaw cueing together with the full vehicle pitch and roll motions. The effect of motion on SS was investigated using the misery scale (MISC) [27] and the simulator sickness questionnaire (SSQ) [28]. Then, the experimental results were used to validate the developed model.

Furthermore, two additional measurements were the perceived motion incongruence (PMI) and head movements. The PMI may be used to quantify a part of the SC theory, which is a qualitative description to explain the cause of MS. However, as the SSQ and MISC measurements are quantitative; it is hard to match the theory with the experimental results. This is also suggested by Stoffregen and Riccio [29], because they argued that the SC is not a measurable variable meaning that it cannot even be falsified. However, a reliable and validated method has been developed by Cleij et al. [30] to measure the PMI. The PMI describes the mismatch between the visual and inertial motion as perceived in a simulator by a human participant [30], which is similar to the visual-vestibular rearrangement as used in the SC theory by Reason [7]. This PMI could be a way to make the SC theory quantifiable, which will substantiate the hypotheses about the sensory rearrangement theory by Reason [7] and help in better understanding MS characteristics.

Head movement strategies might attenuate SS. It has been found that activity and anticipation are both effects that can reduce SS [21], [31]. So, when participants move their head more actively in the direction of the curve, as drivers also do during car driving, they get a clearer picture of the road geometry. This enables the participants to better anticipate their future motion [31], [32]. Therefore, it was investigated if head movements may have a consistent effect on SS.

This paper is structured as follows. Section II presents the proposed SS prediction model. Subsequently, Section III describes the methodology of the experiment. Then, Section IV presents the experimental results. Section V elaborates on the results by means of a discussion. Finally, Section VI concludes the paper.

II. Simulator Sickness Prediction (Model)

An SS prediction model has been developed to predict the simulator sickness incidence (SSI), which is the percentage of people that vomit under the given circumstances. The SSI is related to the motion sickness incidence (MSI) [9], but is specifically defined for the developed model. The SS prediction model combines several model parts from Oman's heuristic mathematical model to explain MS [8], the SVC model from Bos and Bles [10] and its extension to six degrees-of-freedom (DOF) by Kamiji et al. [11]. The model structure can be found in Figure 1 and consists of five blocks: A, B, B', C and D. Block A represents the input selection and kinematics. Here, the signals that are sensed by the human sense organs are selected. Block B includes the human sense organ dynamics and the visual-vestibular interaction part, outputting the sensed signals. Block B' represents the internal model and is copy of block B that generates the expected signal from the CNS. Block C merges the expected and sensed signals to calculate a conflict that is responsible for SS. Finally, block D is responsible for simulating the development behavior of sickness symptoms over time and calculating the SSI.

The model uses a right-handed coordinate system. The direction of the forces are seen from the head reference frame as done by [11]. Hence, the x-axis aligns with the naso-

occipital axis, the y-axis with the interaural axis and the z-axis is orientated perpendicular to the xy-plane where the positive x-direction is to the front, the positive y-direction is to the left and the positive z-direction is upwards because it presents the reaction force of gravity as sensed by a human being, see Figure 2. Other assumptions are that the semi-circular canals are mutually orthogonal to keep the parameters easily identified and to avoid mathematical cross-coupling. Furthermore, this model considers passive motions, meaning that a human is being moved outside his/her control.

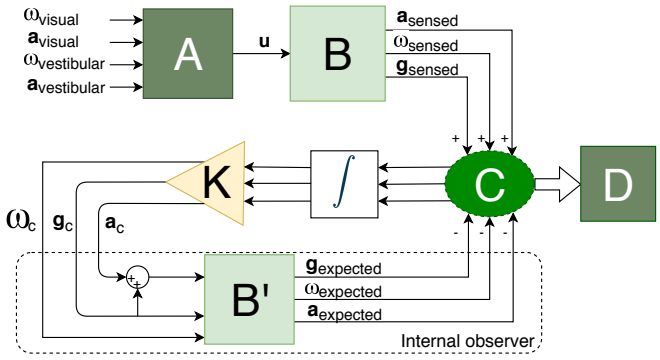

Fig. 1. Simulator Sickness Prediction Model.

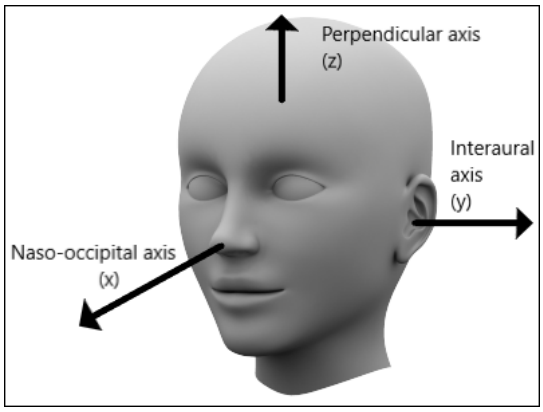

Fig. 2. Human head reference frame. Adapted from [33]

A. Model Requirements

The following requirements were used to make the new SS prediction model verifiable:

Req1 The model should incorporate a part that predicts the sickness incidence and explains the production of symptoms, because the main goal of the model is to predict SS.

Req2 The visual system should be included. When humans drive in simulators, then the visual stimuli can cause sickness. This phenomenon is referred to as visually induced motion sickness (VIMS) [34]. So, the interactions between the visual and vestibular system are of vital importance to get a proper representation.

Req3 The SS prediction model should be able to on the one hand see if the human perception part can estimate certain vestibular motion paradigms, visual sensory paradigms and visual-vestibular paradigms available in literature correctly [8] [35] [36]. On the other hand, the model outputs or SS predictions should be compared with experimentally obtained MS and SS data from literature as well [9].

Req4 The model should be able to be verified and validated for multi-dimensional cases. The experiment to be conducted will involve a multiple DOF motion, which means that 3 dimensions and possibly 6-DOFs need to be taken into account by the model.

B. Theories

The SC theory is generally the most accepted theory that tries to explain the cause of MS and SS [17]. According to the sensory rearrangement theory, all situations that induce MS can be related to some type of sensory rearrangement (of sensory cues). Here, motion signals of the different sense organs can be at variance with each other and with what is expected based on prior experience. The different forms of sensory arrangement are divided in two headings (HE) [7]

He1 The visual-vestibular rearrangements where there is a conflict between information from the sense organs;

He2 The canal-otolith rearrangements where there is a conflict between the vestibular system receptors.

Each heading has three types of conflict. First, a type I conflict arises when the information between sense organs or system receptors is contradictory or uncorrelated. Second, a type II conflict occurs when, for example, the visual system signals motion in absence of the expected corroborating signal from the vestibular system. Thirdly, a type III conflict is the opposite of a type II conflict, so when the vestibular system signals in absence of the expected corroborating signal from the visual system. The neural mismatch model from Reason [7] provides a theoretical framework to implement the SC theory. This model generates a mismatch signal if a comparator detects a conflict or sensory rearrangement as described above. If this mismatch signal is persistent over a certain period of time, then it is used to adapt to existing motions. Furthermore, this mismatch signal is responsible for the cumulative development of sickness symptoms [7], [16].

The SVC theory is a simplification of the SC theory by Bos and Bles (1998) [10] and suggests that MS is primarily provoked by a mismatch between the sensed vertical and the expected or subjective vertical based on prior experience. This conflict appears, for example, in fixed-base simulators when expected motion based on previous experience is unavailable. The determination of the subjective vertical is done by the CNS and based on integrating visual, vestibular and proprioceptive information [37]. Furthermore, the conflicts do not need to be categorized anymore, because there is only one conflict involved, which can be advantageous. This theory also suggests that the assumption of pinning down all provocative motions to a single conflict is justified given the analysis of different types of MS [37]. The developed SS prediction model incorporates the SVC theory, because this theory is of a quantitative nature [10], [11].

C. Input Selection and Kinematics (Block A)

The inputs of the SS prediction model, which are the three-dimensional angular velocity and linear acceleration vectors, are processed by block A, see Figure 1. This block selects the required inputs to be processed by the senses in Block B and calculates the orientation of the gravitational force vector with respect to the human body, which is assumed to be a rigid body. The orientation of the gravitational force vector changes due to the three-dimensional rotations. The following equation is used to determine the relative orientation of gravity based on angular velocity information [11], [21], [35], [38]:

$$\frac{d\vec{g}}{dt} = \vec{g} \times \vec{\omega} = -\vec{\omega} \times \vec{g}, \tag{1}$$

in which $\vec{\omega}$ is the angular velocity of the rigid body in the three dimensional world and $\vec{g}$ is the gravitational force applied.

D. Visual-vestibular interaction (Block B)

After block A, the selected input vector consisting of the specific force, the angular velocity, the linear velocity and gravitational force,($u = [f_h \quad \omega_h \quad v_h \quad g_h]^T$), goes into block B (see Figure 1). This block contains a visual-vestibular interaction model based on [39] including the human motion sensors. The content of block B is visualized in Figure 3.

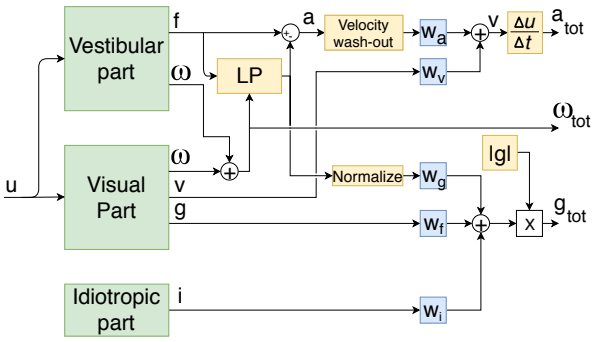

Fig. 3. Visual-vestibular interaction model.

The vestibular part consists of the semi-circular canals (SCC) and otoliths, which are sensitive to angular velocity and specific force, respectively. This model uses a 2^{nd} order transfer function to model the human SCC as done by [11] and [40]:

$$\omega^i_{vest}(s) = \frac{\tau_a \tau_d s^2}{(\tau_a s + 1)(\tau_d s + 1)} \omega^i_h \quad (i = x, y, z), \tag{2}$$

with τ_d as the dominant time constant and τ_a as the adaptation time constant, with values of, respectively, 5 and 80 seconds adapted from Haslwanter et al. [41].

The perception of self-motion through the visual system is based on the reaction to optic flow from the surrounding visual scenes [42], [43]. The human visual system is sensitive to velocity and position, but not to acceleration. However, an individual can see differences or changes in velocities [36]. When an object or visual scene moves within the visually-perceived environment of the observer, then a feeling of self-motion can be induced, even when the observer is stationary [44]. This phenomenon is called vection. Processing the visual flow and the images is a time consuming task due to the complexity and neural delays of the CNS. In this model, linear vection, which increases gradually, is assumed. Therefore, a first-order low-pass filter is used to describe this effect as done in [39]:

$$\vec{v}_{vis} = \frac{1}{\tau_v s + 1} \vec{v}_h, \tag{3}$$

with $\vec{v}_h$ representing the velocity with respect to the head reference system, $\vec{v}_{vis}$ as the perceived velocity by the visual system and $\tau_v = 1\ s$.

Besides velocity, the eyes can perceive rotary motions. These motions can induce circular vection, which is reached after several seconds of motion. Again a low-pass filter is employed, because the sense of angular velocity is just given by the opposite of vestibular angular velocity [36]:

$$\vec{\omega}_{vis} = \frac{1}{\tau_c s + 1} \vec{\omega}_h, \tag{4}$$

with $\tau_c = 10\ s$.

Furthermore, the visual system is able to perceive the direction of gravity (but not it's magnitude), $\vec{g}_{vis}$. Houses and trees are defined as orientation information. This information is used, together with the fact that the horizon is always horizontal, to determine what is upright. Furthermore, perpendicular lines from structures around us are used as frame information. Using orientation and frame information to determine the direction of gravity is relatively a fast process and, therefore, a first-order low pass filter can be used for the approximation [36]:

$$\vec{g}_{vis} = \frac{1}{\tau_g s + 1} \vec{g}_h, \tag{5}$$

with $\vec{g}_e$ as the gravity vector with respect to the earth, $\tau_g = 1s$.

The last green block of the visual-vestibular interaction model as presented in Figure 3 is the idiotropic vector. Humans have the tendency to align their subjective vertical towards their longitudinal body axis [45]. The idiotropic vector has a relatively small magnitude and is added to the total subjective vertical such that the sense of verticality tends to align with the main body axis.

After the senses or perceptual organs, the signals need to be processed by the CNS. The human otoliths are not capable of extracting the gravitational force vector from the sensed specific force information. This problem is called the gravito-intertial force (GIF) resolution problem and is directly linked to Einstein's equivalence principle, which states that the accelerations due to gravity ($\vec{g}$) and motion ($\vec{a}$) are physically equivalent. Angular velocity information ($\vec{\omega}$) from both the visual system and semi-circular canals is required to solve this problem within the CNS [46]. A way of mathematically modeling this solution is given in the block LP (Figure 3) and the output of this equation is the sensed vertical $\vec{g}_{sens}$:

$$\frac{d\vec{g}_{sens}}{dt} = \frac{1}{\tau}(\vec{f} - \vec{g}_{sens}) - \vec{\omega} \times \vec{g}_{sens}, \quad (6)$$

in which the first term on the right represents the specific force or GIF as estimated by the otolith afferent signals only. The second term account for the rotation of the head and the accompanying change of gravity.

Equation (6) also deals with the high-pass characteristics of the semi-circular canals as described by Glasauer and Merfeld [47]. For the low-frequency motions, such as off-vertical angular movements, the sensed vertical is changed according to the outputs of the otoliths. In this case, the semi-circular canals do not signal any motion and the first term with its low-pass filter characteristics passes all information virtually unmodified. For high-frequency motion, the opposite occurs and all the otolith outputs will be filtered out. Bos, Bles and Groen [46] concluded that Equation (6) above gives the most realistic and simplest way in which our CNS is believed to solve the GIF resolution problem.

Subtracting the sensed vertical signal from the original otolith outputs gives the linear acceleration $\vec{a}$ due to motion. The visual system is not able to detect this acceleration, as explained before, and visual information will only enter the path of motion perception after vestibular signals have been integrated temporally. This is also due to Newton's second law, which states that acceleration and force are linearly dependent and force perception does not depend on vision [36]. Normally, the human sense of acceleration vanishes after some time and this is modeled through a high-pass filter in Equation (2). However, there would still be a perception of velocity when simply integrating the acceleration to velocity. Therefore, an additional high-pass filter is added to drive the vestibular velocity perception towards zero [39]. The integration of acceleration to velocity can then be formulated as follows:

$$\vec{v} = \frac{1}{s}\frac{\tau_{av}s}{\tau_{av}s+1}\vec{a} = \frac{\tau_{av}}{\tau_{av}s+1}\vec{a}, \quad (7)$$

and this final result can be regarded as a low-pass filtered acceleration with $\tau_{av} = 5\ s$.

The visual velocity and vestibular velocity outputs are linear weighted using a linear weighted addition as done by Howard [48]:

$$\vec{y} = \frac{w_a\vec{v}_{vest} + w_v\vec{v}_{vis} + \ldots + w_n\vec{u}_n}{w_a + w_v + \ldots w_n}, \quad (8)$$

with $\vec{y}$ as output vector and $\vec{u}$ as the input vector. The weight for the vestibular information is taken as w_a = 0.2 and for the visual system as $w_v = 0.8$, because the visual information is assumed to be dominant [39] [49]. For this model it is assumed that the velocity is differentiated to get the total acceleration (a_{tot}) and feed it back to the internal model. Circular vection behaves contrary to the vestibular angular velocity motion perception. When both sense systems have the same time constant τ_c, the outputs can be added and the sense of self motion is equal to the veridical motion ($\omega_h = \omega_{tot}$):

$$\vec{\omega_{tot}} = \frac{\tau_c s}{\tau_c s+1}\vec{\omega}_h + \frac{1}{\tau_c s+1}\vec{\omega}_h, \quad (9)$$

because now the low-pass filtered part and high-pass filtered part are added such that the original signal becomes the result.

Finally, the attitude or vertical consists of the visual, the vestibular and the idiotropic parts. These should be added as follows. The idiotropic and visual vector only contain orientation information and the vestibular vector contains both orientation and magnitude information. So, Bos and Bles [36] proposed to give all the sources of attitude information only orientation information by defining a unit vector and adding them afterward using Equation (8). The weighting factors that are used have the following values: $w_f = 0.75$(visual), $w_i = 0.05$ (idiotropic) and w_g = 0.2 (vestibular). When there is no source of visual information, then the parameters are chosen as: $w_f = 0.0$, $w_i = 0.05$ and $w_g = 0.95$ [39], [49]. The resulting vertical (g_{tot}) has the length of the gravity as sensed by the vestibular system only [39]. MS is related to the difference between the gravity vector as sensed and the gravity vector as expected by the internal model and, therefore, it needs a magnitude to explain MS.

E. Internal Observer (Block B')

Ideally, the CNS wants to control all various motion states in a noise-free fashion, but the response of the human senses do include sense organ output noise and are not sensitive to all states. For example, humans do not possess senses to measure gravity separately from acceleration or to measure angular acceleration. So, it is not possible to achieve adequate orientation in the spatial environment when only noisy and indirect information about the physical behavior of the body is available, which are in turn subjected to external disturbances. However, there is a solution for the CNS model to adequately control the body, namely by employing a so-called observer [8] (see Block B' in Figure 2). Here, an estimate of the controlled system is generated by the information processing observer consisting of an internal model of the controlled system, giving the observer priori knowledge.

When the system is not subjected to external disturbances it should be able to predict the consequent behavior of the system over time using an accurate set of initial conditions. However, such a system without external disturbances is in practice not available. Therefore, Kalman and Bucy [50] and Wonham [51] showed a strategy to overcome this problem. The internal observer should be able to estimate the state of the controlled system as well as to predict the feedback measurements to be expected from moment to moment if the observer's guess regarding the actual system is correct.

To derive the estimated state, some assumptions are made. For example, the behavioral aspects of the body and its sensory organs are known by the CNS or internal observer. These are the elements in B' and the CNS can employ an estimate of B. A conflict vector can be defined as the difference between the expected signals from B' and the sensed signals from B:

$$\vec{c} = \vec{y} - \hat{\vec{y}}, \quad (10)$$

This conflict $\vec{c}$ contains information that can be used to steer the time rate of change of the estimated state $\hat{\dot{\vec{x}}}$ towards the actual state $\vec{x}$. Now, an observer gain matrix K (Block K in

Figure 1) needs to be chosen consisting out of three gains: K_{ac}, K_{gc} and $K_{\omega c}$. These gains should be chosen such that $\hat{\vec{x}}$ is driven towards $\vec{x}$ and the conflict itself is reduced. A more detailed explanation of the chosen gains for the SS prediction model can be found in Appendix A.

F. Model output (Block D)

Current models that try to predict MS generally use the MSI as output [10], [11], [52], which is the percentage of vomiting subjects [10] and this is an observable marker of behavior [16]. The output of the SS prediction model is the SSI, which is similar to the MSI, but more focused on SS as this is the topic of interest in this paper. Block D in Figure 2 consists of two parts. When using the MSI, or the SSI in the SS prediction model, it should be taken into account that humans cannot become sicker than sick, which is vomiting. This maximum is reached asymptotically [46]. On the other hand, small conflicts can be neglected, because not all actual or apparent motions lead to the development of sickness symptoms. Therefore, an exponential function is suitable at the start. As the conflict vector, $\vec{c}$, can become very large and both positive and negative, a Hill-type function is used that transforms the conflict according to these needs [46]:

$$h(\vec{c}) = \frac{(||\vec{c}||/b)^{n_h}}{1 + (||\vec{c}||/b)^{n_h}} \tag{11}$$

The parameter n_h accounts for the steepness of the function and when n_h is chosen even, the conflict will always be positive, as desired here. For $n_h = 2$ the function is logarithmic for larger conflicts and the function is exponential for smaller conflicts. Parameter b can be chosen such that the model outputs fit the experimental data best [10], as done in Appendix A. Figure 4 shows the output of a Hill function for different values of b. When b becomes larger then the steepness of the function and end values at $||\vec{c}|| = 1$ both decrease.

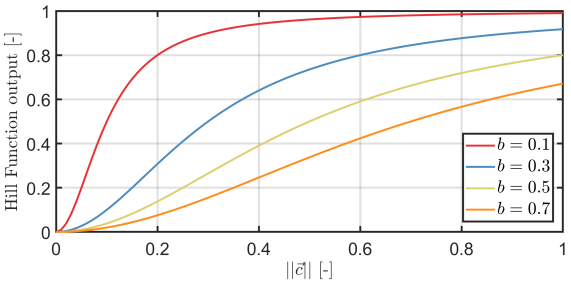

Fig. 4. The output of a Hill function for different values of b.

Then, a leaky integrator models the cumulative behavior of MS to get the MS severity. Small disturbances or short temporal fluctuations in the conflict vector should normally not be sufficiently provocative to induce MS. Therefore, a second-order filter is chosen to ignore the slightly different accumulations at different acceleration levels. The final result becomes:

$$\text{SSI} = \frac{P}{(\mu s + 1)^2} h \tag{12}$$

where μ is time constant of the low-pass filter and P is the percentage of the maximum amount of participants that got motion sick under the given circumstances [10]. The response of a leaky integrator and a normal integrator to a saw-tooth input signal are given in Figure 5 for different time constants of the low-pass filter. A normal integrator keeps the signal at the same level if the conflict returns to zero, but this would mean that humans will become increasingly more sick during their life. The leaky integrator makes sure that the sickness severity returns to zero after cessation of the conflict [10] [46]. The smaller the time constant, the faster sickness develops and the faster it reduces after cessation of the conflict.

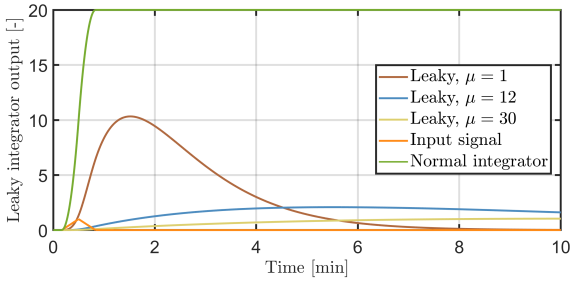

Fig. 5. The response of a leaky integrator and normal integrator to a saw-tooth input signal for different time constants.

G. Results

The complete list of parameters used for the SS model predictions is given in Table I. These parameters have been used to make some first predictions regarding the motion cases to be considered during the experiment. As mentioned before, three motion cases were tested during the experiment. Case 1 considered the no-motion case, where naturally no motion was cued by the simulator. Case 2 considered a purely scaled yaw motion, including pre-positioning, where 58% of the yaw motion was cued by the simulator, see Figures 6 and 9. Case 3 considered the motion as in Case 2 together with the full pitch and roll motions of the vehicle model, see Figures 7 and 10. Additionally, the full vehicle model movement case is considered that consists of the veridical angular and translational movements of the vehicle as presented in Figures 8 and 11.

TABLE I
PARAMETERS OF THE SS PREDICTION MODEL ACCORDING TO [11], [39], [49] AND THE WEIGHT PARAMETER TUNING.

Parameter	Value	Unit	Parameter	Value	Unit
K_{ac}	1.9418	$[-]$	g_0	9.80665	$[m/s]$
K_{vc}	18.6511	$[-]$	b	0.1061	$[-]$
$K_{\omega c}$	1.9418	$[-]$	μ	12	$[min]$
τ_a	190.0	$[s]$	P	85.0	$[\%]$
τ_d	7.0	$[s]$	Weights	Light	Dark
τ	5.0	$[s]$	w_a	0.2	1.0
τ_c	10.0	$[s]$	w_v	0.8	0.0
τ_v	1.0	$[s]$	w_g	0.2	0.95
τ_{av}	5.0	$[s]$	w_f	0.75	0.0
τ_g	1.0	$[s]$	w_i	0.05	0.05

One of the objectives of this paper is to investigate the effect of adding yaw motion to a simulator on SS.

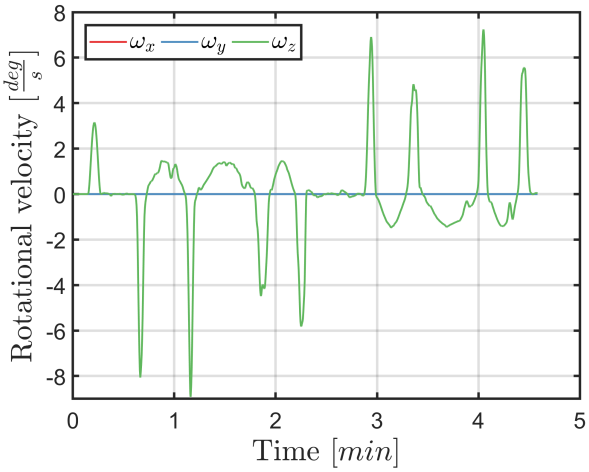

Fig. 6. The angular velocities as cued by the simulator, which is in this case purely down-scaled yaw motion (Case 2).

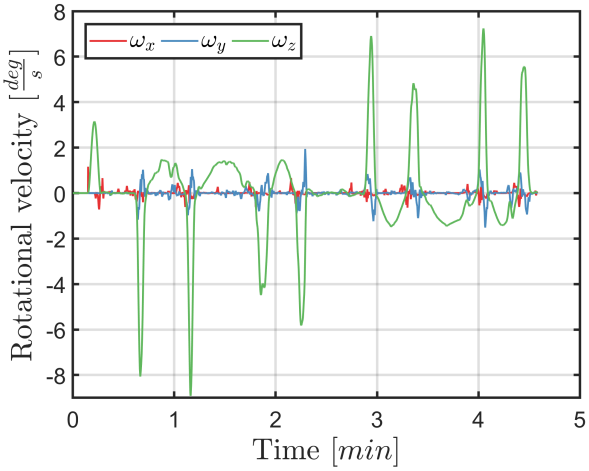

Fig. 7. The angular velocities as cued by the simulator, which are in this case roll, pitch and yaw motion (Case 3).

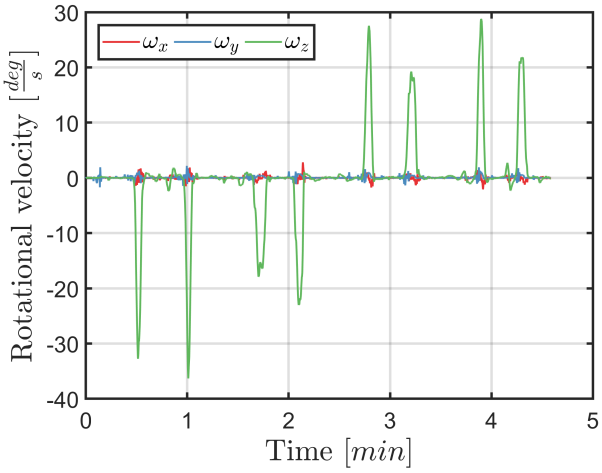

Fig. 8. The vehicle model angular velocities. These angular velocities were always used as input for the visual part of both the experiment and the model.

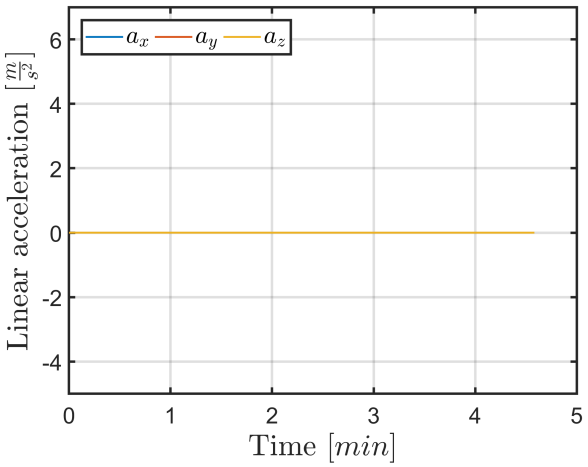

Fig. 9. The accelerations as cued by the simulator, which are zero for the purely yaw motion case (Case 2).

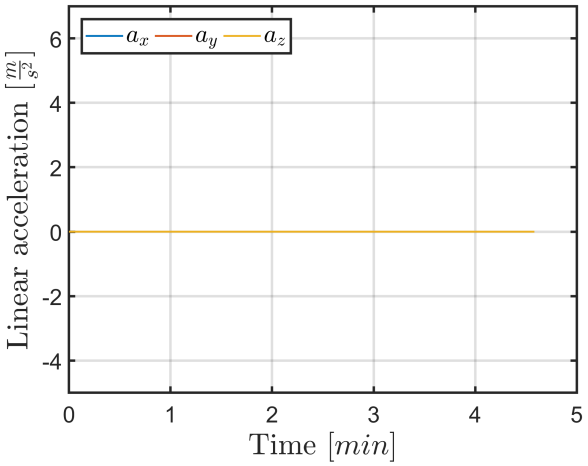

Fig. 10. The accelerations as cued by the simulator, which are zero for the roll, pitch and yaw motion case (Case 3).

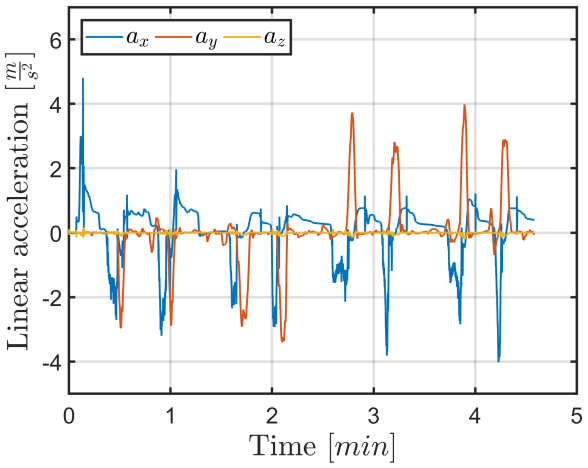

Fig. 11. The vehicle model accelerations. These accelerations were always used as input for the visual part of both the experiment and the model.

To form some first hypothesis for the experiment, the SS prediction model was used to predict the SSI for the different motion cases, see Figures 12 to 14. Transformations from the vehicle center of gravity (CoG) to the head reference frame were neglected in this study. The motion cases, which are Case 2, Case 3 and the full-motion case, were compared to Case 1, the no-motion case. First, Figure 12 presents the prediction results of the SS prediction model of the no-motion case (Case 1, blue line) and the full-motion case (red line). Secondly, the comparison of SSI predictions between Case 2 and Case 1 can be found in Figure 13. Thirdly, the comparison of SSI predictions between Case 3 and Case 1 can be found in Figure 14.

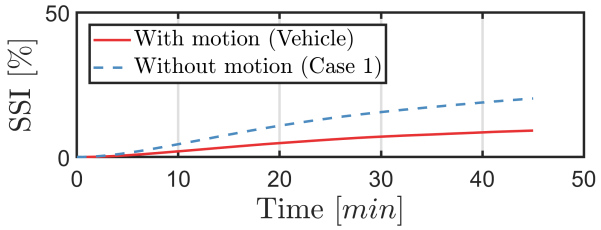

Fig. 12. SS model predictions for both the motion (full vehicle model motion) and without motion case.

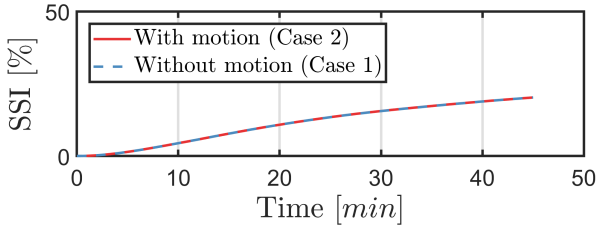

Fig. 13. SS model predictions for the no-motion case (Case 1) versus the scaled yaw motion case (Case 2)

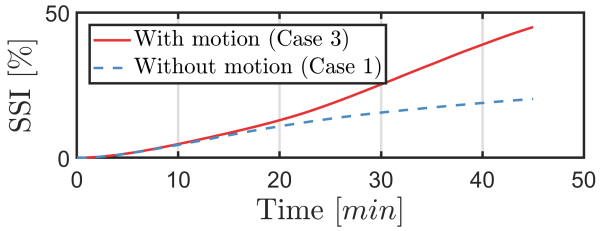

Fig. 14. SS model predictions for the no-motion case (Case 1) versus the roll, pitch, yaw motion case (Case 3).

The results in Figure 12 are as expected based on both the SC and SVC theory: adding roll, pitch and yaw motion should attenuate both the SC and SVC responsible for SS and thereby the SSI. The lines for Case 1 vs. Case 2 overlap (Figure 13), which is inaccurate when considering the SC, but accurate when considering the SVC theory. The SC theory incorporates a sensory rearrangement type that describes a conflict between the visual and vestibular system, see **He1** in Section II-B. Such a conflict is expected for Case 2, since only limited motion signals are provided to the vestibular system and the full motion is provided to the visual system. However, the SVC theory states that there is no conflict in this case, as only pure yaw motions are considered, meaning that there is no mismatch between the subjective vertical and the sensed vertical [10]. Figure 14 indicates that more humans get sick when adding the motion cueing as been considered in Case 3. However, these results are contradicted by both the SC and SVC theory.

Despite the model verification in Appendix A, it has not been designed to cope with transformed motion (i.e., non-veridical) as input. Therefore, an important assumption for the remainder of this paper is that the experimental results will be compared to the model outputs of Figure 12, because these results are in terms of SS model validity, the most reliable ones. Based on the SC and SVC theory and the predictions by the SS prediction model for the full-motion case, it could be hypothesized that adding motion should attenuate the SSI. To test this hypothesis, an experiment was performed as explained in the next section.

III. Experiment

An experiment has been conducted to investigate the effect of adding scaled, but otherwise veridical, yaw motion to a simulator on SS. Hence, the second objective of this paper was to attenuate SS by adding scaled, but reliable and correct motion to a simulator. This has been done by performing a between-subjects experiment in the driver-in-motion (DIM) simulator of the BMW Group in Munich, in which participants were driven around in an urban environment as passenger with left and right 90-degree turns. The three cases were as follows: the simulator either cued no motion (Case 1), purely yaw motion (Case 2), or roll, pitch and yaw motion (Case 3). The participants were passively driven and were asked to give a MISC score every minute and continuously rate the PMI during the turns. The PMI was measured to investigate its relationship with the SSI and if this PMI could be used as a way to quantify a part of the sensory rearrangement theory. At the end of the experiment, participants were required to fill in the SSQ, which served as an extra SS measure. Finally, head motions were measured to try to identify to what extent the participants used a strategy to reduce SS.

A. Participants

The experiment protocol and consent forms were approved by the Human Research Ethics Committee of the Technical University of Delft. Data were collected from 63 healthy participants that were randomly assigned to one of the three cases. They all possessed a driver's license. There were 31 males participating in the experiment and 32 females, with a large spread in age, see Table II. Participants were divided such that the age and susceptibility to MS variations were equal among the groups. It has been shown that age may have an effect on SS [53]. Furthermore, Hock [1] suggests to always recruit a mixed sample group. A short version of the motion sickness history questionnaire (MSHQ) was filled out, that considered the participants' susceptibility to MS using a Likert-scale. Besides the age and MS susceptibility, Table II shows that the number of females and males for each case are almost the same. Another factor that was involved in dividing the participants over the different cases was simulator experience.

For each case there were 5 participants that had some prior simulator experiences. All participants gave informed consent prior to performing the experiment. Finally, the number of participants per case differs, because there were relatively more technical failures during the experiment trials in Case 2 and Case 3. Some of the participants that encountered these technical failures were excluded from the analysis. Therefore, more participants were tested in Case 2 and 3 to have a more similar number of participants per case during the analysis.

TABLE II
OVERVIEW OF THE NUMBER OF MEN AND WOMEN THAT PARTICIPATED IN THE 3 CASES WITH THE CORRESPONDING MEAN AGE AND STANDARD DEVIATION BETWEEN THE BRACKETS.

	Case 1: No Motion		Case 2: Yaw Motion		Case 3: Yaw, Pitch, Roll motion	
	N	Age	N	Age	N	Age
Females	9	41.89 (12.33)	11	41 (9.66)	12	39.5 (11.86)
Males	11	39.09 (12.31)	10	44.5 (11.37)	10	38.6 (10.44)
Total	20	40.35 (12.40)	21	42.67 (10.66)	22	39.09 (11.24)

B. Apparatus

The VI-grade driver-in-motion (DIM) simulator of the BMW Group in Munich was used as driving simulator in the experiment to present the visual and vestibular stimuli, see Figure 15. A car mock-up was positioned on top of a platform that was attached to multiple actuators. The actuators provide a 9-DOF motion space from which 6-DOF were produced by a hexapod that was placed on top of a 3-DOF tripod. The hexapod was capable of cueing high-frequency movements ($\pm 5 - 30\ Hz$) and the tripod was capable of cueing low-frequency movements ($\pm 0 - 5\ Hz$). Both parts were used to cue the complete yaw motion during the experiment. For the pitch and roll motions, only the hexapod was used.

Table III summarizes the simulator performance of the combined hexapod and tripod system. The climate within the mock-up of the simulator was controlled by the participants. Vibrations were not simulated, because an accurate vibration template module was not available. Sound was available in the form of road, motor, and other environmental noises. A wraparound projection screen provided a 220° field of view displaying the visuals. Figure 16 shows the field of view that a participant was able to see from inside the motion cabin.

TABLE III
DIM SIMULATOR CHARACTERISTICS.

	Stroke	Max. Velocity	Max. Acceleration
X	1.08 $[m]$	3.7 $[m/s]$	37 $[m/s^2]$
Y	1.00 $[m]$	3.2 $[m/s]$	35 $[m/s^2]$
Z	0.22 $[m]$	1.6 $[m/s]$	35 $[m/s^2]$
Roll	20 [°]	135 $[°/s]$	2500 $[°/s^2]$
Pitch	20 [°]	130 $[°/s]$	1000 $[°/s^2]$
Yaw	45 [°]	300 $[°/s]$	3900 $[°/s^2]$

Fig. 15. DIM Simulator.

Fig. 16. Visible field of view of a corner seen from behind the simulator motion cabin.

C. Experimental conditions

As mentioned in the introduction, the main known remedy for SS is adaptation. Simultaneously this could be disadvantageous when employing a within-subjects design with multiple cases per participants. Therefore, a one-factorial between-subjects design was used here. The independent variable, motion, consisted out of three cases. The first case was without movement, so subjects were driven around the track with purely visual inputs. For the second case, participants were exposed to purely yaw motions, which were scaled to 58% of the actual vehicle motion. Prepositioning with a maximum of 3°/s was added as well to stay within the actuator limits and get a larger yaw movement space. The third case presented the same yaw motion to the participants as case 2, but in addition, the full pitch and roll motion of the vehicle model were cued. Participants were passively driven around an eight-shaped track as can be seen in Figure 17. An urban environment was simulated including 80 sharp 90-degree curves, pedestrians and large city buildings. Thus, the scenery can be characterized as eliciting a rather high optic flow.

D. Measurements

The first measurement was the motion sickness history questionnaire (MSHQ) [54]. For the MSHQ, participants

Fig. 17. Driving track. The crosses indicate objects such as buildings, pedestrians etc.

were asked six questions, of which the first five considered the participants' experience with MS while traveling in different forms of transport. Subjects were also asked to give a self-rating of their overall susceptibility to MS compared to other people based on the options below:

1 Clearly less than average
2 Less than average
3 Average
4 More than average
5 Clearly more than average

Second, a specific tool to measure SS is the simulator sickness questionnaire (SSQ) by Kennedy, Lane, Berbaum, and Lilienthal [28]. This questionnaire is seen as the single most important questionnaire regarding simulator, cyber or virtual reality sickness [55]. The 16 items on the SSQ were rated by the participants on a 4-point Likert-scale ranging from "not at all" to "severe". These items are divided over three sub-scales [28] [55]. Eventually, a total SSQ score and scores for every sub-scale can be calculated. The three sub-scales are:

- Disorientation (e.g., vertigo, concentration issues)
- Nausea (e.g., general discomfort, nausea)
- Oculomotor issues (e.g., eyestrain, focusing issues)

Third, the misery scale (MISC) was employed, which is an 11-point Likert-scale as well ranging from zero to ten. It gives a more sensitive measure of sickness than the MSI, which is desirable when studying a small group of participants as done in the present experiment [27]. This scale was used as a verbal rating scale and monitored every minute throughout the experiment trials. Participants were only asked to give a number, which took only a couple of seconds, as soon as they were familiar with the rating scale. A copy of the MISC was placed in the car mock-up next to the steering wheel for reference. Furthermore, the rating as indicated by the participants was repeated by the experiment leader to confirm the number and the accompanying symptoms when the rating was changing. The MISC according to [27] can be found in Table IV. A maximum of 6 to 7 on the misery scale was allowed during the experiment, which means participants at most suffered from minor to medium nausea effects. If people got this far on the MISC, the simulation was stopped immediately and the participants were defined as sick. These drop-outs were used to determine the SSI.

TABLE IV
MISERY SCALE (MISC).

Symptom		Score
No problems		0
Uneasiness (no typical symptoms)		1
Dizziness, warmth, headache, stomach awareness, sweating, ...	vague	2
	slight	3
	fairly	4
	severe	5
Nausea	Slight	6
	fairly	7
	severe	8
	(near) retching	9
Vomiting		10

Furthermore, a rotary knob on the center console was used to continuously rate the deviation between the expected movement from a real car that is in accordance with the presented visuals and the movement cued by the simulator, i.e., the perceived motion incongruence (PMI) [30]. The PMI has been found to be a reliable and valid measure to be used during vehicle motion simulation [30]. The deviations or PMIs can occur in different forms. Movements could have been completely absent, meaning that there was not enough movement in a specific driving maneuver, but they could also been partly available and giving a the feeling that something was missing. These deviations were evaluated according to one's own feelings. The scale ranges from 0 to 10, where 0 represents no deviation from a real vehicle motion and 10 a very large deviation from the real vehicle motion.

The current scale value was indicated by a bar in the presented driving scene. It was important for the participants to use the full scale, because participant could only use such a rating scale properly when the maximum incongruence during the experiment is known [30]. The PMI scale is displayed in Figure 18. Only the movement of the simulator should have been evaluated. The following was not included in the rating:

- Visualization error, for example, pixelations, end of the screen;
- Missing road conditions, such as potholes, sewage covers;
- Sound effects, such as engine sound, wind;
- Noise from the simulator, for example electric actuators;
- Immediate beginning and end of the ride. The simulator moves to the neutral position, this is not part of the test drive;
- Unrealistic conditions in the driver's compartment, for example steering wheel and foot pedals do not move;
- Odors.

Finally, Tobii eye-tracking glasses including a gyroscope and accelerometer were put on before the experiment started to measure head movements, see Figure 19. These glasses needed

to be calibrated shortly. Head movement data that came from the internal gyro and accelerometer provided orientation and inertial acceleration data.

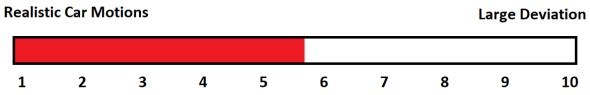

Fig. 18. Continuous rating bar to rate motion realism.

Fig. 19. Tobii eye-tracking goggles.

E. Procedure

An overview of the complete experiment procedure can be found in Table V. Participants started by reading the experiment instructions and filling out the mentioned questionnaires. They got a safety briefing in the simulator before starting the simulation and information contained in the instructions was repeated. Once started, two practice drives, one with motion and one without motion, were performed to practice with the continuous rating task and the verbal rating scale. This training session was performed until a sufficient level of capability was achieved determined by the experiment leader. After this familiarization, the Tobii glasses were calibrated and participants were presented with one of the three given scenarios and driven for a maximum of 45 minutes. Screens and sound were provided to the experiment leader to closely monitor the participants' condition. When the participants indicated a MISC index of 6 two times in two minutes or a single 7, the simulation was aborted immediately. After the experiment, the SSQ was filled in again and there was some time for questions of the participants.

F. Data analysis

The MSHQ data can be categorized as ordinal data meaning that a non-parametric test needed to be selected. A Pearson Chi-Square test has been applied to see if there is a significant difference between the three cases concerning the distribution of participants' MSHQ scores. This specific test has been chosen, because MSHQ data are categorical data and a between-subjects design has been chosen. For the MISC data, two operations have been performed to restructure the data. First, the number of drop-outs was determined based on the number of MISC scores above 6 or two times 6 and indicated with a zero (completed experiment) or one (dropped out). Subsequently, a Pearson Chi-Square test was performed on the data, for the same reasons as for the MSHQ data, to test if there was a difference between the three cases (Case 1 vs. Case 2 vs. Case 3). A Pearson Chi-Square test was also performed to test the effect of just motion on the number of drop-outs (Case 1 vs. Case 2 + 3).

TABLE V
EXPERIMENTAL PROCEDURE.

Step	Duration $[min]$	Notes
Pick-up and welcome	5	
Instructions at desk	3	Reading
Pre-test Interview	5	Fill in SSQ/MSHQ
Instructions in simulator	2	Safety instructions
Familiarization	5	Drive two test scenarios
Experiment	45	Drive one of the three scenarios
Post-test Interview	5	Fill in SSQ
Q&A	3	Question and Answers
Departure	2	
Buffer	15	For technical failure/other delays
Total	90	

The SSQ and PMI results were both continuous data. A one-way ANOVA test was performed, since the independent variable was categorical, more than two predictors (Case 1, 2 and 3) were involved, a between-subjects design was employed and all data sets are normally distributed. As post-hoc procedure, either a Tukey procedure was applied, when the sample sizes are equal, or Gabriel's procedure is used when the sample sizes are slightly different. Levene's test was executed on the data to see if the assumption of homogeneity of variances was violated. When this assumption was violated, the Welch F was reported instead of the usual F-ratio. Besides the difference in PMI between the three cases, these data were used to see if it can be related to the MISC. On the one hand, the SSI was calculated according to the procedure in Section II-F with $c = \text{PMI}$. On the other hand, the integrated PMI over time was calculated, $\int \text{PMI}\, dt$. Subsequently, Pearson's correlation coefficient was determined between the calculated SSI or integrated PMI and the MISC data to determine the strength of the relationship.

The integrated head yaw data with respect to the rotating cabin was acquired by subtracting the yaw motions of the simulator from the Tobii yaw data acquired in Case 2 and Case 3. Then a cumulative yaw rate score was calculated per participant, which consisted out of the head movements that were consistent with the direction of a left or right curve. This has been done for separately the right and left curves, but also for all corners. Subsequently, the participant results were divided over two cases: a group with MISC scores larger than 3 (MISC > 3) and a group with MISC scores smaller or equal to 3 (MISC ≤ 3). A Kruskal-Wallis test was performed to determine the significance of the cumulative yaw rate score difference between these two groups, because the assumption of a normal distribution was violated.

Finally, the SSI as predicted by the SS prediction model was compared to the experimentally obtained SSI. The model predicted the SSI for the no-motion case and for the case with motion. This means that the model predicted SSI for the no-motion case was compared to the experimental results from

Case 1 (no-motion case). Subsequently, the model predicted SSI for the case with motion was compared to experimental results from Case 2 and Case 3 (with motion cases). The data sets violated the assumption of being normally distributed. Therefore, Kendall's tau was used as non-parametric correlation test since a small sample size was considered.

G. Hypotheses

The following hypotheses were formulated prior to the experiment, based on Section II:

H1 *Adding motion to a static driving simulator while driving in an urban environment will result in a decreasing frequency of sick people.* The SC theory states that MS increases when there is a conflict between the sensed and expected afferent signals [7]. When adding motion, the sensory conflict will, in theory, attenuate and therefore the SSI will decrease. Furthermore, this hypothesis is also based on the SS prediction model outputs showing a higher SSI for the no-motion case than for the motion case;

H2 *A positive correlation exists between the PMI and sickness scores over time.* This hypothesis is based on a **He1** sensory rearrangement producing MS as stated by Reason [7] and Section II;

H3 *Head yaw movements affect simulator sickness.* When participants move their head along with the direction of the curve, they are more actively involved. Furthermore, they are able to observe the road geometry more easily and thereby anticipate their motion in the near future. Activity and anticipation are effects that were reported to reduce simulator sickness [31] [21] [32];

H4 *A positive correlation can be found between the SSI as predicted by the SS prediction model and the experimentally obtained SSI.* The proposed SS prediction model is based on human perceptual mechanisms and theories on the explanation of MS and SS. Therefore, it is expected that the model output is related to the experimental output.

IV. Results

The results of the experiment were analyzed using the Statistical Package for Social Science, (IBM, SPSS, v.25) with a priori alpha of 0.05, or the Statistics and Machine Learning Toolbox software from Matlab. Out of the 63 participants, 5 participants were excluded, because a too long break was required to restart the system somewhere during the experiment execution. After the break, there was not enough time to perform the whole 45-minute drive again. Because MS and SS develop over time, this could be a confound. Participants that had a break but could finish the full 45 minutes without jumps in the data before/after the break were included. For example, a jump in the data could be that the MISC score was 4 before the break and 1 after the break. Eventually, 58 participants were left for the analysis.

A. MSHQ

The MSHQ was used to ensure similar MS susceptibility across all groups at baseline. In Figure 20 a stacked bar plot presents the division of the participants and their indicated MS susceptibility score over the three cases. After excluding five participants that were dropped, it becomes clear that the distribution of participants in Case 3 suffers the most. In the end, the distribution over the different cases is similar. A Pearson Chi-Square test was performed and resulted in non-significant differences of the MSHQ indications between Case 1, 2 and 3, $\chi^2(6) = 2.67$, $p(0.85) > 0.05$. This outcome substantiates the results that the distribution of the participants over the different cases is fairly done.

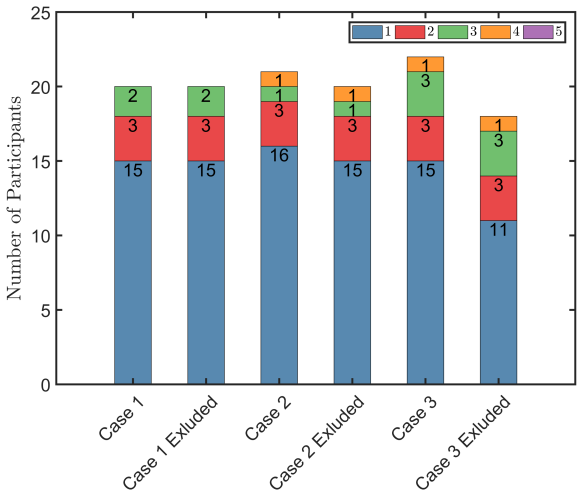

Fig. 20. MS susceptibility division over three cases.

B. Drop-outs

Of the 58 participants, for 13.8% (n=8) the experiment was stopped by the experiment leader before the end of the experiment. These participants reported high MISC levels (MISC > 6) at some point in time. The number of participants that completed and dropped out per case are given in Figure 21. For Case 1, 25% of the participants dropped out, for Case 2 this was 10% and for Case 3 this was 5.6%. The pie-charts display the largest drop-out number at Case 1. The non-parametric Pearson Chi-square test revealed that the drop-outs in the different cases were not significantly different, $\chi^2(2) = 3.38$, $p(0.18) > 0.05$. When comparing the motion cases (2 and 3 in Figure 21) with the no-motion case (Case 1) in Figure 21, then there are significantly more drop-outs in the no motion cases than the motion case, $\chi^2(2) = 10.55$, $p(0.005) < 0.025$. To prevent a Type 1 error, a Bonferroni correction was applied.

C. MISC

First, Figures 22 to 24 give the occurrence of MISC levels per minute for the three cases. Four groups have been made with different MISC scores in ascending order: 0-1 means

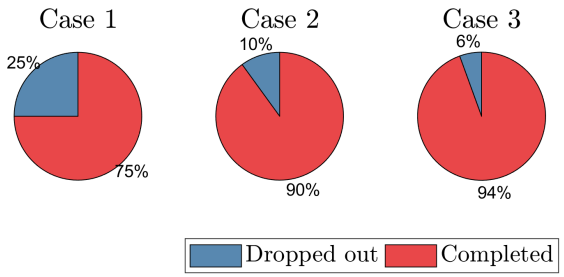

Fig. 21. Number of participants that completed the full experiment or dropped out per case.

there can be some uneasiness without clear symptoms, 2-3 means some uneasiness with symptoms, 3-5 means more severe uneasiness with symptoms and 6-7 means that participants show nauseated behavior. Most participants that reach a MISC level of 6 to 7 can be found in Case 1, which is in accordance with the drop-out behavior shown previously. Case 3 shows relatively the highest number of MISC levels between the 4 and 5, which is already on the edge of getting nauseous. Based on these graphs, Case 2 shows the best results with the majority of participant only reaching MISC levels between the 0 and 3.

Furthermore, Figure 25 shows the box-plots for the MISC scores at the end of the experiment duration time per case. This final MISC data is presented considering the full data-set and a data-set without the participants that dropped out of the experiment. The full data-set displays the highest median for Case 1 compared to the other cases. When pulling out the participants that dropped out, the medians of Cases 1 and 3 are equal and the median of Case 2 drops to zero. Overall, Case 2 again shows the best results in terms of sickness since it has the lowest MISC median. The outcome of the Pearson Chi-Square indicates that no significant differences have been found between the MISC end values of the cases, $\chi^2(2) = 11.27$, p (0.67) > 0.05. Furthermore, a significant difference has not been found between the no-motion case (Case 1) and motion cases (Case 2 and Case 3) as well, $\chi^2(1) = 5.82$, p (0.56) > 0.05.

The statistical tests points out that none of the visual trends are significant. Figure 26 shows the simulator sickness incidence, which is the percentage of people that became sick over time per case. Here, sickness is defined as reaching a MISC level of two times 6 in two minutes or one 7. Hence, the end of the experiment can be at, for example, 20 minutes when someone already reaches 6 multiple times or even a 7 and dropped out. At the end of the experiment time (45 minutes), 25% of the people became sick for Case 1 and for Case 2 and 3 this was 10% and 6%, respectively. Again, the no-motion case (Case 1) lead to the most people that were sick.

D. SSQ

The results of the SSQ are shown in Figures 27 to 30 . First, the total score (TS) is displayed with underneath the three

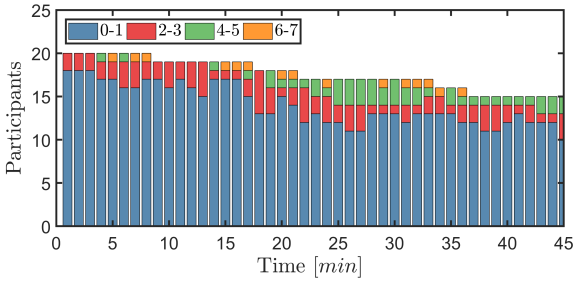

Fig. 22. MISC indications for each minute in Case 1.

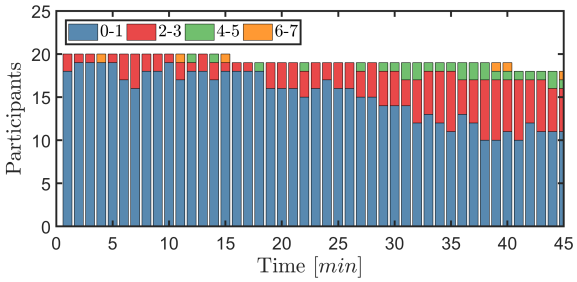

Fig. 23. MISC indications for each minute in Case 2.

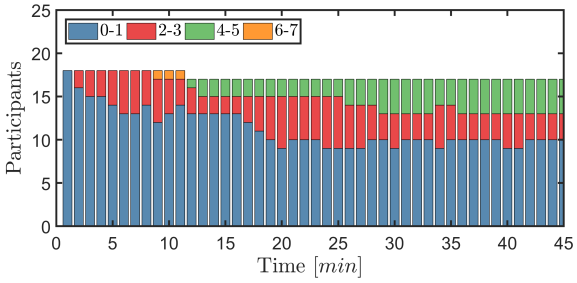

Fig. 24. MISC indications for each minute in Case 3.

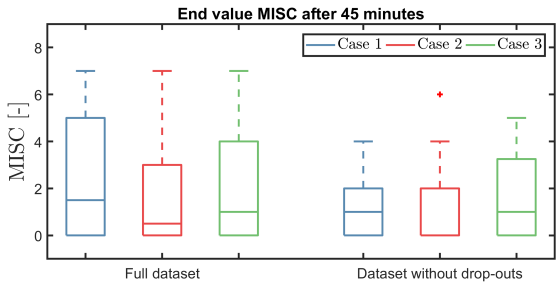

Fig. 25. MISC boxplot of three cases for the full data-set and data-set without the dropped out participants.

distinct symptom cluster scores, which are Nausea scores (NS; nausea, stomach awareness, increased salivation, burping), Oculomotor scores (OS; eyestrain, difficulty focusing, blurred vision, headache) and Disorientation scores (DS; dizziness, vertigo).

Generally, the box-plots display similar behavior for the before and after SSQs. However, the after SSQ scores median is higher for all cases and categories compared to the before SSQ scores median. So, participants became more sick after the simulation trial according to these results. Furthermore,

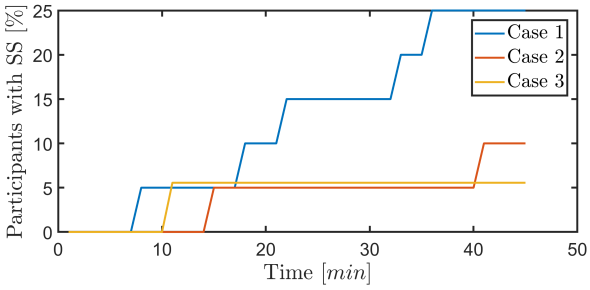

Fig. 26. Percentage of participant becoming sick over time for each case.

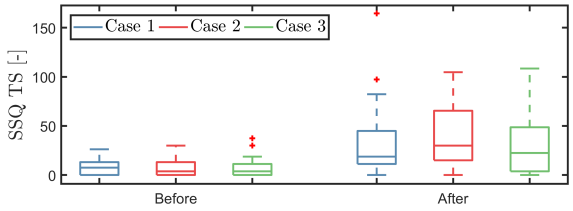

Fig. 27. SSQ total score (TS) before and after per case.

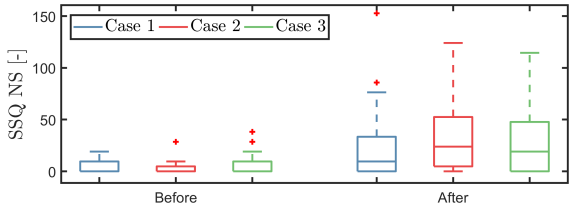

Fig. 28. SSQ nausea score (NS) before and after per case.

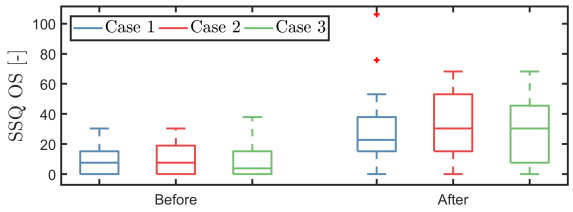

Fig. 29. SSQ oculumotor score (OS) before and after per case.

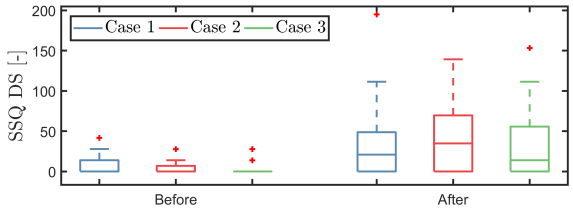

Fig. 30. SSQ disorientation score (DS) before and after per case.

Case 2 shows generally the highest scores for all categories. This is not in line with the results in Section IV-C, where the MISC scores are relatively the lowest compared to the other cases. No significant difference has been found between the different cases for all the total scores and the three different symptom cluster scores considering both the before and after SSQs ($p > 0.05$), see Table VI.

TABLE VI
THE KRUSKAL-WALLIS TEST STATISTIC H AND THE SIGNIFICANCE P-VALUES FOR THE DIFFERENT CASES, SCORES AND SSQS.

	Before (H)	Before (p)	After (H)	After (p)
TS	0.60	0.74	0.97	0.62
NS	1.04	0.59	1.20	0.55
OS	0.4	0.82	0.83	0.66
DS	0.30	0.86	0.49	0.78

E. PMI

For the analysis of the PMI, one extra participant from Case 1 was excluded from the data-set due to the apparent inability to properly rate the motion during the simulation trial. This means that 57 participants were included for the analysis of the PMI. The yaw rate ($\dot{\psi}$) of the vehicle, together with the PMI rating of a participant are given in Figure 31 for the time required to finish one round on the eight-shaped track. First, to analyze the PMI for the corners only, the data within the green dotted lines in Figure 31 was required. The PMI data for $\dot{\psi} < 3.72°/s$ is excluded from the data-set to keep only the PMI data generated during the corners. When using this number as threshold value for $\dot{\psi}$, then the small yaw motions on the straight sections are omitted. To check if this was done correctly, the start and end point of each corner was plotted based on the procedure above.

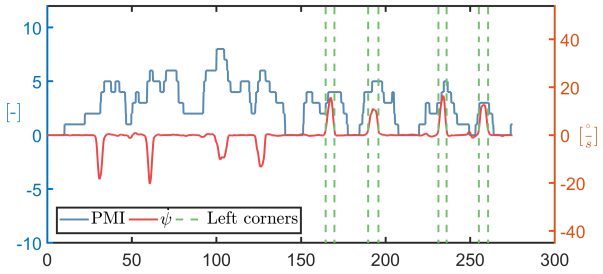

Fig. 31. Vehicle yaw rate and PMI rating during the simulation time of one eight shape on the track for a random participant in Case 3.

Figure 31 shows this for the first part of the simulation trial and only the left corners. As not all corners require the same amount of time, it would be wrong to take averages of PMI in the corners. Therefore, the maximum PMI value for each corner is chosen to act as dependent measure for the analysis.

The PMI ratings of the dropped-out participants and of the participants that completed the trial are compared in Figures 32 and 33. Here, the mean maximum PMI of the participants is displayed for all right and left corners. The group with the participants that completed the simulation trial, the non-sick group, show a constant maximum PMI rating over time. This was not the case for the group with the dropped-out participants, the sick group. From the Figure 33 it can be seen that the PMI rises after more corners are passed. However, it should be taken into account that the group size also decreases as shown by the red striped line and therefore calculating the mean over the remaining participants is disputable.

The comparison of the PMI between the different cases can be found in Figures 34 and 35. The two figures show the mean

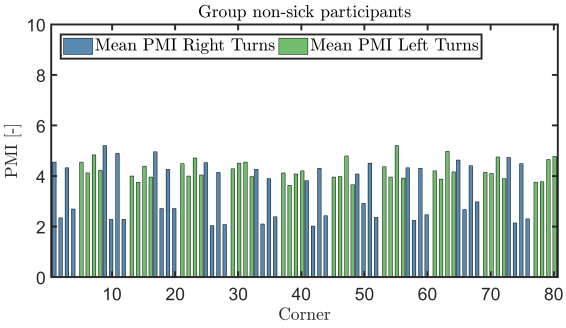

Fig. 32. Mean maximum PMI of participants that completed the full simulation trial per corner for left and right turns.

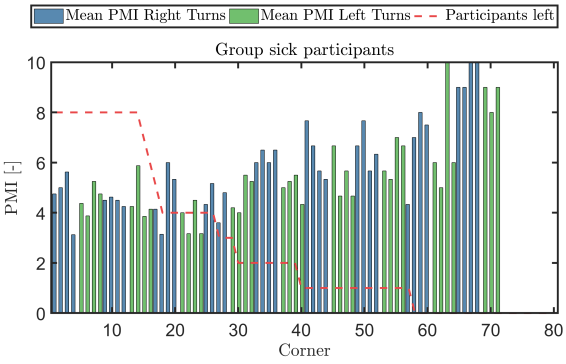

Fig. 33. Mean maximum PMI of participants that dropped out during the simulation trial per corner for left and right turns.

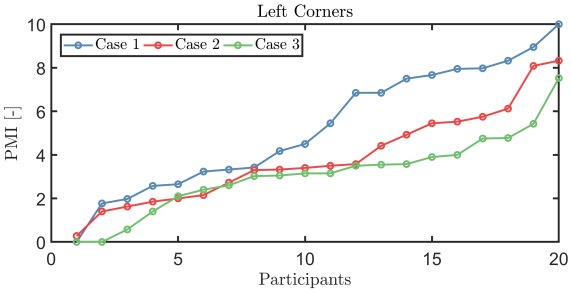

Fig. 34. Mean maximum PMI of participants for left corners in the three cases.

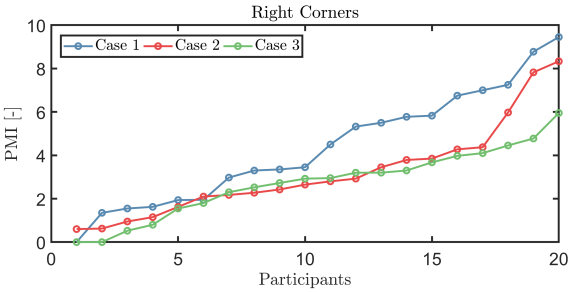

Fig. 35. Mean maximum PMI of participants for right corners in the three cases.

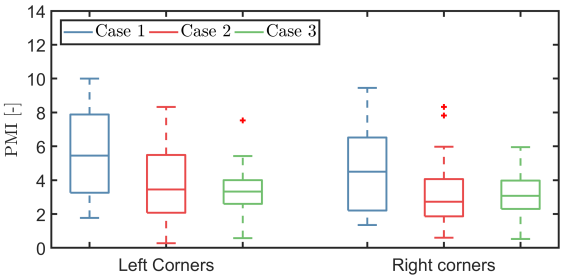

Fig. 36. Boxplot of mean maximum PMI of participants for left and right corners in the three cases.

maximum PMI over, respectively, the left and right corners for each participant. Case 1 shows generally the highest PMI for both left and right corners, which can be substantiated using Figure 36. This figure shows the distribution of the mean maximum PMI for the different participants. The median of the ratings in Case 1 is higher than for the other cases for both the left and right corners. This means that participants indicate a larger deviation between the expected movement from a real vehicle and the presented visual together with the movement as cued by simulator. Naturally, this was expected, because Case 1 does not involve any actual movement at all. Furthermore, Figures 32 to 35 show that the mean maximum PMI's are larger for the left turns than for the right turns.

The sample sizes of each group are slightly different ($N_{case1} = 19, N_{case2} = 20, N_{case3} = 18$) and therefore the post-hoc procedure, Gabiel's pairwise test, was chosen. In this case, the Welch F has been used to test the significance. This statistic was applied on the left corners and showed that there is a significant effect of motion on the PMI, $F(2, 35) = 4.22$, $p(0.02) < 0.05$. A significant difference was found with Gabriel's procedure between Case 1 and Case 2, $p(0.02) < 0.05$ and a nearly sifnificant difference was found between Case 1 and Case 3 as well, $p(0.06) > 0.05$. Levene's test was significant for the right turns as well ($p < 0.05$). The welch F reported a nearly significant effect of motion on the PMI for the right corners, $F(2, 34) = 2.86$, $p(0.071) > 0.05$.

When integrating this PMI or conflict it can be compared to the MISC, since both can be regarded as an integration of the sensory conflict as perceived by humans. Two scatter plots are shown in Figures 37 and 38, which indicate the relationship between the integrated PMI and the MISC, and between the SSI based on the PMI as conflict input (see Section II-F with $c =$ PMI,) and the MISC. A trend line is included as well, obtained from a fitting function in Matlab, to get a clearer visualization of the relationship. Both figures show a positive correlation, which means that when people become sicker, the indicated integrated PMI and MSI increase as well. One outlier can be found in both Figures 37 and 38. At the start of experiment, participants felt somewhat strange and therefore often indicated a larger MISC score, which explains the outlier. However, it was observed that within a few minutes this values often dropped back to zero. The Pearson correlation coefficient between the integrated PMI and MISC is 0.691 ($p < 0.05$). This means that there is a significant relationship between the aforementioned variables. This also holds for the MSI and and the MISC, with a correlation coefficient of 0.706 ($p < 0.05$).

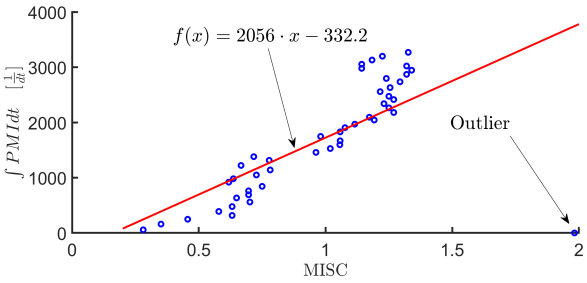

Fig. 37. Integrated PMI versus the MISC outcomes.

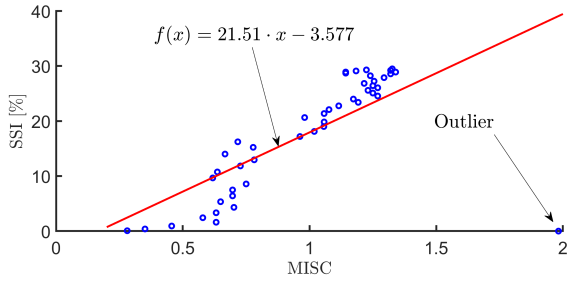

Fig. 38. SSI with c = PMI versus the MISC outcomes.

F. Head movement data

The gyroscope data are plotted against the vehicle model yaw rate and the simulator yaw rate for a single participant who was grouped in Case 3, see Figure 39.

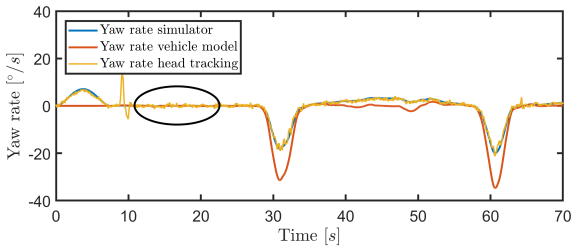

Fig. 39. Yaw rate of vehicle, simulator and head tracking output data for the first 70 seconds of the simulation trial.

A rate gyro bias needed to be removed. This has been removed by taking the average of the straight part (between $t \approx 12\ s$ and $t \approx 26\ s$) (see black ellipse) and subtract it from the head tracking yaw rate data. After this subtraction, looking forward without head movements now also means that the yaw rate of the Tobii data is zero. The next step was to get the data in just the corners and this has been done by applying the same procedure exclude the PMI data outside the left and right corners. First, the root-mean-square (RMS) of the head yaw data is calculated to quantify the amount of head motions made by the human participants in group with MISC scores larger than 3 (MISC $>$ 3) and in a group with MISC scores smaller or equal to 3 (MISC $\leq$ 3).

The box-plot in Figure 40 shows the distribution of the RMS scores for the participants of the two groups. These results show a similar distribution of the two data groups and, also that they have a similar median. Figure 41 shows the cumulative head yaw rate scores for the human participants in the group with MISC scores larger than 3 (MISC $>$ 3) and in a group with MISC scores smaller or equal to 3 (MISC $\leq$ 3). The cumulative head yaw rate score is determined by summing the positive yaw rate values when the participants drive through a left turn. Conversely, the absolute value of the negative yaw rates are summed when the participants drive through a right turn. This means that only yaw rates are summed when the participants look along with the geometry of the corner. For the all corners both the positive yaw rate values for the left turns and the absolute value of the negative yaw rate for the right turns are added altogether.

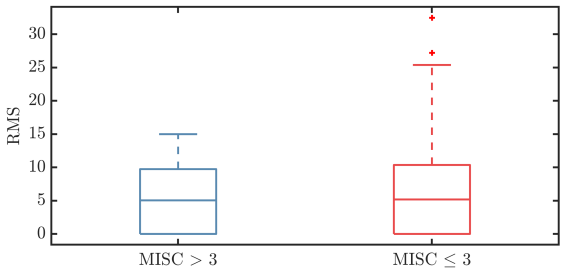

Fig. 40. Boxplot of the RMS between the head yaw data and vehicle yaw data for the participants in the three cases.

For the left turns, right turns and all turns, the results imply that the people in the MISC $\leq$ 3 group move their head more along with the direction of the corner than the people who have larger MISC scores. A Kruskal-Wallis test was employed to substantiate the boxplot results and a significant difference was found in head movements along the corner between two MISC score groups for the left corners, $H(1) = 7.32$, p (0.007) < 0.05, the right corners, $H(1) = 6.35$, p (0.012) < 0.05 and all corners $H(1) = 7.42$, p (0.006) < 0.05.

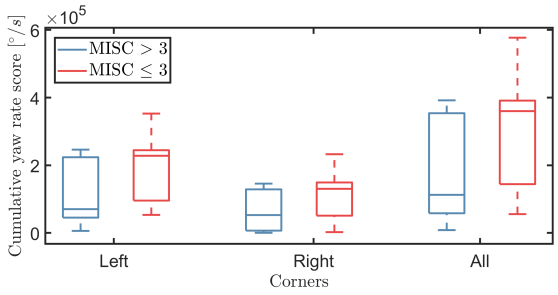

Fig. 41. Boxplot of the cumulative yaw rate scores between human participants in group with MISC scores larger than 3 (MISC $>$ 3) and in a group with MISC scores smaller or equal to 3 (MISC $\leq$ 3).

G. Experimental vs. Model Results

To compare the model results with the experimental results, there are two cases to compare: the motion and the no-motion cases. This means that Case 2 and Case 3 of Figure 26 are combined into a single motion case (N = 38). Case 1 is considered as the no-motion case (N = 20). Again, the SSI

based on the experiment was determined by taking the number of people that had a MISC score of 7 or two times a 6 in a row. The SSI that is predicted by the model has been calculated by taking the inputs of simulation trials of the experiment. Subsequently, the results of the experimentally-obtained SSI and the model-predicted SSI are compared in Figure 42. This graph shows that the experimental and model data are similar in terms of their absolute value. The scatter plots in Figures 43 and 44 give an indication of the the relationship between the experimental and model data as well.

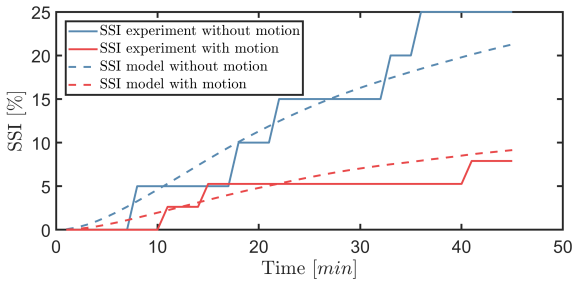

Fig. 42. SSI of the participants during the experiment and the SSI predicted by the SS prediction model for both the motion and no-motion case.

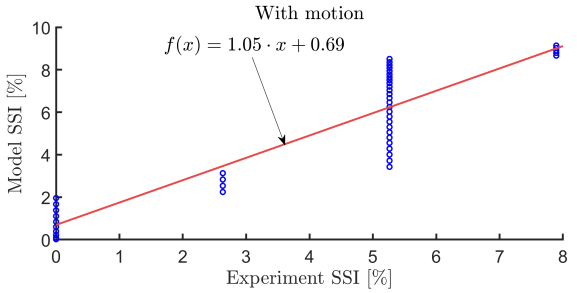

Fig. 43. Experimentally-obtained SSI vs. Model-predicted SSI for the case with motion.

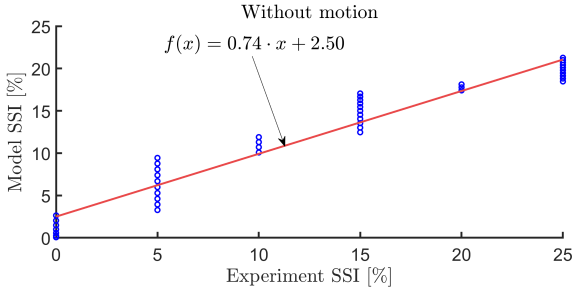

Fig. 44. Experimentally-obtained SSI vs. Model-predicted SSI for the no-motion case.

From these last two graphs, it can clearly been seen that there are large gaps between the data locations. This has to due with the experimental results as displayed in Figure 42 (thick lines). This figure shows this discontinuous behavior. When one participant becomes sick in the no-motion case (Case 1), then this is already around 5% of the group ($N_{c1} = 19$). Both scatter plots show a positive correlation, which means that when the experimental SSI rises, the model predicted SSI increases as well. Besides the scatter-plots, Kendall's tau has been determined. A significant positive relationship was found between the experimentally obtained SSI data and model predicted SSI data for the no-motion case, $\tau = 0.91$, $p < 0.05$. This holds for the case with motion as well, $\tau = 0.781$, $p < 0.05$.

V. Discussion

This research had two objectives. First, the objective was to better understand and predict SS when driving in urban environments, which involves strong vehicle yaw motions, by explaining a mathematical model that incorporates some well-known perceptual mechanisms and that is able to predict SS. Second, the goal was to investigate the effect of adding scaled, but otherwise veridical yaw motion to a simulator on SS. This was tested by means of an experiment, where participants were seated in a simulator and driven around in an urban environment. There were three cases with either no motion, yaw motion only, or roll, pitch and yaw motion. Participants filled out the SSQ before and after the experiment. During the experiment, a MISC score was indicated by the participant every minute and the PMI was measured continuously together with head yaw rate data.

A. Experiment and Hypotheses

For the first hypothesis (**H1**) it was expected that adding motion to a simulator while driving in an urban environment would results in a decreasing frequency of sick people. When comparing the no-motion case (Case 1) with the motion case (Case 2 and 3) it can be concluded that adding motion to a static driving simulator while driving in an urban environment results in less people becoming sick. This means that the first hypothesis (**H1**) is retained. This statement can also be substantiated by the results of the MISC scores. It has been shown that more human participants reached a MISC score of 6 or 7 for Case 1, which was defined as "sick" in this research, than the other two cases. However, the statistical analysis could not substantiate these results. An assumption of the Pearson Chi-Square test, which was executed on the MISC data, is that the expected frequency or values should be larger than 5 [56]. Here, these values were found to be below 5 and therefore, there is a loss of statistical power. Collecting more data to boost the proportion of cases falling into each category is a way to resolve this problem [56].

On the other hand, the SSQ results do not substantiate **H1**, since there was no difference in SSQ scores be found between the participants of the three cases. The disadvantage of the SSQ is that participants fill it in before and after the stimuli, i.e., when sickness symptoms have already been partly attenuated. Despite the request to fill in the questionnaire according to the sensations at the end of simulation, it is possible that the subjective judgments of these sensations are inaccurate. The MISC scores are less sensitive to these subjective judgments, since the participants are constantly monitored and can be corrected if symptoms arise. In the end, when a participant feels sick, he or she wants to quit the simulation, which is a clear indication of sickness. Therefore, the number of drop-outs and the MISC scores are assumed to be more reliable compared to the SSQ scores.

When considering the PMI results, several remarks can be made. First, for the sick participants it was seen that the PMI increased over time for the different corners and remained constant for the non-sick participant group. This already suggests that there may be a relationship between the PMI and MISC scores. Secondly, the highest PMI scores were given in Case 1, which was expected, because there was no motion presented, meaning a large conflict between the expected motion and sensed motion. These results could only partly be substantiated by the statistical results, because only a significant difference was found between the PMI of Case 1 and Case 3 for the left corners. A limitation for the statistical analysis was again the sample size per case ($N < 21$), the unequal sample sizes per case, and the violation of the assumption of equal variances.

Still, when looking at the data, it could be seen that the PMI is generally highest for Case 1. The same holds for the MISC scores and this indicates again the relationship between the MISC and PMI. For the second hypothesis (**H2**) it was expected that a positive correlation would exist between the PMI and sickness scores over time. A positive correlation between the PMI and sickness scores over time has been confirmed, meaning that **H2** is retained as well. Thereby, it could be suggested that the PMI could be a way to quantify the visual-vestibular sensory rearrangement by a human participant as explained in Section II-B. When using the PMI as quantifiable conflict, it can be used to enhance the verification and validation of the SS prediction model.

Assuming that the PMI is positively related to SS, an explanation between the found difference in mean maximum PMI between the right and left corners could be based on their dynamic characteristics. A corner to the left requires more time together with a larger radius and higher lateral or tangential acceleration, resulting in a more low-frequency motion characteristic. MS is associated with low-frequency motions around 0.2 Hz [6], [9], [10], [16]. Therefore, the PMI may be indicated larger for left turns.

Subsequently, for the third hypothesis (**H3**) it was expected that head yaw movements affect SS. Participants that reported low MISC scores during the simulation trial (≤ 3) did move their heads relatively more along the angular direction of the corner. This suggests that head movements do have an effect on SS and **H3** can be retained. However, the head tracking measurements were not started simultaneously with the real-time simulation, resulting in a manual synchronization afterwards. This could have had some effect on the conclusions, but all the measurements were checked on their alignment with the simulator output and showed minor differences, as can be seen when zooming in on Figure 39 as done in Figure 45 (yellow line vs. blue line). Based on these results, a potential SS attenuation method could be to taught humans to move their head along the corner direction. This has as results that participants are more actively involved, are able to observe the road geometry more easily, and thereby anticipate their motion in the near future, in order to attenuate SS.

For the last hypothesis, (**H4**), it was expected that a positive correlation could be found between the SSI as predicted by the SS prediction model and the experimentally obtained SSI.

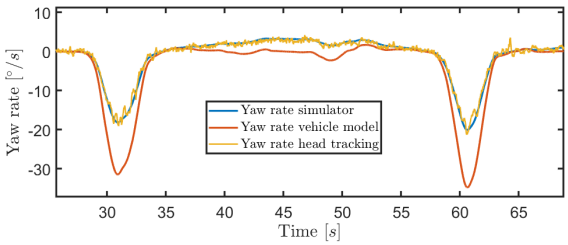

Fig. 45. Yaw rate of vehicle, simulator and head tracking output (zoomed in).

The prediction model output was found to be highly correlated with the experimental outputs. However, it should be taken into account that the motion cases from the model and experiment differ. The model predictions are based on the full vehicle motion outputs. On the contrary, the experimental results are based on a roll, pitch and yaw motion case, a purely yaw motion case and a no motion case. The SS prediction model is not yet capable of providing reliable predictions for reduced motion cases at this stage. However, **H4** is still retained while taking the mentioned assumption into account.

Furthermore, acceleration transformations from the vehicle CoG reference frame to the head reference frame were neglected in this study. The course material of Th. Holierhoek and Melkert [57] is used to investigate the effect of the transformation of the accelerations to the head reference frame. Still, a rigid body is assumed and the distance vector between the CoG and the head is estimated to be $[0.10.51.0]$. The mean percentage error between the SS prediction model outputs without transformations and the SS prediction model outputs with transformation has found to be 0.27% (maximum error was 1.00%) and 1.14% (maximum error was 5.20%) for the no-motion case and motion case respectively.

Finally, only two sets of weighting parameters are currently provided, one for the light condition and one for the dark condition [39], see Table I. However, there is currently not a parameter set available for the reduced motion condition. A way to resolve this, is by adapting the weighting parameters from Figure 3 (blue blocks) such that the conflict causing SS becomes larger when a scaled or reduced motion is presented, while keeping the conflict level below the level of having no motion at all.

B. SS prediction model

The SS prediction model lacks the description of the adaptation to a rearranged sensory environment. Like other models, it remains a challenge to include habitation and restitution to the stimuli causing MS and SS [16]. More research should be done on the implementation of expectations or familiar stimulus patterns since motion history is likely to play a role [58]. Furthermore, visual information is of vital importance for this model and Bos, Bles and Groen [52] presented a framework to understand, explain and predict visually induced motion sickness, which is closely related to SS. This framework focuses more on the perception of verticality by not just relying on the vestibular cues, but also on the frame and polarity information.

The way of integrating these cues enables the model to account for effects such as foreground/background motion, field of view, image velocity, head movements and frame rates and delays [52]. Research should be done on implementing this framework mathematically and use it to extend the current SS prediction model

After the MS experimental data verification, the perception part of the model was assessed by comparing the model output data to some motion and sensory paradigms to see if the data matches the earlier performed research in this area [35], [59], [60]. The model output shows similar behavior to the data considering the different kinds of motion and sensory paradigms. However, the availability of experimental subjective perceptual data is limited [59]. Future efforts should focus on validating the proposed SS prediction model. The model should be tested against more complex or different motion or sensory paradigms such as the visual-pseudo-coriolis illusion [59].

Despite it's limitations, the current SS prediction model combines several advances from previously implemented models of SS and meets the requirements as stated in Section II-A on which is elaborated below. First, it implements mechanisms that model the production of sickness symptoms and predict the SSI (**Req1**). Secondly, the advantage of the SS prediction model is the implementation of a visual-vestibular interaction model (**Req2**) while taking into account vection delays, which is omitted in Newman's model [59]. The visual part of the model is of vital importance since SS caused by visual stimuli is of main interest during simulator studies and so to this research. Furthermore, [58] suggested that the overall motion perception is not a simple addition of the perceived translational and rotational components. For this model, a linear weighted addition has been implemented to integrate the visual and vestibular estimations as also implemented in the visual-vestibular interaction model by Bos and Bles [39].

The developed model has been verified for some experimental data on MS and visual sensory and visual-vestibular motion paradigms (**Req3**), see Appendix A. Initially, the part that involves the accuracy of predicting SS has been verified. The results of this verification step show that the model's simulation output more accurately fits the experimental data by McCauley [9] than other available models, for example, these of Kamiji [11] and Bos and Bles [10]. However, the amount of data to verify the model for its effectiveness of correctly predicting sickness and the production of symptoms remains limited. So, more SS data are required to verify the SS predictions made by the SS prediction model and test its validity.

Furthermore, the SVC theory as proposed by Bos and Bles [37] has been mathematically implemented ensuring that the conflict is a measurable variable increasing the models prediction power, while being able to make predictions for multi-dimensional cases (**Req4**). Despite the characteristic of being a suitable theory to get a better understanding of MS and SS, the SVC theory does not explain why humans become sick when experiencing pure yaw rotations around an earth-vertical axis [14]. An extension of the model should be a mechanism that complements this failing part of the SVC-theory. This mechanism should enable the model to predict SSI or MSI when a participant is subjected to pure earth-vertical yaw rotations.

VI. Conclusion

The aim of this research was to better understand simulator sickness (SS) by developing a mathematical model that can predict SS while driving in urban environments and to understand the effects of adding motion to a simulator on SS. For the SS prediction model, the 6 degree of freedom (DOF) subjective vertical conflict (SVC) model was combined with the visual-vestibular interaction model by Bos and Bles. This model is capable of predicting SS for multiple-DOF motions while incorporating visual stimuli as well. The human spatial orientation part of this model has been verified for several motion and sensory paradigms that substantiate its capability to correctly estimate the angular and translational motions. The SS prediction model results agree with the experimental results, but the assumption of using different motions as input for the experiment and model should be taken into account. It can be concluded that this is an appropriate first iteration towards a SS prediction model and helps in better understanding the mechanisms behind SS.

For the experiment, a correlation between the development of sickness and the perceived motion incongruence (PMI) was found. Therefore, the PMI can be used to quantitatively substantiate the hypothesis regarding the sensory conflict (SC) theory and the it can be used to enhance the verification and validation of the SS prediction model. Furthermore, the head data results suggest that turning the head along with the corner direction can be a strategy to become less sick. Finally, it was investigated if human participants became less sick when a form of yaw-motion was provided to a simulator. As expected, it can be concluded that less participants dropped out of the experiment when providing these kinds of motion. This means that the number of participants that drop out during a simulator experiment can already be reduced by using, for example, a simple yaw platform. This will save time and money for the automotive industry.

References

[1] Hock, P., Kraus, J., Babel, F., Walch, M., Rukzio, E., and Baumann, M. How to Design Valid Simulator Studies for Investigating User Experience in Automated Driving. In *Proceedings of the 10th International Conference on Automotive User Interfaces and Interactive Vehicular Applications - AutomotiveUI '18*, pages 105–117, 2018.

[2] Brooks, J. O., Goodenough, R. R., Crisler, M. C., Klein, N. D., Alley, R. L., Koon, B. L., Logan, W. C., Ogle, J. H., Tyrrell, R. A., and Wills, R. F. Simulator sickness during driving simulation studies. *Accident Analysis & Prevention*, 42(3):788–796, 2010.

[3] Kay, P. Feasibility of Virtual Environments to Develop Future Driving Cycles. In *International Powertrains, Fuels & Lubricants Meeting*, sep 2018.

[4] De Winter, J., Happee, R., and Leeuwen, van P. Advantages and disadvantages of driving simulators: a discussion. *Proceedings of Measuring Behavior*, (January):47–50, 2012.

[5] Birren, J. Motion sickness: its psychophysiological aspects. A survey report on human factors in undersea warfare. Technical report, Committee on Undersea Warfare, National Research Council, Washington, D.C., 1949.

[6] Dobie, T. G. Motion Sickness: A Motion Adaptation Syndrome, 2019.

[7] Reason, J. T. Motion sickness adaptation: a neural mismatch model. *Journal of the Royal Society of Medicine*, 71(11):819–29, 1978.

[8] Oman, C. M. A Heuristic Mathematical Model for the Dynamics of Sensory Conflict and Motion Sickness. *Acta Oto-Laryngologica*, 94(SUP 392):4–44, 1982.

[9] McCauley, M. E., Royal, J. W., Wylie, C. D., O'Hanlon, J. F., and Mackie, R. R. Motion sickness incidence: exploratory studies of habituation, pitch and roll, and the refinement of a mathematical model. Technical report, 1976.

[10] Bos, J. E. and Bles, W. Modelling motion sickness and subjective vertical mismatch detailed for vertical motions. *Brain Research Bulletin*, 47(5):537–542, 1998.

[11] Kamiji, N., Kurata, Y., Wada, T., and Doi, S. Modeling and validation of carsickness mechanism. In *SICE Annual Conference 2007*, pages 1138–1143, 2007.

[12] Groen, E. L. and Bos, J. E. Simulator Sickness Depends on Frequency of the Simulator Motion Mismatch: An Observation. *Presence: Teleoperators and Virtual Environments*, 17(6):584–593, oct 2008.

[13] Wada, T., Fujisawa, S., Imaizumi, K., Kamiji, N., and Doi, S. Effect of Driver's Head Tilt Strategy on Motion Sickness Incidence. *IFAC Proceedings Volumes*, 43(13):192–197, 2010.

[14] Nooij, S. A., Pretto, P., Oberfeld, D., Hecht, H., and Bülthoff, H. H. Vection is the main contributor to motion sickness induced by visual yaw rotation: Implications for conflict and eye movement theories. *PLoS ONE*, 12(4):1–19, 2017.

[15] Keshavarz, B., Philipp-Muller, A. E., Hemmerich, W., Riecke, B. E., and Campos, J. L. The effect of visual motion stimulus characteristics on vection and visually induced motion sickness. *Displays*, 2018.

[16] Lewkowicz, R. Modeling Motion Sickness. *The Polish Journal of Aviation Medicine, Bioengineering and Psychology*, 22(3):32–42, 2017.

[17] Johnson, D. M. *Introduction to and review of simulator sickness research*. Number Approved for public release; distribution is unlimited. Rotary-Wing Aviation Research Unit, U.S. Army Research Institute for the Behavioral and Social Sciences, Fort Rucker, AL, 2005.

[18] Benson, A. J. Motion sickness. *G. Dhenin & J. Ernsting (Eds.), Aviation Medicine*, pages 468–493, 1978.

[19] Reason, J. T. and Brand, J. J. *Motion sickness.* Academic Press, London, 1975.

[20] Clark, T. K., Newman, M. C., Karmali, F., Oman, C. M., and Merfeld, D. M. Mathematical models for dynamic, multisensory spatial orientation perception. *Progress in Brain Research*, pages 65–90, 2019.

[21] Wada, T., Fujisawa, S., and Doi, S. Analysis of driver's head tilt using a mathematical model of motion sickness. *International Journal of Industrial Ergonomics*, 63:89–97, 2018.

[22] Sharkey, T. and Mccauley, M. E. Does a motion base prevent simulator sickness? *Flight Simulation Technologies Conference*, 1992.

[23] Klüver, M., Herrigel, C., Preuß, S., Schöner, H.-P., and Hecht, H. Comparing the Incidence of Simulator Sickness in Five Different Driving Simulators. *Driving Simulation Conference 2015*, pages 16–18, 2015.

[24] Blana, E. Driving simulator validation studies: A literature review. Technical report, Institute of Transport Studies, University of Leeds, Leeds, 1996.

[25] Stoner, H., Fisher, D., and Mollenhauer, M. Simulator and Scenario Factors Influencing Simulator Sickness. *Handbook of Driving Simulation for Engineering, Medicine, and Psychology*, 2011.

[26] Mourant, R. R., Rengarajan, P., Cox, D., Lin, Y., and Jaeger, B. K. The Effect of Driving Environments on Simulator Sickness. *Proceedings of the Human Factors and Ergonomics Society Annual Meeting*, 51(18):1232–1236, 2007.

[27] Bos, J. E., MacKinnon, S. N., and Patterson, A. Motion sickness symptoms in a ship motion simulator: effects of inside, outside, and no view. *Aviation, space, and environmental medicine*, 76(12):1111–8, 2005.

[28] Kennedy, R. S., Lane, N. E., Berbaum, K. S., and Lilienthal, M. G. Simulator Sickness Questionnaire: An Enhanced Method for Quantifying Simulator Sickness. *The International Journal of Aviation Psychology*, 3(3):203–220, 1993.

[29] Stoffregen, T. and Riccio, G. *An Ecological Critique of the Sensory Conflict Theory of Motion Sickness*, volume 3. sep 1991.

[30] Cleij, D., Venrooij, J., Pretto, P., Pool, D. M., Mulder, M., and Bülthoff, H. H. Continuous subjective rating of perceived motion incongruence during driving simulation. *IEEE Transactions on Human-Machine Systems*, 48(1):17–29, 2018.

[31] Rolnick, A. and Lubow, R. *Why is the driver rarely motion sickthe Role of controllability in motion sickness*, volume 34. aug 1991.

[32] Kuiper, O. X., Bos, J. E., Schmidt, E. A., Diels, C., and Wolter, S. Knowing What's Coming: Unpredictable Motion Causes More Motion Sickness. *Human Factors: The Journal of the Human Factors and Ergonomics Society*, page 001872081987613, 2019.

[33] Second Picture, S. 3D Modeling a Human Head, 2007. [Online; accessed June 27, 2019].

[34] Keshavarz, B., Hecht, H., and Lawson, B. Visually induced motion sickness: Characteristics, causes, and countermeasures. In *Handbook of Virtual Environments: Design, Implementation, and Applications*, pages 648–697. sep 2014.

[35] Merfeld, D. M., Young, L. R., Oman, C. M., and Shelhamer, M. J. A multidimensional model of the effect of gravity on the spatial orientation of the monkey. *Journal of Vestibular Research*, 3(2):141–161, 1993.

[36] Bos, J. E., Bles, W., and Hosman, R. J. A. W. Modeling human spatial orientation and motion perception. In *AIAA Modeling and Simulation Technologies Conference and Exhibit*, 2001.

[37] Bles, W., Bos, J. E., De Graaf, B., Groen, E., and Wertheim, A. H. Motion sickness: Only one provocative conflict? *Brain Research Bulletin*, 47(5):481–487, 1998.

[38] Glasauer, S. *Interaction of Semicircular Canals and Otoliths in the Processing Structure of the Subjective Zenith*, volume 656. 1992.

[39] Bos, J. E., Hosman, R. J. A. W., and Bles, W. Visual-vestibular interactions and spatial (dis)orientation in flight and flight simulation. Technical report, TNO, 2002.

[40] Merfeld, D. M. and Zupan, L. H. Neural Processing of Gravitoinertial Cues in Humans. III. Modeling Tilt and Translation Responses. *Journal of Neurophysiology*, 87(2):819–833, 2002.

[41] Haslwanter, T., Jaeger, R., Mayr, S., and Fetter, M. Three-dimensional eye-movement responses to off-vertical axis rotations in humans. *Experimental Brain Research*, 134(1):96–106, 2000.

[42] Correia Grácio, B. J. *The Effects of Specific Force on Self-Motion Perception in a Simulation Environment*. PhD thesis, Technical University of Delft, 2013.

[43] Gibson, J. J. *The perception of the visual world.* Houghton Mifflin, Oxford, England, 1950.

[44] Steen, van der F. and Kamphuis, H. H. The environment provides the reference frame for self-motion perception. In *Conference on human decision making and manual control*, page 65, Delft, 1995. Delft University of Technology.

[45] Mittelstaedt, H. A new solution to the problem of the subjective vertical. *Naturwissenschaften*, 70(6):272–281, 1983.

[46] Bos, J. E. and Bles, W. Theoretical considerations on canal-otolith interaction and an observer model. *Biological Cybernetics*, 86(3):191–207, 2002.

[47] Glasauer, S. and M. Merfeld, D. *Modelling Three Dimensional Vestibular Responses During Complex Motion Stimulation*. 1997.

[48] Howard, I. P. Interactions Within and Between the Spatial Senses. *Journal of Vestibular Research*, 7(4):311–345, 1997.

[49] Groen, E. L., Jenkin, H. L., and Howard, I. P. Perception of self-tilt in a true and illusory vertical plane. *Perception*, 31(12):1477–1490, 2002.

[50] Kalman, R. E. and Bucy, R. S. New Results in Linear Filtering and Prediction Theory. *Journal of Basic Engineering*, 83(1):95–108, 1961.

[51] Wonham, W. On the Separation Theorem of Stochastic Control. *SIAM J. Control*, 6, 1971.

[52] Bos, J. E., Bles, W., and Groen, E. L. A theory on visually induced motion sickness. *Displays*, 29(2):47–57, 2008.

[53] Park, G. D., Allen, R. W., Fiorentino, D., Rosenthal, T. J., and Cook, M. L. Simulator Sickness Scores According to Symptom Susceptibility, Age, and Gender for an Older Driver Assessment Study. *Proceedings of the Human Factors and Ergonomics Society Annual Meeting*, 50(26):2702–2706, 2006.

[54] Griffin, M. and Howard, H. Motion Sickness History Questionnaire. *ISVR Technical Report*, (No. 283), 2000.

[55] Keshavarz, B. and Hecht, H. Validating an efficient method to quantify motion sickness. *Human Factors*, 53(4):415–426, 2011.

[56] Field, A. P. *Discovering statistics using SPSS: (and sex and drugs and rock 'n' roll)*. SAGE Publications, Los Angeles [i.e. Thousand Oaks, Calif.], 2009.

[57] Holierhoek, J. G. and Melkert, J. A. Advanced Dynamics. Technical Report September, TU Delft, Delft, 2008.

[58] Nooij, S. A., Nesti, A., Bülthoff, H. H., and Pretto, P. Perception of rotation, path, and heading in circular trajectories. *Experimental Brain Research*, 234(8):2323–2337, 2016.

[59] Newman, M. C., Oman, C. M., and Darmofal, D. L. *A multisensory observer model for human spatial orientation perception*. PhD thesis, Massachusetts Institute of Technology, 2009.

[60] BORAH, J., YOUNG, L. R., and CURRY, R. E. Optimal Estimator Model for Human Spatial Orientationa. *Annals of the New York Academy of Sciences*, 545(1):51–73, dec 1988.

APPENDIX A
MODEL VERIFICATION

First, the parameters tuning method being employed is explained, which enables the model output to predict McCauleys experimental data to some extend. Secondly, the capability results of predicting the right outputs for some motion and sensory paradigms are given.

Sickness part

First, to see if the model is capable of generating the right MSI data it can be compared to experimentally obtained MS data from McCauley [9]. McCauley subjected participants to vertical sinusoidal motions in a ship-motion simulator and the results of the experiment can be found in Figure 46 together with their fitted data. When comparing the experimentally obtained data and their own data fit, then the root mean square error (RMSE) is 6.1%. However, the SS prediction model shows a large deviation (RMSE = 32.97%) between model data and McCauley's data while using the parameters according to Kamiji and Wada [11] [13].

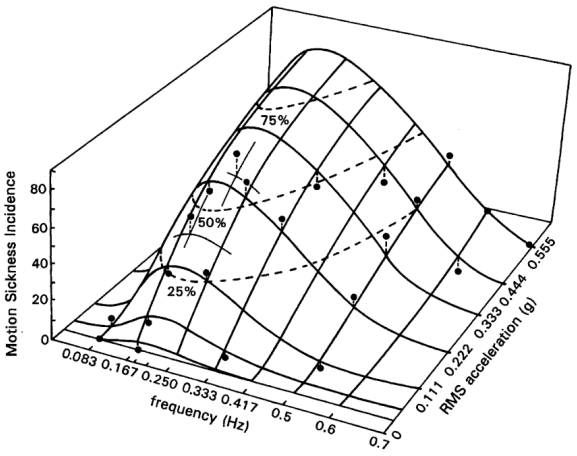

Fig. 46. Experimentally obtained results of MSI's for different accelerations and frequencies. Reprinted from [9]

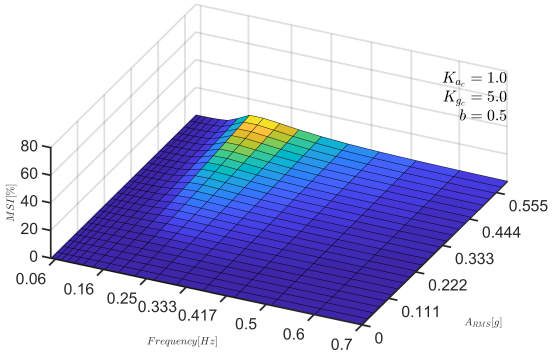

Fig. 47. MSI results from SS prediction model before parameter tuning.

But, McCauley's model lacks a vestibular basis and predicts only the MSI for vertical sinusoidal motions [10]. A sensitivity analysis was done to see which parameters had a positive effect on attenuating this error. For this linear motion case, so vertical accelerations in the z-axis, the parameters K_{a_c}, K_{v_c} and b were tuned such that the RMSE was as low as possible. These gains are chosen because K_{a_c} and b influence the peak of the graph and K_{v_c} influences the position of the center frequency or the frequency where the peak of the graph is located. Furthermore, only linear translations are considered here meaning that K_{w_c} has no influence on the outcome because rotational motions are not considered. To get this lowest RMSE, an optimization algorithm in Matlab was employed. This optimization function is called the "fminsearch" function and is a multidimensional unconstrained nonlinear minimization that makes use of the Nelder-Mead method. The cost function used within this algorithm is the SS prediction Matlab Simulink model in which the changing parameters were K_{ac}, K_{vc} and b. After performing the optimization algorithm on the parameters K_{ac}, K_{vc} and b, an RMSE of 14.44% has been achieved when comparing the results to the original data of McCauley. The RMSE deviation between the experimentally obtained data and McCauley's model data is still better than the RMSE deviation of the SS prediction model. The 1-DOF SVC model of Bos and Bles [10] has an RMSE deviation of 22.25%. Furthermore, the 6-DOF SVC model of Kamiji and Wada [11] gave an RMSE deviation of 21.42%, which is already better. In the end, the developed and tuned SS prediction model presents the best results.

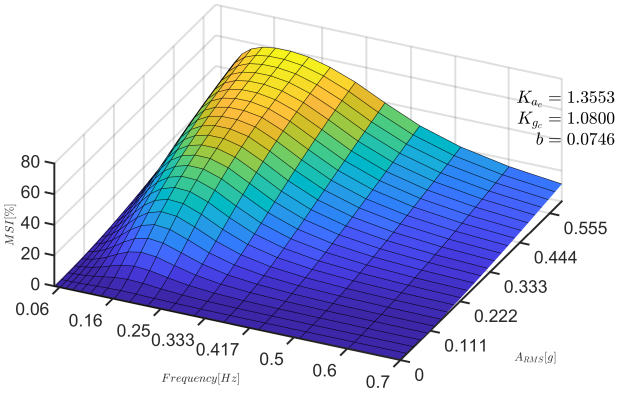

Fig. 48. MSI results from SS prediction model after parameter tuning.

The change of MSI over time for one specific frequency of 0.25 Hz and three different acceleration according to McCauley's data is displayed in fig. 49. On the right of this figure, the results for the SS prediction model can be found with the belonging parameter settings. They are now quite similar, so the prediction of the model is more accurate already.

Verification motion and sensory paradigms

Other model results regarding the motion and sensory paradigms can be found in the figures below.

Constant Velocity Rotation about an Earth Vertical Axis fig. 51 shows the results of Newman's model predictions for

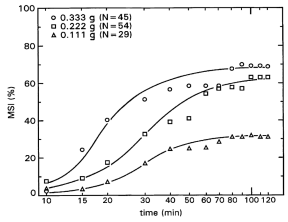

Fig. 49. Experimentally obtained results of MSI's overtime for one specific frequency (0.25 Hz) and three different acceleration conditions. Reprinted from [9]

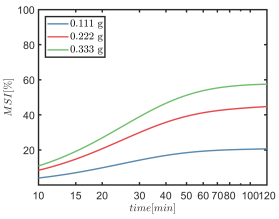

Fig. 50. SS model predictions MSI over time for 0.25 Hz and three different acceleration conditions.

a constant velocity rotation around an earth vertical axis as reported in [59] together with model predictions of the SS prediction model. A participant is sitting upright in a rotation chair while being rotated in light and dark conditions with an angular velocity of 0.26 rad/s for 30 seconds. A second case is where the visual surroundings are rotated in light conditions with the same angular velocity around participant (circular vection). The third case considers dark conditions and the results are similar to the results from Merfeld [35], because now the visual information is not available. When comparing these results to the results of the proposed SS prediction model, then it can be seen that the behavior is almost the same, but the values deviate. However, it still shows proper behavior in different conditions. For example, a sustained sensation of rotational motion that decays towards a value that is near the actual input stimuli ($\omega_{z_{input}}$). It also properly predicts circular vection when just the visual field rotates around the participant in the absence of motion.

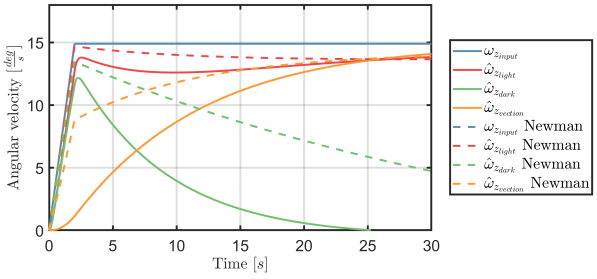

Fig. 51. SS model predictions for constant velocity rotation about an Earth vertical axis compared to the model outputs of Newman for the same motion paradigm.

The difference with Newman's results can be found when considering the fast-rising component followed by a slow rising component because it is harder to distinguish between these components for the SS prediction model results. However, the model takes into account the delay of the circular vection, which is typical for human participants [59] and this part lacks in the model of Newman. This motion paradigm is of particular importance since this research will focus mainly on strong yaw motions during a corner in urban environments.

Somatogravic Illusion

The Somatogravic Illusion can be described as the development of a pitch up movement sensation when being forward accelerated at a constant rate on a sled. Again, the results of both Newman's model and the SS prediction model for this visual-vestibular sensory paradigm can be found in fig. 52 and fig. 53. The observer model of Newman displays similar results as the actual visual-vestibular interaction mechanism responsible [59]. On the other hand, the results from the SS prediction model are displaying a deviation. At the start of the simulation, the rise time of the linear acceleration and pitch angle is slower than Newman's model. Furthermore, the rise time of the light condition is slower than the dark condition, which means there is a difference that is not visible in Newman's model. However, the behavior at the end is again quite similar. In light conditions, there will be a constant sensation of acceleration due to the addition of the visual and vestibular input suppressing the somatogravic illusion.

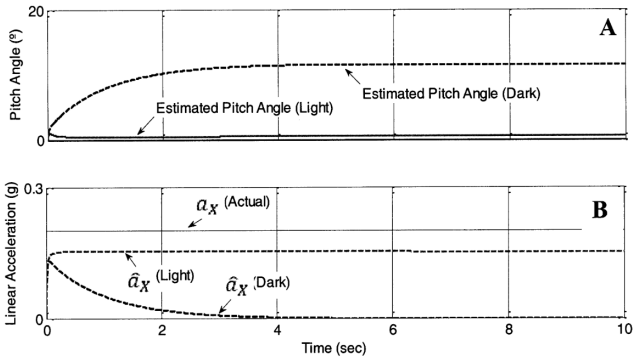

Fig. 52. Newman's model predictions for a forward linear acceleration on a sled (Somatogravic Illusion). Reprinted from [59].

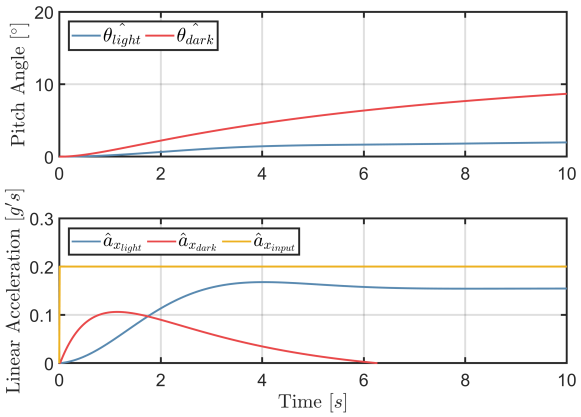

Fig. 53. SS model predictions for a forward linear acceleration on a sled (Somatogravic Illusion).

Forward Linear Vection

For this visual sensory paradigm, a human participant is seated upright and subjected to a 15 cm/s step visual linear velocity input. The CNS gradually accepts the visual input resulting in vection, an illusory sensation of linear motion [59]. fig. 54 and fig. 55 present the results of a forward linear vection stimulus from Newman's model and the SS sickness model. Newman's

model fails to predict the vection onset delay as seen with the constant velocity rotation around an earth vertical axis in contrary to the SS prediction model. There is also a slight overshoot visible from the SS prediction model results that differ from Newman's model predictions.

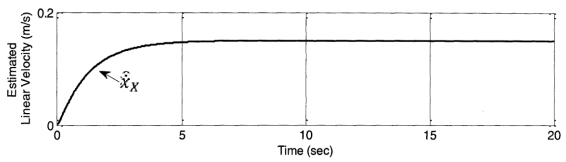

Fig. 54. Newman's model predictions of a forward linear vection stimulus. Reprinted from [59].

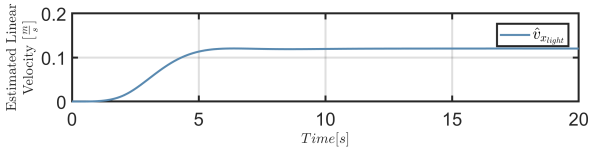

Fig. 55. SS model predictions of a forward linear vection stimulus.

Post-Rotary Tilt

The post-rotary tilt is simulated with an initial constant yaw rotation of 100 deg/s about an earth-vertical axis. After 50 seconds, the SCC responses should have decayed to zero and the simulated subject is decelerated to 0 deg/s in one second. After stopping, an immediate angular roll velocity is applied with 45 deg/s for 2 seconds such that the participant is rolled 45 degrees to the right. This can be seen in the upper figure of fig. 56. Here the results of the SS prediction model show quite some deviations. First, for the expected angular velocity a y-component is missing after the roll rotation.

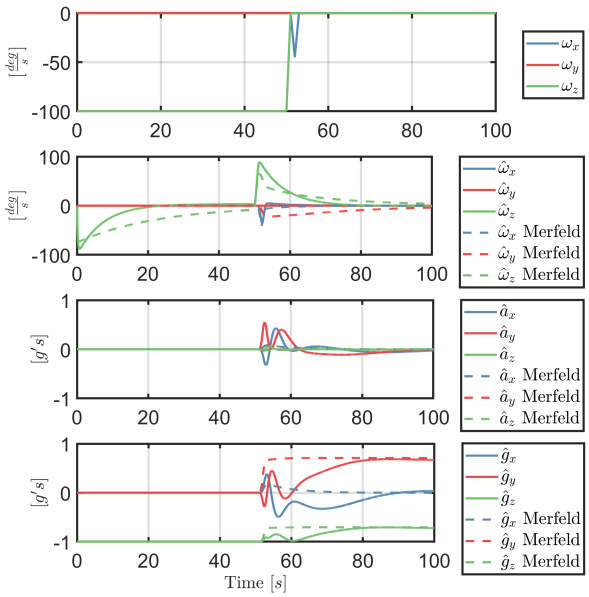

Fig. 56. Results SS prediction model for the Postrotatory tilt motion paradigm in Matlab Simulink versus the results from Merfeld's velocity storage model for the same motion paradigm.

This component is induced due to the strong post rotary tilt sensation that causes the SCC afferent signal $\vec{\omega}$ to be not aligned with gravity anymore. Furthermore, the expected acceleration and gravity deviate as well around to the roll-rotation point. A strong oscillation is visible that should not be there when comparing these results to Merfeld's model outputs. However, the end values correspond again.

Ferris wheel illusion

The next example considers the Ferris wheel illusion, which nicely illustrates the deficient functioning of our SCC under unnatural conditions, see fig. 57. When a participant starts to rotate around an earth-horizontal axis (x_{earth}), he or she will first sense the true or veridical motion. But after some time, when a constant angular velocity is reached, the SCC afferent signals will go back to their resting values (normally $\hat{\omega} = 0$) as can be seen in the middle graph of fig. 58. Now the orientation of the subject is lost and the motion will be interpreted as a circular motion with a fixed orientation [46], which is presented in the right part of fig. 57 and the bottom graph of fig. 58.

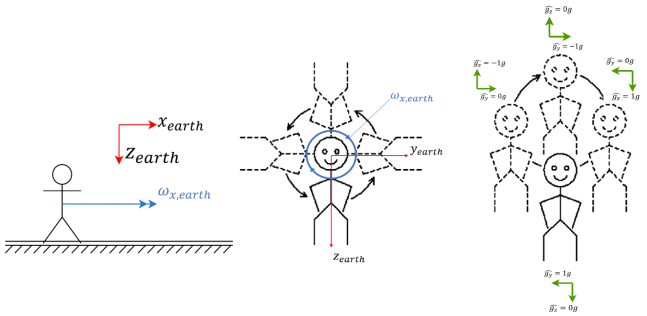

Fig. 57. Ferris wheel illusion. A subject rotating with a constant angular velocity about an earth-horizontal axis (left) perceives a motion like a gondola of a Ferris wheel after his canal signals have returned to their rest value (right), Reprinted from [46].

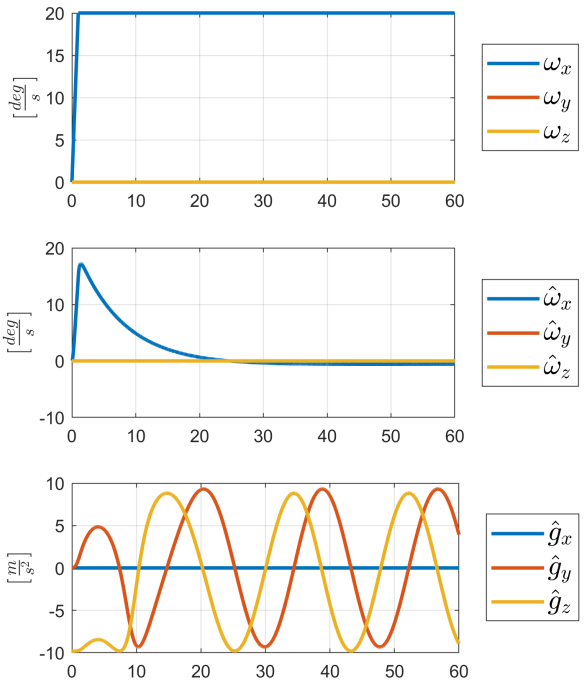

Fig. 58. Top graph: the constant angular velocity input around an earth horizontal axis (ω_x). Middle graph: the effect on the perceived or expected angular velocities, $\hat{\omega}$, by the human. Bottom graph: the effect on the perceived or expected gravity, $\hat{g}$, by the human

APPENDIX B
NOMENCLATURE

Abbreviations

CoF	Center of Gravity
DOF	Degrees of Freedom
DS	Disorientation score
FOV	Field of View
GIF	Gravito Inertial Force
MISC	Misery Scale
MS	Motion Sickness
MSHQ	Motion Sickness History Questionnaire
MSI	Motion Sickness Incidence
NS	Nausea score
OS	Occulumotor score
PMI	Perceived Motion Incongruence
SC	Sensory conflict
SS	Simulator Sickness
SSI	Simulator Sickness Incidence
SSQ	Simulator Sickness Questionnaire
SVC	Subjective Vertical Conflict
TS	Total score

Latin Symbols

Symbol	Description	Unit
$\vec{a}$	Linear motion acceleration	$\frac{m}{s^2}$
b	Fitting parameter Hill function	-
$\vec{c}$	Conflict vector of expected and measured afferent signal	-
$\vec{f}$	Specific force or GIF	g's
$\vec{g}$	Linear gravitational acceleration	g's
$\vec{g}_e$	Linear gravitational acceleration with respect to earth	g's
$\vec{g}_h$	Linear gravitational acceleration with respect to the head	g's
g_{sens}	Sensed vertical	g's
$\vec{g}_{tot}$	Resulting vertical	g's
$\vec{g}_{vis}$	Visual linear gravitational acceleration	g's
K_{ac}	Acceleration conflict gain	-
$K_{\omega c}$	Angular velocity conflict gain	-
K_{gc}	Gravitational conflict gain	-
n_h	Parameter that accounts for the steepness of the hill function	-
P	Maximum amount of participants that get sick under the given circumstances	%
$\vec{v}$	Velocity	$\frac{m}{s}$
$\vec{v}_{vis}$	Velocity as perceived by visual sysem	$\frac{\frac{s}{m}}{s}$
w	Weight factor in linear weighting addition	-
w_a	Vestibular velocity weighting vector	-
w_f	Visual vertical weighting vector	-
w_g	Visual vertical weighting vector	-
w_i	Idiotropic vertical weighting vector	-
w_v	Visual velocity weighting vector	-
$\hat{\vec{y}}$	Expected afferent signal from internal observer	-
$\vec{y}$	Measured afferent signal from human sense organs	-

Greek Symbols

Symbol	Description	Unit
μ	Time constant leaky integrator	s
τ	Time delay	s
τ_a	Adaptation time constant	s
τ_{av}	Time delay high-pass filter velocity perception vestibular system	s
τ_c	Time constant SCC	s
τ_d	Dominant time constant	s
τ_g	Time constant low-pass filter gravity perception visual system	s
τ_v	Time constant low-pass filter linear velocity perception visual system	s

ω	Angular velocity	rad/s
ω_c	SCC angular velocity	rad/s
ω_h	Head angular velocity	rad/s
ω_{vest}	Vestibular angular velocity	rad/s
ω_{vis}	Visual angular velocity	rad/s

II

Preliminary Research Report

This part has already been graded under AE4020

Understanding and Attenuating Simulator Sickness when driving in Urban Environments

M. Hogerbrug

2

Motion Sickness

Despite the many published papers on motion sickness (MS), this phenomenon is still barely understood. Although there are some theories and models that are generally accepted, such as the sensory conflict theory, MS remains a complex problem without a clear-cut model explaining its etiology or in other words: the cause of this condition. Simulator sickness (SS) is closely related to MS and therefore a review on this topic is necessary to get a good understanding of both phenomena [18]. But before diving into these phenomena, it is relevant to start at the beginning, the human sensors. They detect the motion signals coming from the environment such that the brain can process them properly and these signals cause the unpleasant feeling of MS eventually. How the human body uses these systems and sensors to perceive motion and orientates itself in a spatial environment is explained in Section 2.1. This chapter continuous with a historical background on MS (Section 2.2), its definition (Section 2.3) and its symptoms and effects (Section 2.4). The focus of this thesis is SS, which is elaborated in Section 2.5. In simulators, the motion perceived by the vestibular organs often lacks and the main contributor to the inducement of sickness is the visual system. This specific case is often referred to as visually induced motion sickness (VIMS), which will be explained in Section 2.6. At the end of this chapter a short discussion presents the main findings of the literature study on MS and the relevance for this research (Section 2.7).

2.1. Human sensation of motion

When humans move through an environment, virtually all sensory systems acquire signals with self-motion information [34]. And as been said before, the human sense of motion plays an important role in understanding SS and MS. Therefore, the human visual system (Section 2.1.1), vestibular system (Section 2.1.2) and somatosensory systems (Section 2.1.3) will be described in more detail. Secondly, the central nervous system (CNS) integrates vestibular information to distinguish between linear motion acceleration and linear gravity acceleration. This distinction is important to consider since it should be included in the human perception models as well. Therefore, Section 2.1.4 will elaborate on this principle called the gravito-inertial force resolution problem. Finally, the main focus of this initial thesis is on the perception of strong yaw motions on which will be elaborated in Section 2.1.5.

2.1.1. Visual system

The perception of self-motion through the visual system is based on the reaction to optic flow from the surrounding visual scenes [35] [36]. An expanding optic flow pattern entering the retina results in a feeling of forward self-motion and the other way around, a contracting pattern results in a feeling of backward self-motion. When an object or visual scene moves within the visually perceived environment of the observer, then a feeling of self-motion can be induced, even when the observer is stationary [34]. This phenomenon is called vection.

Two other sources that contribute to the sensation of an upright position are the vertical and horizontal lines of the environment (the frame) and the visual polarity of objects with a distinct top and bottom [37] [35]. The frame of the visual environment, i.e. windows and columns of a building, can be

used by the human to estimate its orientation with respect to the earth's vertical. Polarity information is used for the same purpose since it also gives information about the vertical direction.

2.1.2. Vestibular system

The vestibular system of a human is located in the inner ear, see Fig. 2.1. It consists of two organs, the otolith organ (a calcium carbonate structure in the saccule or utricle) and the semicircular canals (SCC), which are sensitive to linear and rotational acceleration respectively [34] [35] [38]. Each canal of the SCC (Superior, Posterior, Horizontal) consists out of three approximately orthogonal canals containing a fluid called endolymphe. This fluid lags behind head rotations due to inertia. The cupula, which is a kind of valve, is sensitive to the fluid flow and has the same density as the endolymphe, which makes the SCC insensitive to linear motion. In other words, the SCC are the human angular acceleration sensors, be it that their output is proportional to angular velocity in the frequency range of naturally made head and body movements [38] [39]. The otoliths register the specific force or gravito-inertial force (GIF), a vectorial sum of linear motion acceleration and linear gravitational acceleration:

$$\vec{f} = \vec{a} + \vec{g} \tag{2.1}$$

The vestibular otolith consists out of the utricle and saccule containing a layer of sensory hair cells with crystals on top. These crystals have a higher density than the surrounding fluid. The otoliths can be seen as more or less perfect three-dimensional direct current (DC) accelerometers in which the utricle senses the accelerations in the horizontal plane and the saccule is more responsive to vertical accelerations (gravity) and for- and backward accelerations [40].

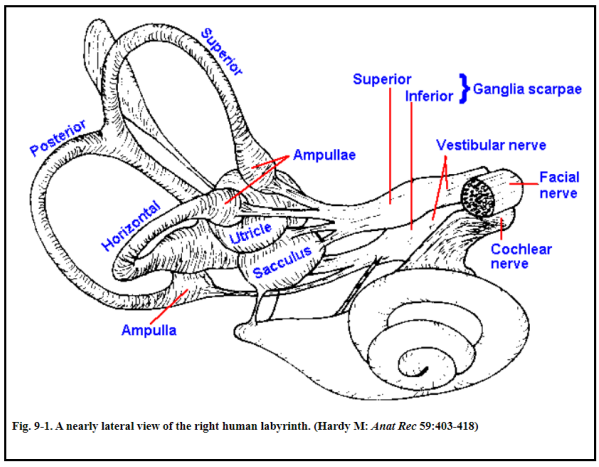

Figure 2.1: A nearly lateral view of the right human labyrinth. Reprinted from The Nervous System In Action by M.D. Mann, 2011, retrieved from http://michaeldmann.net/mann9.htmlfrom by M.D. Mann.

2.1.3. Somatosensory system

Finally, the somatosensory system is also able to tell an individual about its movements and spatial orientation. In brief, this system consists of different kinds of receptors that are sensitive to pressure, stretch, and vibration. Furthermore, in joints and tendons, some receptors can feel accelerations of the body in different directions [40]. According to Correia Gárcia (2013), it is difficult and ethically questionable to measure the outputs of the somatosensory system experimentally, since it needs some medical procedures that went beyond the scope of his thesis [35]. The somatosensory system will therefore not be distinguished from the vestibular system in the rest of this thesis to overcome this difficulty.

2.1.4. GIF resolution problem

The GIF resolution problem can be derived from Einstein's equivalence principle, which states that the otoliths are physically not capable of distinguishing between linear acceleration and gravitational acceleration [41]. A real-life example will be explained to get a better understanding of how our CNS

deals with the GIF-resolution problem. Furthermore, the basic operations that should be realized to solve the GIF-resolution problem based on otolith and SCC afferent signals are described as well.

Problem explanation

An example to visualize and get a better understanding of the GIF-resolution problem can be found in Fig. 2.2. In this figure the gravitational acceleration is directed upwards because it presents the reaction force of gravity as sensed by a human being [41]. Hence, when humans move on earth they only perceive the GIF as given by Eq. (2.1). Now, angular information is required to distinguish between $\vec{a}$ and $\vec{g}$, because otherwise a forward movement may be confused with a head tilt where the head referenced GIF is the same for both situations [41].

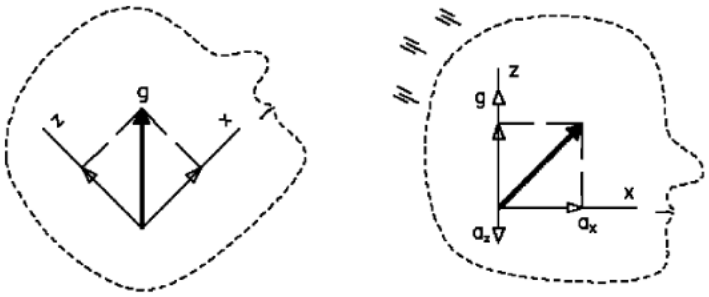

Figure 2.2: By head rotation the GIF components may be as shown left. These GIF components may be exactly equal to those of a condition of combined forward a_x and downward a_z acceleration (such as during walking). Reprinted from [41].

The required angular information can be obtained from the SCC, which is sensible for angular velocity ω. Thus, both the afferent signals from the otolith (GIF information) and SCC are necessary to describe the six degrees of motion (three rotations and three translations) in three-dimensional space. Two examples can be given to better understand how the CNS resolves the GIF-resolution problem. The first one is the somatogravic effect, in which a subject is placed onto an accelerating platform. The subject will be accelerated for ten seconds. Now the subject experiences a forward acceleration and gravitational acceleration (a and g), resulting in a tilted GIF. It is being observed that the subjective vertical (SV) approach this GIF asymptotically, see Fig. 2.3. This illustrates that we do not employ an actual thrust-worthy sense of verticality, but adapt to the GIF instead [41].

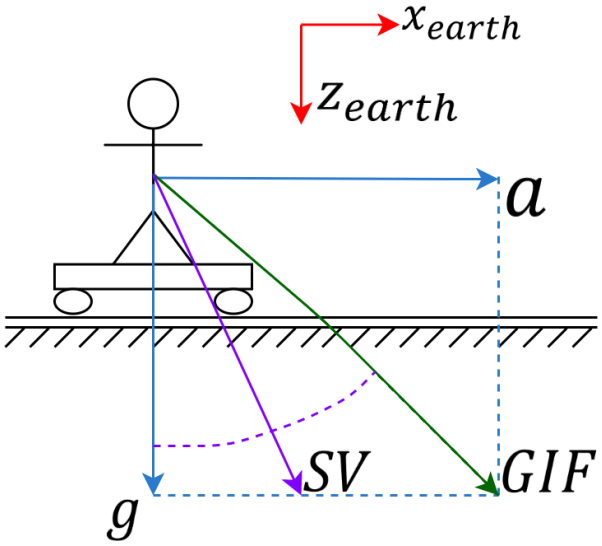

Figure 2.3: The somatogravic illusion. Here it can be seen that the SV follows the GIF.

The second example considers the Ferris wheel illusion, which nicely illustrates the deficient functioning of our SCC under unnatural conditions, see Fig. 2.4. When a participant starts to rotate around an earth-horizontal axis (x_{earth}), he or she will first sense the true or veridical motion. But after some time, when a constant angular velocity is reached, the SCC afferent signals will go back to their resting values (normally $\hat{\omega} = 0$) as can be seen in the middle graph of Fig. 2.5. Now the orientation of the subject is lost and the motion will be interpreted as a circular motion with a fixed orientation [41], which is presented in the right part of Fig. 2.4 and the bottom graph of Fig. 2.5.

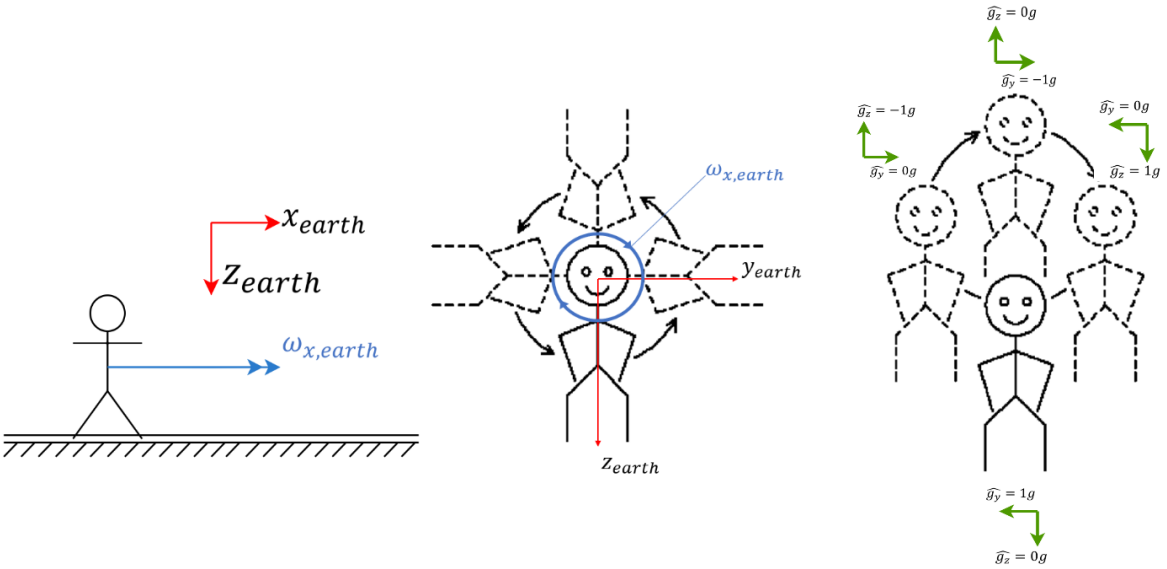

Figure 2.4: Ferris wheel illusion. A subject rotating with a constant angular velocity about an earth-horizontal axis (left) perceives a motion like a gondola of a Ferris wheel after his canal signals have returned to their rest value (right), Reprinted from [41].

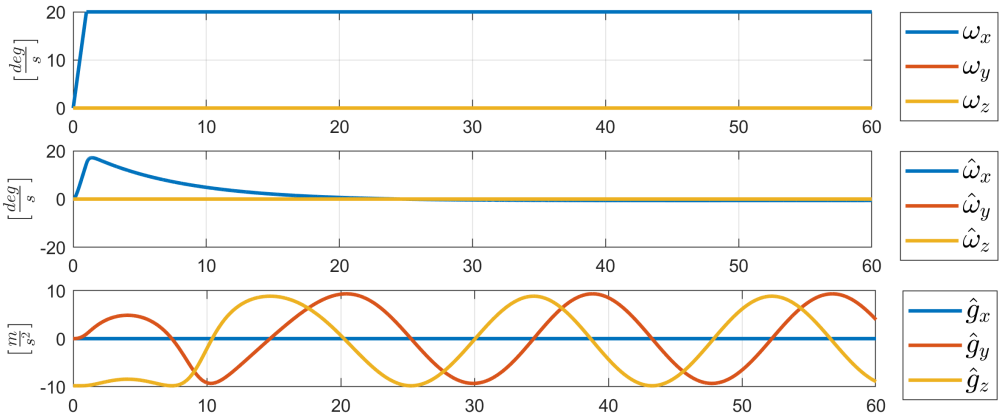

Figure 2.5: Top graph: the constant angular velocity input around an earth horizontal axis (ω_x). Middle graph: the effect on the perceived or expected angular velocities, $\hat{\omega}$, by the human. Bottom graph: the effect on the perceived or expected gravity, $\hat{g}$, by the human

GIF-resolution problem

Bos and Bles (2002) suggested that:

> *...knowledge (in a perceptual, and not in a cognitive sense) about gravity can only be gained during life, and due to the equivalence principle, filtering out gravity is a matter of inference, and not of physics. As a consequence, any model that relies on initial settings for motion and gravity, therefore, cannot represent the true function of our vestibular system (Bos and Bles, p.193, [41]).*

A solid starting point to solve this problem is the earlier mentioned equation: $\vec{f} = \vec{a} + \vec{g}$. Here, $\vec{g}$ is defined in an earth fixed frame of reference and the GIF ($\vec{f}$) is defined in a head frame of reference. So in order to get the GIF into a earth-referenced vector, an Euler rotation matrix $\mathbf{R}_\omega$ is determined by the SCC afferents $\vec{\omega}$:

$$\vec{a} = \mathbf{R}_\omega(\vec{f}) - \vec{g} \tag{2.2}$$

Mayne [42] tells us that there is one characteristic that can separate gravity from the inertial acceleration: the constancy of the one and the transient nature of the other [42]. In this case, gravity is the constant part and linear acceleration is identified as the transient response [41] [42]. Three low-pass filters for the three orthogonal systems involved can now be used to filter out gravity if there are only linear accelerations involved that are normally of short duration or periodic. So for each Cartesian component with index i, this can be described by the following equation in Laplace notation or ordinary differential equation [41]:

$$\vec{g}_{sens} = \frac{1}{\tau s + 1}\vec{f} \tag{2.3}$$

$$\frac{d\vec{g}_{sens}}{dt} = \frac{1}{\tau}(\vec{f} - \vec{g}_{sens}) \tag{2.4}$$

in which g_{sens} is the gravitational vector that is sensed by the human body. It should be noticed that if head motions are coplanar, meaning there exists a geometric plane that contains all these motions, the sensed vertical corresponds to the true GIF immediately. Only if the otolith and SCC inputs are not connected, this will result in a delayed tilt sensation as being explained by the somatogravic effect [41]. According to Bles and Bos (2002) this can be explained as follows: the low-pass filtering to estimate $\vec{g}_{sense}$ should be done in an earth-fixed frame of reference as displayed in Eq. (2.2), because gravity is constant relative to earth. One way to continue determining the sensed vertical is by using rotation matrices, quaternion representation, and multiple-step integration. But there is an easier way. The following equation presents a differential equation to determine the sensed vertical without using rotation matrices:

$$\frac{d\vec{g}_{sens}}{dt} = \frac{1}{\tau}(\vec{f} - \vec{g}_{sens}) - \vec{\omega} \times \vec{g}_{sens} \tag{2.5}$$

in which the first term on the right side of the equation represents the specific force or GIF as estimated by the otolith afferent signals only. The second terms account for the rotation of the head and the belonging change of gravity. The full derivation of this formula can be found in Appendix A. This equation deals also with the high-pass characteristics problem of the SCC as described by Glasauer [43]. For the low-frequency motions the sensed vertical is changed according to the outputs of the otoliths. In this case, the SCC do not signal any motion and the first term with its low-pass filter characteristics passes all information virtually unmodified. For high-frequency motion, the opposite will naturally occur and all the otolith outputs will be filtered out. It can be concluded that the equation above gives the most realistic and simplest way how our CNS solves the GIF-resolution problem [41].

2.1.5. Perception of strong yaw motions

Nooij et al. (2016) did research on the perception of path, rotation and heading during circular trajectories. They addressed the integrated perception of the translational and rotational motions of a

moving participant along a curved trajectory [44]. According to Nooij, there are four characteristics that describe motion perception in the dark [44]:

- The integration of the otolith and SCC signals to resolve tilt and translation;
- The somatogravic effect;
- The decreasing perception of rotational velocity and linear velocity during constant velocity motion;
- The integration of velocity over time to acquire an estimate of the traveled distance.

Nooij's research investigates if these four characteristics can be used to understand the combination of the translational and rotational components in a horizontal plane while moving though a curve [44]. Specifically, they focused on the perceived yaw rotations. A perception model by Merfeld [45] and Newman [46] was employed to question if the perceived motion follows the model predictions. This model assumes linear addition of rotational and translational components. Participants were subjected to circular trajectories and their task was to indicate the perceived angular displacement and perceived traveled path. Another experiment considered their heading estimation. The main finding was that the rotation perception corresponded to the model prediction, but the heading perception was perceived more in line with the true motion than the model predicted [44]. The heading bias could also not be influenced by changing the model parameters. However, some factors were described that could have prevented this bias [44]:

- The initially perceived heading is essential for the remaining trial and can be used to shape the perception of the subsequent part. This can be done by presenting extra-retinal information very briefly that modifies the initial perception at the start of the visual stimulus [44] [47];
- Familiar and expected stimulus patterns influence the overall motion perception;
- The overall motion perception does not depend on just the simple addition of translational and rotational variables. Expectation and knowledge about the relationship between these variables need be taken into account.

2.2. Historical background

MS documentation dates back to the ancient Greeks [18]. The amount of documentation and incidences increased rapidly when mankind decided to travel oversea. Adopting this new kind of transportation gave humans the possibility to trade on a wider scale than possible on land. But traveling through ships did not suit everyone, because lots of humans became the victim of the "plague at sea", i.e. seasickness [48]. Nausea or seasickness can be derived from the Greek word "naus", which means ship [20]. In these times there were already quite some proper ideas about what might cause this sickness. For example, waves cause an experience of passive movements and these were identified as critical stimuli by different cultures [48]. Besides, more experienced sailors were also more resistant to seasickness than novice sailors or in other words: habituation plays an important role in reducing seasickness. Furthermore, according to the Chinese, young children were more susceptible to seasickness. The greek way of explaining seasickness was done by the humoral theory of Empedokles and Aristoteles, which says that the four body fluids (yellow bile, phlegm, black bile, blood) are out of balance at such times. On the other hand, the Chinese studied this phenomenon and its effects on human well-being as well and explained the malfunction is caused by certain body substances and the life force Qi [48].

Some centuries ago, people were naturally still suffering from seasickness, which largely affected many wars and exploration voyages. For example, Houdini was able to escape almost from anything except the seasickness when he took his act to the lands of Europe [7]. Later, more provocative forms of transport arose such as automobiles, air vehicles, trains, carnival rides, swings, tilted rooms, camel riding, newly prescribed eyeglasses and even space vehicles, all creating new kinds of MS. Even more recently, new problems occurred with the arrival of simulators, virtual environments, and widescreen movies. However, it is not just the forms of MS that count as complexity, but even more that individuals differ in their susceptibility to several provocative motion stimuli [7].

2.3. MS Definition

It is important to have a good understanding of MS to place SS in the right context [18]. Already in 1931 researchers discovered that MS occurs when there is a variance between the visual and vestibular cues compared to normal patterns experienced. On top of that, in 1881, Irwin already noted that seasickness can be produced when humans experience a difference between the true visual impression and a certain “visual habitat” [8]. An essential definition of MS is given by Steele in 1968 [49]:

> Motion sickness constitutes a maladaptation to a novel inertial environment (Steel, p.89 [49]).

This maladaptation term has to do with the fact that symptoms do not develop inevitably in the presence of motion, but can also be caused by the new dynamic environment. The inadequacy of the subject to adapt to the dynamic aspects of his environment is the one element that differs from the unaffected [49]. Birren (1949) [6] describes MS as a psycho-physiological phenomenon. Dobie (2019) [7] thinks this is a very important statement since it can help with understanding the several disturbance features of MS in terms of incidence, variability and methods of management. According to Birren, these features should all be tackled by both the physiological and psychological point of view. He also gives a more accurate and constructive title of this disturbance: ”A Motion Adaption Problem” and adds that it should be taken into account that sickness can be explained by primarily psychological reason and therefore can be unrelated to the motion profile. Despite the several perspectives on the definition of MS, there is one definite finding that is already known for decades. Humans without a properly functioning organ of balance in the inner ear are called labyrinthine defective (LD) and incapable of experiencing MS and SS [18] [20] [50]. This was already concluded by Irwin in 1881 because he observed that deaf-mute individuals were immune during sea voyage [51] [52].

According to Birren (1949) [6], more than half of the people suffer from MS and almost everyone can be made motion sick when under the appropriate conditions. Still, it should be taking into account that the individual difference in susceptibility plays an important role. A couple of examples from the conclusions drawn by Dobie (2019) [7] are that women are more susceptible than men. According to recent evidence, this is a result of the distinction in hormones between the sexes. When looking at different age groups, then there is still not a clear-cut conclusion about the difference in susceptibility. For example, Reason and Brand [20] reported that MS susceptibility fluctuates with age and that humans are most susceptible between the age of 2 -12. Above the 50 years, humans are becoming almost immune to MS and it occurs very rarely [18]. However, Cheung and Money performed a study with squirrel monkeys over a period of ten years. They concluded that there was no change in susceptibility to MS when the squirrel monkeys got older. Finally, Fig. 2.6 gives a summary of the outcomes of different simulator studies considering drop out rates (Matas, Nettelbeck, & Burns, 2015, p.161) for different ages [53]. From this summary, it becomes clear that the drop-out rate for older adults is higher than for younger adults.

Some say that it is not the age specifically that influence the susceptibility of MS, but it is the experience of the individual that often comes with age. Habituation to different forms of provocative motions and how this individual developed behavioral strategies to cope with them helps in adapting to MS in specific environments [7] [20] [54] .

2.4. Symptoms and effects

There is a large range of different symptoms that MS brings to human beings. The cardinal signs, or primary clinical symptom, by which the diagnosis of MS is made, are pallor, sweating and vomiting. These signs can become so severe, that some individuals get into an almost pathological state of depression, apathy and listlessness [18] [20]. Other symptoms are dizziness, headache, drowsiness, and mental disorientation. Responses to MS are developed over a certain period, based on the individual susceptibility, the severity and the duration of the stimulus [7]. It is also useful to mention that MS has the word sickness as a misnomer in it. Sickness is normally associated with a disease or malady, which MS is not. A more proper name for MS is: ”a motion maladaptation syndrome” since it is a

Table 1
Reported dropout rates in driving simulation studies.

Study	Older adult dropout	Younger adult dropout	Group difference (Fisher's exact test)	Notes
Bélanger et al. (2010)	37.5% (12/32)	0% (0/20)	Significant	Age 25–42 vs age 65–83
Brooks et al. (2010)	27.8% (15/54)	6.7% (4/60)	Significant	Age 18–50 vs age 65–81
Caird et al. (2007)	34.6% (9/26)	9.3% (7/75)	Significant	Over 65 vs under 65.
Domeyer et al. (2013)	30% (12/40)	12.5% (5/40)	Non-significant	Young 18–28; old 60–90. (Middle age 30–58, 20% (8/40)). For remaining participants, there was no difference in SS scores between age groups after accounting for baseline scores.
Edwards et al. (2004)	40% (8/20)	14% (2/14)	Non-significant	Age 65–83, age 19–22.
Kaber et al. (2012)	16.7% (2/12)	0% (0/10)	Non-significant	Under 25 vs over 65
Kawano et al. (2012)	17.6% (5/17)	0% (1/15)	Non-significant	Younger adults mean age 35.2 ± 5 SD vs over 60 (mean 66.6 ± 4.7 SD).
Lee, Lee, et al. (2003)	0% (0–129)	–	–	9% experienced SS, but 0 dropped out. Age 60+.
Park et al. (2006)	37.3% (25/67)	13.7% (7/51)	Significant	Age 21–50 vs age 70–90
Roenker et al. (2003)	11.5% (3/26)*	–	–	Age 55–86 Participants assigned to simulator training group
Schwebel et al. (2007)	10% (10/101)	–	–	Age 75+
Shanmugaratnam et al. (2010)	17.5% (5/18)	4.5% (2/44)	Significant	Age under 40 vs age over 40
Shechtman et al. (2007)	35% (10/30)	17% (4/23)	Non-significant	Age 25–25 vs age 65–85
Sklar et al. (2014)	37.9% (22/58)	4.5% (3/67)	Significant	Age 55–70 vs age 25–35.
Trick et al. (2010)	44% (15/34)	–	–	Age range not reported. Mean age of non-dropouts 70.8 years ± 5.98. Participants were judged "at-risk" after completing screening and a practice drive and were removed from the study.
Yang et al. (2006)	–	0% (0/24)	–	Novice and experienced drivers aged 16–45

Figure 2.6: Reported dropout rates in driving simulation studies. Reprinted from [53].

> ... normal response of a healthy individual, without organic or functional disorder, when exposed for a sufficient length of time to unfamiliar motions of sufficient severity (Benson, p. 469 [19]).

On the other hand, some people are incapable of experiencing MS and in this case, these people are the ones with the pathology, which is an absent or nonfunctional vestibular system [18] [20].

The effects of MS can be so severe, that people are unable to continue their work properly. In 1943, Schwab experimented with 115 naval personnel, whom all suffered from MS [7] [55]. He classified the individuals into two classes, type I and type II according to the severity of MS as experienced previously. He then determined how efficient they were under these disturbing conditions compared to their normal efficiency on land capabilities. Type I sailors were almost unable to work on a ship because on large ships they could only work at 40 % of their normal pace on land efficiency and on medium-sized and small ships only 5 till 10 %. Type II sailors were able to work at a reduced level of efficiency and were less affected. This group could work for 90 % of their shore efficiency on large vessels, 60 % on medium vessels and about 40 % on small ships [7] [55]. Although he did not give any details on how he arrived at his results, it is inevitable to say that the main problem of MS is performance degradation, certainly when dealing with human operator systems. In this case, their ability to effectively perform their task may decrease [7]. On the other hand, Birren concluded that some people who are experiencing a transient effect of MS can find themselves back and carry on adequately when the need requires them to do so [6]. Similar symptoms and effects can be found for SS on which will be elaborated next.

2.5. Simulator Sickness

The term SS is newer because simulator studies have for example only been conducted since the 1960s within the automotive industry [2]. Over the course of the last 10 years, simulator studies have become increasingly popular and this has to with the increased interest in autonomous driving. The amount of publications considering autonomous driving increased from 22 to 85 per year in the period from 2012 to 2017. According to [2], when the term ”driving simulator” is added, then the amount of publications increased continuously from 3 to 27. Simulator studies are focusing on system acceptance, cooperative strategies, usage of automation, takeover behavior, etc. But as explained before the challenge remains to overcome SS, which is a serious problem [2].

As stated before, SS is a form of MS, but some specific characteristics explain SS. For example, the symptoms are somewhat different, because participants suffer less from nausea, but more from vision and disorientation symptoms according to [56]. Also, vomiting occurs less for SS, which is a common

sign for MS [18] [29]. One aspect that considerably influences the symptoms of SS is the environment. Mourant (2007) used a mini SS questionnaire (mini-SSQ) to asses SS in urban environments with a lot of left and right turns and on the other hand, in-country and sub-country environments with mainly straight roads [27]. He reported that subjects driving on straight roads showed significantly lower mini-SSQ scores than subjects driving a lot of left and right turns in the city environment. Furthermore, a wide visual display field of view (FOV) visual screen is also a provocative factor for SS symptoms [18] [57] [58] [59].

Besides the environment and visual FOV, there are a couple of other facts specific for SS [7]:

- The incidence of SS varies with the **type of simulator** (fixed-based, motion-based) used and has been reported with various types of visual systems such as flat-screens, domes, etc;
- The **intensity and duration** of the simulation have a clear negative effect on SS;
- **Experienced** pilots seem to suffer more from SS than novice pilots or students.

Also, the most effective treatment of SS is the same as for the relief of MS, namely adaptation [18].

A more recent studied aspect of SS that does not apply to MS is the intra-visual conflict [59]. This can be described as the unrestricted view of a participant in which he or she can see the edges of the screen and some aspects of the laboratory environment. SS can even be increased by this phenomenon and should, therefore, be taken into account within the experimental design. Finally, participants need to deal with the sensation of illusory self-motion in simulators, also called ”vection”, and strong visual flows that are related to sickness induction [60] [16]. The development of discomfort while being presented to purely dynamic visuals is called visually induced motion sickness (VIMS). The sensation of discomfort during VIMS is comparable with MS, but now physical movements are often absent or limited. To close the circle; VIMS in flight or driving simulators can in its turn be called SS [61].

A way to overcome the inconvenience of having no motion when experiencing VIMS, is by adding a motion cueing algorithm to the simulator. When the expected motions of a human are known from the perception part of the MS or SS models in a specific dynamic motion and visual environment, this information can be used to propose a motion cueing approach that ensures these expectations are conceded. This will result in a decrease of the conflict and thus a decrease in sickness severity and incidence according to the theory. Motion bases have been added to simulators to increase their fidelity, but later also to decrease SS [25]. It is however impossible to exactly duplicate the motion of a real driving vehicle. These so-called motion cueing algorithms are applied to take into account the motion space of a simulator. Here, scaling is applied to prevent the motion base of reaching its limits. Besides scaling, wash-out is used to steer the simulator back to its neutral position after a movement has been executed. It is however unclear whether providing a motion base to a simulator has its desired effects. For example, Sharkey and McCauley noted that adding a motion base to a simulator did not have the predicted effect of reducing SS and could even make it worse [22]. Furthermore, Klüver found that SS is only marginally smaller in motion-based simulators compared to fixed-based simulators [23]. On the other hand, there are also some positive results on the reduction of SS by adding motion cueing [25] [24]. In other words, this approach requires further investigation.

2.6. Visually Induced Motion Sickness (VIMS)

As stated in the previous section, sickness can also be induced by the visual surrounding rotating around the vertical axis of a stationary observer and give this observer a sense of self-motion called vection [60]. The traditional example to explain vection is when one sits in a stationary train and an adjacent train starts to move, then one may perceive this as self-motion [34] [35]. When this individual looks to the opposite side of the window and sees the stationary environment again, then this illusion will disappear immediately. Research to vection can be traced back to the late 19th century where Wood [62] experimented with the ’haunted swing illusion’. Humans were placed as stationary observers in a rotating furnished room that generated a complete head over heels self-rotation feeling [63]. It is a very important aspect in virtual environments since it can enhance the realism for humans [64]. Vection can be saturated at the moment that the environment is perceived as earth-stationary and only the body is

perceived as moving. Nowadays, research to vection is often done by experiments in which humans are placed into a vertically alternating black and white striped painted cylindrical drum. When rotation is started, the moving visual pattern evokes circular vection and optokinetic nystagmus (OKN). OKN is a reflex of compensatory eye movements to keep the image of visual field fixed o the retina [65]. Vection is perceived in the opposite direction of the actual movement of the drum and increases gradually. Eventually, a state of full vection is achieved when the observer or participant within the drum perceives the rotating drum as earth-stationary. It attributes all the perceived motion to self-motion [15]. When a participant is exposed long enough to these kinds of motions (i.e., 20-30 min), MS can occur, which is referred to as VIMS.

Besides vection, OKN has been proposed as a contributing factor in the genesis of VIMS [15]. OKN can be described as a reflexive eye movement that reacts on the motion of the whole, or part of, the visual surroundings. OKN helps to stabilize the image on the retina by using a slow phase where the eyes will move along with the visual stimulus together with a resting phase in the opposite direction of the movement [60]. Furthermore, head movements and postural instability are also seen as a causal factor for VIMS. Nooij (2017) did research to the relative contribution of vection, OKN, and postural instability and concluded that there is not a clear-cut answer to the cause of VISM. Only vection-gain is found to be the main contributor in VIMS during yaw rotation, but it remains a complex problem in group assessments, since inter-individual differences in VIMS susceptibility may stay hidden in this case [15]. On the contrary, Keshavarz concluded that vection can be experienced without experiencing VIMS, but suggested that there is a link between the two that should be further investigated [16].

2.7. Discussion

The following is essential for the remaining of this research project. MS is closely related to human spatial orientation. For example, humans without a vestibular system cannot be made sick. Understanding the functioning and dynamics of human sensation of motion forms therefore the basis of a MS or SS prediction model. For this research, SS is the main topic and in this case it is not just the vestibular system that is key in understanding the etiology, but together with visual system and the visual-vestibular interactions. When designing a model to predict SS, it is therefore crucial to first implement these characteristics properly. Besides these characteristics, a model that has the focus on prediction SS in urban environments with strong yaw motions should take into account the four characteristics as described in Section 2.1.5. Additionally, this model should integrate the lawful relationship between the rotational and translational component during a curved motion not just by linear addition, but by taking into account the expected relationships between these components as well [44].

Generally, MS and SS are complex problems that have already been encountered by many scientists over the last centuries. As with many problems including humans, the individual differences are hard to take into account in a model. Another human characteristic is adaptation. An individual that has more experience with moving and seeing through several kinds of motion and visual environments, is more used to these circumstances and therefore less susceptible. As explained before, adaptation remains the ultimate remedy against MS. So, when designing an experiment involving MS, these factors and others, such as age and gender differences, should be taken into account. Experience and individual differences are relevant for the design of a SS prediction model as well. Although, these human aspects are hard to implement mathematically into a model. So, developing a mathematical model that describes the etiology of SS properly while taking into account visual-vestibular interactions has initially the main focus in this research.

3

Theories on Motion Sickness

This chapter concerns the etiology of MS motion sickness (MS) and simulator sickness. As for the terminology, MS will be used in this chapter to refer to both motion and simulator sickness. Several theories try to explain the physiological mechanisms underlying the responses of MS [7]. Although the sensory conflict theory is generally accepted and the most prominent in the available literature [8] [18] [61] [66] [14] [67] [9], there is still not an absolutely clear agreement on the underlying etiology of MS. Therefore, Section 3.1 will give an overview of theories that are developed in the last decades. Then, the sensory conflict will be explained in more detail (Section 3.2). A simplified version of the sensory conflict theory, the subjective vertical theory, will be explained in Section 3.3. More recent mathematical models on MS, such as those from Kamiji [12] and Wada [68], are using this theory from Bos and Bles [67]. Finally, a discussion will be given in Section 3.4 that points out the essential parts of this chapter for this research.

3.1. Theories on MS

Vestibular Overstimulation theory
As discussed in Section 2.6, the vestibular system plays a vital role in the physiological responses to MS. Without this organ, humans are immune to MS [18]. Vestibular overstimulation theory was thought to be responsible for the malady called MS. Here it was thought that provocative motions inducing large angular and linear accelerations sensed by the inner ear organ cause MS. The severity and duration of those accelerations are related to the severity and incidence of MS, but many unfamiliar stimuli such as sudden stops in rotating chairs are not provocative [7]. Furthermore, visual stimuli alone without any vestibular activity can produce MS as well. Eventually, the vestibular over-stimulation theory with its flaws has been replaced by the sensory conflict theory [69]

Sensory Conflict theory
One of the first proponents of the sensory conflict theory was Irwin [7], whose view is already quite similar to the currently known theory:

> *In the visual vertigo of seasickness, there appears to be a discord between the immediate or true virtual impressions and a certain visual habit or visual sense of the fitness and order of things, which passes into consciousness as a distressing feeling of uncertainty, dizziness and nausea (Irwin, p. 908 [51]).*

According to Dobie [7] and Oman [9], it was Cleremont in 1931 who came up with a full description of the sensory conflict theory. He observed that MS occurs when there is an incongruity between visual and vestibular stimuli compared to normal patterns established in everyday life [9] as already shortly addressed in Section 2.2. So it is not a single vestibular event, but the body's response to inharmonious sensory information that reaches a so-called comparator in the brain [7]. A conceptual model for an adapted version of the sensory conflict generation was proposed by Reason in 1978 [8]. Reason's

neural mismatch model is a corollary of the sensory rearrangement theory of Held [70] and draws on the reafference principle of von Holst [71]. The sensory conflict model is stated as following: it is not just inharmonious sensory information, but it is a conflict between the present sensory information and that retained from the past [7] [8] [9].

Subjective Vertical Conflict theory
Then in 1998, Bos and Bles came up with a simplification of the sensory arrangement theory, which is called subjective vertical (SV) theory. This theory considers only one conflict, which is the conflict between the subjective or expected vertical and the actual sensed vertical. An elaborated explanation of the sensory arrangement theory and the SV-theory is given in Section 3.2 and Section 3.3.

Evolutionary theory
Another theory on MS that suggests similar finding as the sensory conflict theory is the evolutionary hypothesis from Treisman in 1977 [72]. He also suggests that MS is triggered by provocative situations when the visual, vestibular or proprioceptive inputs are repeatedly and unpredictably be perturbed. On the other hand, he tries to explain why humans vomit and state that these reactions are consistent with a reaction designed to eliminate toxins. It is simply an accidental byproduct in response to motion of this natural system of eliminating ingested neuro-toxins [72].

Postural Instability theory
In 1991, Riccio and Stoffregen came up with the postural instability theory. In contrast to the sensory conflict theory, this theory suggests that it is not the change in stimulation of perceptual systems, but the novel demands on the control of orientation and posture that produce MS. They argue that prolonged postural instability, which is a specific property of animal-environment interactions, causes the symptoms for MS. Thus, MS occurs when animals do not yet possess the ability or strategy that are effective to maintain postural stability [73]. The focus of this theory is on the posture,

> *because postural control is fundamental to all behavior-to any perception-action interaction between the animal and the environment (Riccio and Stoffregen, p.233, [73].*

Dennison found that subjects with greater levels of cybersickness exhibited fewer variations in postural sway and concluded that postural instability theory has a weak link to cybersickness [74]. Besides Dennison, Warwick-Evans et al. (1998) did two experiments to evaluate the sensory conflict and postural instability theory of MS. They concluded that the sensory conflict theory gives the best overall explanation of the cause of MS [75]. More recently, Nooij concluded that the sensory conflict theory can explain VIMS most properly compared to the postural instability theory and the subjective vertical conflict theory, but a more detailed and refined definition of the nature of the conflict should be provided [15].

3.2. The sensory conflict theory

As mentioned in the previous section, Reason proposed a conceptual model for sensory conflict generation that is based on the reafference principle and sensory rearrangement theory. First, Section 3.2.1 elaborates on the reafference principle and Section 3.2.2 explains the sensory arrangement theory. The last subsection combines the two mentioned principles and introduces the notion of a neural mismatch as been introduced by Reason in 1978 (Section 3.2.3).

3.2.1. Reafference principle

The reafference principle contributes to answering the question about how the central nervous system (CNS) can distinguish between the visual input generated by body movement and the visual input generated by the movement of the entire visual surroundings [9] [76]. Von Holst came up with two sources of sensory information (”afference”), namely muscular stimuli and external factors, which he called reafference and ex-afference respectively. The last one is independent of motor impulses [71]. The hypothesis of the described mechanism proposes:

that the efference leaves an "image" of itself somewhere in the CNS, to which the re-afference of this movement compares as the negative of a photograph compares to its print; so that, when superimposed, the image disappears (von Holst, p. 91 [71]).

An illustration made by Von Holst to explain his principle can be found in Fig. 3.1. Fig. 3.1a shows a motor command C from a higher center (HC) that causes a specific activation in a lower center (LC), Fig. 3.1b. Due to this activation, a certain stimulus-situation gives rise to a specific efference (motor outflow) (E) to the effector (EF), which can be a muscle, a joint or a complete organism, see Fig. 3.1c. In this case, the "image" of the efference is the central stimulus situation and can be called the efference copy (EC). The effector, which can be a muscle, generates a re-afference (R) that is transmitted back to the LC and nullifies the efference copy by superposition (Fig. 3.1d-f). When the efference copy and the reafference compensate each other exactly, nothing will happen. If the afference is too small or lacking, then a "+" will remain and if the afference is too large, then a "-" will remain. In both cases, there will be some definite effects in which the movement itself can be influenced or the difference can ascend to the higher center and produce a perception.

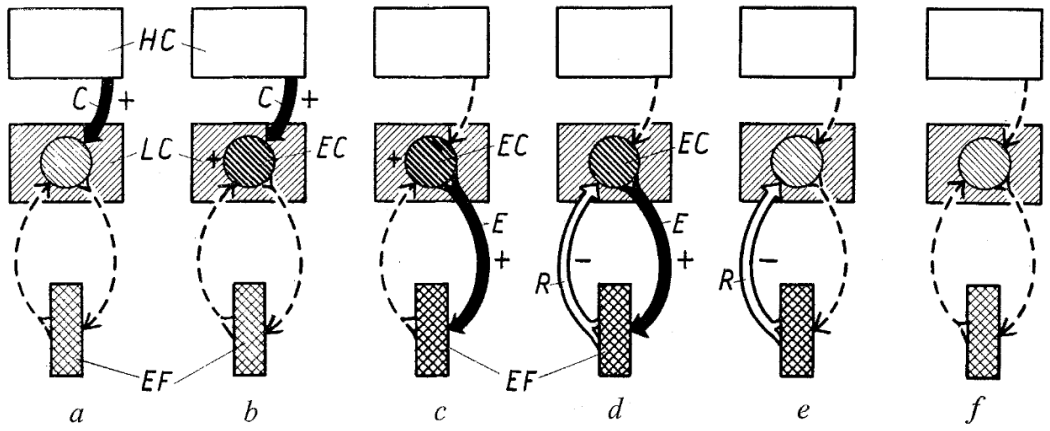

Figure 3.1: Illustration of the re-afference principle. Reprinted from [71].

3.2.2. Sensory rearrangement theory

Held (1961) [70] adapted the scheme from von Holst with a hypothetical structural element called the correlation storage. Now, the re-afferent signal is compared in a comparator with a signal that is selected from the correlation storage by the monitored efferent signal. The correlation storage is meant as a database where previously established combinations of concurrent efferent and re-afferent signals are located. This means that the currently induced efferent signal selects the identical efferent signal and the belonging re-afferent signal, which will be activated. Then, the activated re-afferent signal is sent to the comparator for comparison with the incoming produced re-afferent signal. The outcome of the comparator determines whether to take action or not [9] [70]. When the re-afferent signals are indicated as distorted to one or more sense organs, Held speaks of sensory rearrangement [9].

The sensory rearrangement theory as described by Reason and Brand (1975) states that all situations that induce MS can be related to some type of sensory rearrangement (of sensory cues) in which the motion signals of the sense organs are at variance one with another and with what is expected based on experience [8] [20]. Furthermore, suppose some conditions result in a specific combination of an efferent and re-afferent signal and these conditions change systematically. Then new combinations of the signals will be stored. Thus, this part also takes the adaptation aspect into account as mentioned in Section 2.2. When a human is continuously exposed to the nauseogenic stimulus, then the symptoms of MS will eventually disappear. Or as Reason explains:

It is this crucial temporal comparison between present and past patterns of spatial stimulation that provides the necessary explanatory link between the sensory rearrangement notion and protective adaptation (Reason, p. 280 [8]).

3.2.3. Neural mismatch model

Reason took the correlation storage concept as the basis for his formal psycho-physical model for conflict generation and adaptation in MS. He defined the output of the comparator as a ”neural mismatch” signal that is responsible for producing the MS symptoms. There are two basic structural components of the model according to Reason and their interrelation can be seen in Fig. 3.2.

The first basic component is the neural store containing the efferent and re-afferent signals combinations representing the characteristics of previously encountered sensory environments [8] [9]. He uses a schematic representation to display how two quite disparate re-afferent traces can be linked to the same command signal, see Fig. 3.3. A head tilt is taken as the command signal and the left side of the scheme represents a strongly consolidated well-established bond between the efferent and re-afferent signal. Here the inputs from the eyes and vestibular system are correlated when a head tilt was done in a normal on earth situated environment. The right hand contains the same inputs from the orientation senses, but here they are weakly associated with the command signal. This can be a result of an encounter with some form of sensory rearrangement, such as a situation of weightlessness [8]. Reason originally described six types of sensory rearrangements that could cause MS, but eventually, he mentioned two main categories of motion cue mismatches that were commonly described according to the sensory systems involved [7] [67]:

- A visual-inertial mismatch in which the vestibular system and non-vestibular proprioceptors represent the inertial part and;
- the canal-otolith mismatch.

Additionally, these mismatches can be divided into two types: a type 1 conflict is due to simultaneous contradictory information of two sensory systems and a type 2 conflict is caused when one system signals motion information and the expected signal from the other system is absent.

Eventually, the strongest combination is sent to the comparator, which is the second basic component in Fig. 3.2, for matching with the current reafference. If there is a match, the adaption process is terminated, but if this comparator detects a discrepancy between the present inputs and the stored patterns, a mismatch signal is generated that is fed back into the neural store. This theory also proposes that this signal triggers the various neural and neurohumoral mechanisms that are causing the disturbing feeling of nausea or MS. The neural store reacts on the mismatch signal by selecting the next strongest re-afferent trace combination and sends it again to the comparator. This process repeats itself until the possible combination traces are exhausted or until a consolidated re-afferent trace has been found that is accepted by the comparator. But if the comparator does not accept the presented and available trace combinations, a third process will be executed. In this process, the neural store selects the trace combinations that will once be sufficiently consolidated to function as a proper match in the unknown force environment. But before the comparator accepts the trace combinations as a match, they need to be further consolidated by repeating the same combinations of sensory inputs. In other words, the subjects need to tilt their heads many times in the just mentioned weightless environment to experience the same re-afferent combination of visual and vestibular inputs over and over again. At some point, a strong enough consolidated re-afferent trace combination is developed for the comparator to accept it as a match. The adaptation process will then be terminated [8].

Hence, the description above is valid in case of active self-movement. When the human is passively moved by some means outside its control, there is no command signal generated, so the stimulus traces will not be accessed as quickly as with active self-movement. Somehow the retrieval and consolidation of the re-afferent traces can eventually occur despite the absence of the corresponding efference traces, because the human is still able to adapt, albeit slowly [8]. The neural store could now only bias selection of re-afferent traces in favor of recently-stored trace combinations.

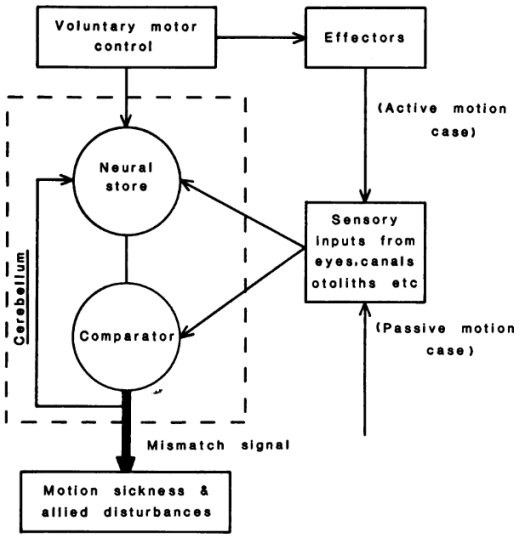

Figure 3.2: The basic structural components of the neural mismatch model. Reprinted from [8].

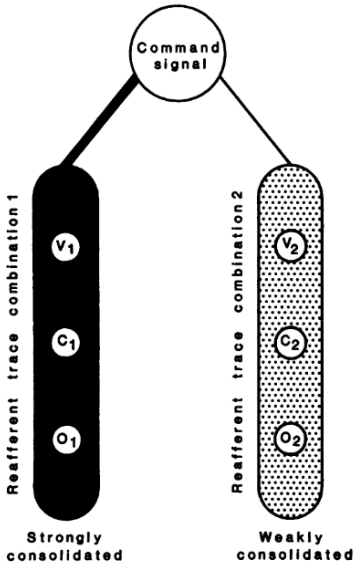

Figure 3.3: A schematic representation of a hypothetical spatial engram. V, visual input; C, canal input; 0, otolith etc. inputs. Reprinted from [8].

There are some assumptions made governing the strength of the mismatch signal. The severity of MS depends on the size of the neural mismatch in any of the sensory inputs, the number of sensory conflicts (e.g. visual-vestibular, canal-otolith, etc.) and the degree of consolidation. The first two are proportional related, but the last one is inversely proportional related to MS symptoms.

Despite the general acceptance of this model, it is criticized among other researchers. The sensory rearrangement theory and neural mismatch model cannot be regarded as an established theory yet, because it has still some weaknesses [18] [9]. Even the proponents of the theory say it has some flaws, such as the large individual differences in incidence, severity, and duration of MS given a constant and unique laboratory motion environment [18] [20]. Furthermore, Stoffregen and Riccio argued that the sensory conflict is not a measurable variable. This means that the sensory conflict theory of MS cannot be falsified [73].

3.3. Subjective Vertical Conflict Theory

First, the human subjective vertical helps in getting an understanding of the upright position. In other words, it is a sense of verticality [41]. There are several senses involved to perceive the world such that it is not inverted or tilted. For example, the visual system helps in perceiving trees, houses, towers, which are naturally vertically orientated as described in Section 2.1. The vestibular system gives a sense of movement and orientation with respect to the world and gravity. In this thesis, the sensed vertical as being sensed by the humans' senses to estimate gravity will be denoted as $\mathbf{g}_{sens}$ and the expected or subjective vertical as determined by the human's internal model based on previous experience will be denoted as $\mathbf{g}_{exp}$.

Bles and Bos (1998) suggested that MS is primarily provoked due to a mismatch between the sensed vertical and the subjective vertical, from which the last is the internal representation of gravity or the expected gravity. Two examples are used to illustrate this statement, see Fig. 3.4. The first one concerns an experiment with long-time duration centrifugal motion in which only head movements (pitch and roll) relative to the gravity vector provoked MS. When the subject experiences just yaw movements while sitting in an upright sitting position, only motion illusions were provoked (left side Fig. 3.4). The same holds when the subject is placed in a supine position, but in this case roll motion does not provoke MS (right side Fig. 3.4). Altogether, this shows that MS is not always a consequence of sensory mismatches, but only when the determination of the subjective vertical is at stake [67]. The second

example concerns experiments that use an optokinetic drum to study optokinetic circular vection, see Fig. 3.5. The MS incidence is lower than 1% even though there is a clear difference in expected and sensed sensory information [67].

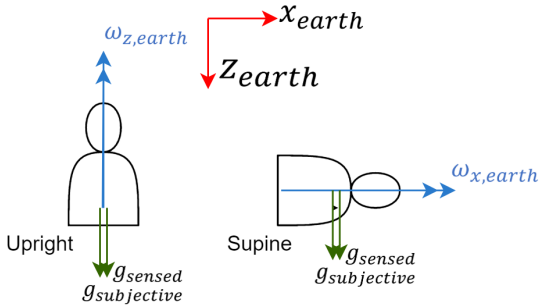

Figure 3.4: Upright and supine position with explained rotations. Here, g_{sensed} and $g_{subjective}$ have the same orientation and magnitude meaning that there is no conflict according to [67] and subsequently no MS.

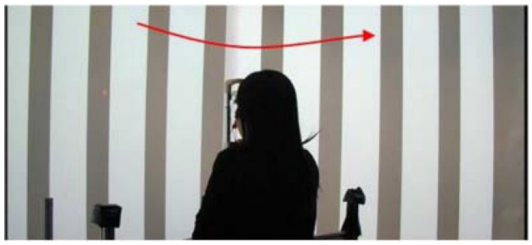

Figure 3.5: A participant standing in front of the rotating striped pattern used in an optokinetic drum inducing circular vection. Adapted from [77].

According to Bles and Bos (1998), the sensory rearrangement theory of MS should be redefined as follows:

> *All situations which provoke motion sickness are characterized by a condition in which the sensed vertical as determined on the basis of integrated information from the eyes, the vestibular system and the nonvestibular proprioceptors is at variance with the subjective vertical as predicted on the basis of previous experience (Bles and Bos, p.481-482, [67]).*

This so-called subjective vertical conflict theory (SVC-theory) is a simplification of the classic sensory rearrangement theory. Here the conflicts do not need to be categorized anymore, because there is only one conflict involved, which can be advantageous. Another important fact is that the assumption of pinning down all provocative motions to one conflict is justified given the analysis of different types of MS [67]. Furthermore, they argue that the subjective vertical determination can be critical to determine one's upright postural position. And this statement can be related to the postural instability theory, which proposed that the control of orientation provides a better understanding of the cause of MS than the classical theory of sensory rearrangement or sensory conflict [7] [67].

Although this SVC theory seems a suitable theory to get a better understanding of MS and SS, it does not explain all situations in which the symptoms of the condition occur. In particular, it does not explain the results of the observed VIMS effects during Earth-vertical yaw rotations [15]. As described above, SS cannot occur when there are only yaw rotations around a vertical axis according to the SVC-theory. The occurred nausea during these situations are an effect of inadvertent head movements, also known as the Coriolis effect [67]. When a participant tilts his or her head on the shoulder during a constant velocity rotation in the dark, then a sensation of pitch rotation will arise (see Fig. 3.6, often together with signs of nausea [78]. This effect is often referred to as the Coriolis effect. However, Nooij used an experimental set-up that minimized these head movements during only visually induced earth-vertical yaw rotations. The results pointed out that inadvertent head movements only occurred sparsely, with low frequency, low angular velocity and minimal head orientation drift over time. But human participants still got sick. So they concluded that both head movements and head tilt were no significant predictors of VIMS and they think that it is unlikely that pseudo-Coriolis effects contribute to the effects of VIMS in this study [15]. This means that the SVC theory does not provide a clear-cut answer to the observed VIMS results regarding Earth-vertical yaw vection. On the other side, they explicitly state that the theory is successful in explaining other types of VIMS as described in [52].

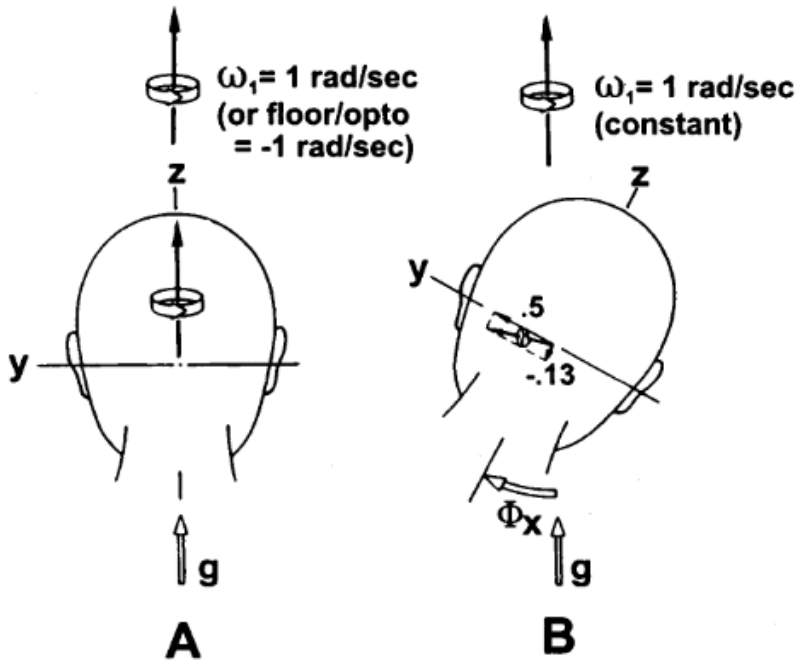

Figure 3.6: Central vestibular angular velocity responses for different stimulus conditions. (A) Response vector due to stimulation of the semicircular yaw-canal, optokinetic and, or somatosensory yaw motion stimulation. (B) Response vectors immediately after a 30 degrees head tilt during constant velocity rotation in darkness, the Coriolis effect. Reprinted from [78].

3.4. Discussion

As stated before, the sensory conflict theory is generally the most accepted theory within research to MS. This qualitative theory is able to explain the key factors of MS as discussed in Chapter 1, namely incidence, adaptation and susceptibility. However, the individual differences among human beings is not explained by this theory. Furthermore, it's qualitative character has little predictive power due to the fact that the produced conflict by the selected re-afferent traces is not measurable. On the other hand, the SVC-theory has been applied to quantitatively explain MS. It is a simplification of the sensory conflict theory that only considers one conflict, which is easier to implement into a model compared to the multiple conflicts as described by the sensory conflict theory. Both theories are useful for this research because they can complement each other. The SVC-theory does not explain results regarding VIMS, which the sensory conflict theory does. And on the contrary to the sensory conflict theory, the SVC-theory has been quantified and generates a measurable conflict, which increases the predictive power of this theory.

4

Motion Sickness Modeling

A motion sickness (MS) model generally consists of two parts: a human spatial orientation perception part and a part where a perceptual conflict is used to model the production of symptoms [12] [9] [11]. There are quite some human spatial perception models that can be found in literature, but not all have been related or used to asses MS. All the models discussed in this chapter have some potential to be used for the to be proposed mathematical simulator sickness (SS) prediction model. Furthermore, the models are observer-based, which is a deterministic modeling approach. And particularly these ”observer” models use similar mechanisms as the brain [21]. This strategy uses residual weights that can be tuned as free parameters, which is for example not possible for Kalman Filter based models [46]. Then, section 4.1 describes the heuristic mathematical MS model of Oman [9] and goes more into detail about its different parts that are partially used in the other models as well. Then, Section 4.2 goes into detail about the one-dimensional and three-dimensional sensory conflict model of Merfeld [45] and elaborates on some extensions. The SVC model that is based on the SVC theory is explained in Section 4.3. Kamiji and Wada extended this model to a 6 degrees of freedom (DOF) vestibular model, which is described in Section 4.4. Merfeld's model is extended as well by Newman [46] with among others the visual system and this model can be found in Section 4.5. An overview of the different models will be made to indicate their performance and potential for this research project (Section 4.6). Finally, this chapter ends with a discussion (Section 4.7) that presents the knowledge that is essential to consider when identifying a new SS prediction model.

4.1. A heuristic mathematical motion sickness model

A heuristic mathematical model for the dynamics of the sensory conflict from Reason and MS was proposed in 1982 by Charles Oman [9]. The objective was to combine the neural mismatch model of Reason and the previously mentioned concepts by Held (1961) [70] and von Holst (1954) [71] together with a control theoretical view on the CNS. First, Section 4.1.1 describes the shortcomings that Oman tries to overcome with this model. Thereafter, the two parts of the heuristic mathematical model will be explained in detail to get a good understanding of the several mechanisms (Section 4.1.2). Finally, Section 4.1.3 discusses its advances compared to the neural mismatch model together with its limitations.

4.1.1. Shortcomings neural mismatch model

The neural mismatch model based on the sensory arrangement theory was at that time a widely accepted framework to describe MS. But it had its limitations from which some of them are already been mentioned in Section 3.2. The objective of the heuristic mathematical model is

> *to reexamine the conflict hypothesis for motion sickness, and attempt a quantitative restatement with modifications aimed at meeting the objections... and also to attempt to bring the theory into some congruence with existing models of spatial orientation perception (Oman, p.11 [9]).*

Oman describes the following deficiencies that he wants to overcome [9]. First, there are forms of MS that cannot be explained by the neural mismatch model. Secondly, the model in its current form has a limited practical value, because expectations based on experience are not individually measurable. Furthermore, the theory does not explain why some individuals do get sick in a given situation and how fast they will adapt. Thirdly, the time course of symptoms is not represented, since there was a lack of information on neural pathways [7] [9]. The final two flaws were that the model did not explain why a vestibular system is required to be susceptible to MS and that the model lacks a purpose. As mentioned before, Treisman suggested for example that it was some kind of alarm signal to trigger vomiting to protect the individual from ingested toxins [72]. But the neural mismatch model did not explain why the nervous system should go to such elaborate lengths to compute sensory conflicts [9].

4.1.2. An adaptive movement control model

The heuristic mathematical model consists of two parts and the first part can be found in Fig. 4.2. This part describes how the body makes spatial orientation estimations and how it controls the body movements. It is a multi-input multi-output (MIMO) system and requires several detailed individual dynamic models for neuromuscular and sensory system elements. The behavior of the body and its neuromuscular and sensory systems that respond to commands from the CNS and external disturbances are converted into a model of linearized differential equations with belonging state variables. Oman took a set of differential equations that describe body sway dynamics for a human participant that stands on a horizontally oscillating platform with the eyes closed as example, see Fig. 4.1. He used simple models to describe the inverted pendulum dynamics where the SCC afferent respond to pitching body motion and the otolith afferent respond to gravito-inertial linear accelerations. A state-space representation is used to represent the entire physical system under CNS control, and the sensory organs providing feedback:

$$\dot{\vec{x}} = A\vec{x} + B\vec{u} \tag{4.1}$$

$$\vec{y} = S\vec{x} + \vec{n_a} \tag{4.2}$$

In this system, the matrix A represents the body and sense organ differential equation coefficients. The matrix B consists out of the mass and inertia coefficients. Together with the actual state $\vec{x}$ and the forcing vector $\vec{u}$, both matrices influence the time rate of change of $\vec{x}$ itself. Eq. (4.1) can be solved given the time histories of the vector $\vec{u}$ [9]. Eg. (4.2) outputs the afference of the system, which are the measurements of the several sense organs corrupted by noise. Besides the input forces from the muscular system $\vec{m}$, the body has to deal with disturbances $\vec{n_e}$ such as obstacles or moving surfaces. Therefore, the forcing vector $\vec{u}$ should be written as:

$$\vec{u} = \vec{m} + \vec{n_e} \tag{4.3}$$

The state-space model representation can be found in the blue box of Fig. 4.2. The strategies of movement control is largely influenced by the S-matrix because this matrix decides which components of the system behavior are observed by the CNS [9]. And ideally, the CNS wants to control all various states in a noise-free fashion, but the response of the human senses do include sense organ output noise or afferent noise (n_a) and are only sensible to some of them. This means that most of the variables in the S-matrix are zero because, except the ones that are associated with sensory organ response gains. So, it is not possible to achieve adequate control when only noisy and indirect information about the physical behavior of the body is available, which is also subjective to external disturbances causing noise on the efferent signal (n_e). But there is a solution for the CNS model to adequately control the body, namely by using a so-called ”observer” [9]. Here an estimate of the controlled system is generated by the information processing observer, which consists of a mathematical model of the controlled systems that gives a priori knowledge. When the system is not subjected to external disturbances it should be able to predict the consequent behavior of the system over time using an accurate set of initial conditions. However, such a system without external disturbances is in practice not available. Therefore Kalman and Bucy [79] and Wonham [80] showed a strategy to overcome this problem. The internal observer should be able to estimate the state of the controlled system as well as to predict the feedback measurements to be expected from moment to moment if the observer’s guess regarding the

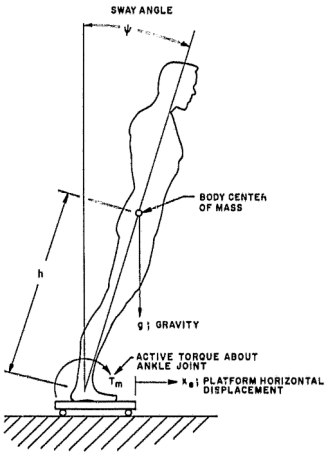

Figure 4.1: Postural control example. Reprinted from [9].

actual system is correct. Eventually, the difference between the expected afferent and actual afferent signals is used to steer the observer state estimates towards reality. This application by Kalman, Bucy and Wonham has close relations to the theories of von Holst [71] and Held [70] regarding internal models, correlation storage, efference copy and closed-loop sensory-motor function. Later, this approach of computationally simulating a model of the system and sensor dynamics to produce expected measurements is encapsulated in the engineering estimation structure of the classic Luenburger observer.

The red box in Fig. 4.2 represents the internal model or "observer". Here a desired state vector of the body $\vec{x_d}$ is compared with the estimated state vector $\hat{\vec{x}}$, which is the output of the observer. The difference between the vectors is the error signal in movement control and is used to determine the efferent signal $\vec{m}$. This error signal is multiplied by an appropriately chosen control strategy matrix C [9]:

$$\vec{m} = C(\vec{x_d} - \hat{\vec{x}}) \tag{4.4}$$

To derive the estimated state, some assumptions are made. For example, the behavioral aspects of the body and its sensory organs are known by the CNS. These are the elements in matrix A and the CNS can employ an estimate of A, which is denoted as $\hat{A}$. Furthermore, the motor outputs $\vec{m}$ are internally available to the CNS and the CNS knows what the effect is of $\vec{m}$ on the system state. Similarly, as employing an estimate of A, the CNS is capable of doing this for B, so $\hat{B}$. Without external disturbances and if A = $\hat{A}$, B = $\hat{B}$ (so a correct internal model), the CNS could achieve open-loop control. This is because the system can predict what the body was doing in response to motor commands. In reality, the body and vehicle which is controlled by the human will be subjected to external disturbances. To solve this problem, a strategy by Kalman, Bucy and Wonham, suggests to employ an internal estimate of the sensory organs as well, denoted as $\hat{S}$ [79] [80]. Now the expected afferent signal can be predicted using the following equation:

$$\hat{\vec{y}} = \hat{S}\hat{\vec{x}} \tag{4.5}$$

Thereafter, a conflict vector can be defined as the difference between the actual sensory afferent and expected sensory afferent signals:

$$\vec{c} = \vec{y} - \hat{\vec{y}} \tag{4.6}$$

This conflict $\vec{c}$ contains information that can be used to steer the time rate of change of the estimated state $\hat{\vec{x}}$ towards the actual state. The information of the conflict vector is somewhat blurred by the variations produced by $\vec{n_a}$, but since it has zero mean it can still gradually steer properly. Now, a K needs to be chosen such that $\hat{\vec{x}}$ is driven towards the actual state and the conflict itself is reduced. Kalman and Bucy (1961) described a process of determining K such that $\vec{c}$ is statistically minimized

when noise processes are known [79]. The higher the uncertainty in measurements, the lower is this weight. Finally, the basic internal model of the CNS or observer is given by [9]:

$$\hat{\dot{\vec{x}}} = \hat{A}\hat{\vec{x}} + \hat{B}\vec{m} + K\vec{c} \tag{4.7}$$

When considering a persistent increasing conflict vector, the internal model should be revised, since this may have to do with changing behavioral characteristics of the body or senses. This persistent sensory conflict would develop in any case if $\hat{A} \neq A, \hat{B} \neq B, \hat{S} \neq S$. The last inequality can be used as a mathematical definition because it describes every situation in which the afferent signals that result from efferent signals have been systematically changed [9]. When the sensory inflow resulting from motor outflow has been systematically changed, for example in the case of weightlessness, then the model predicts the occurrence of orientation and motor control deficits. Now, the body does not behave in a familiar manner requiring a re-identification of the system characteristics A, B and S with appropriate modification of $\hat{A}$, $\hat{B}$, $\hat{S}$, K and C as shown in Fig. 4.2.

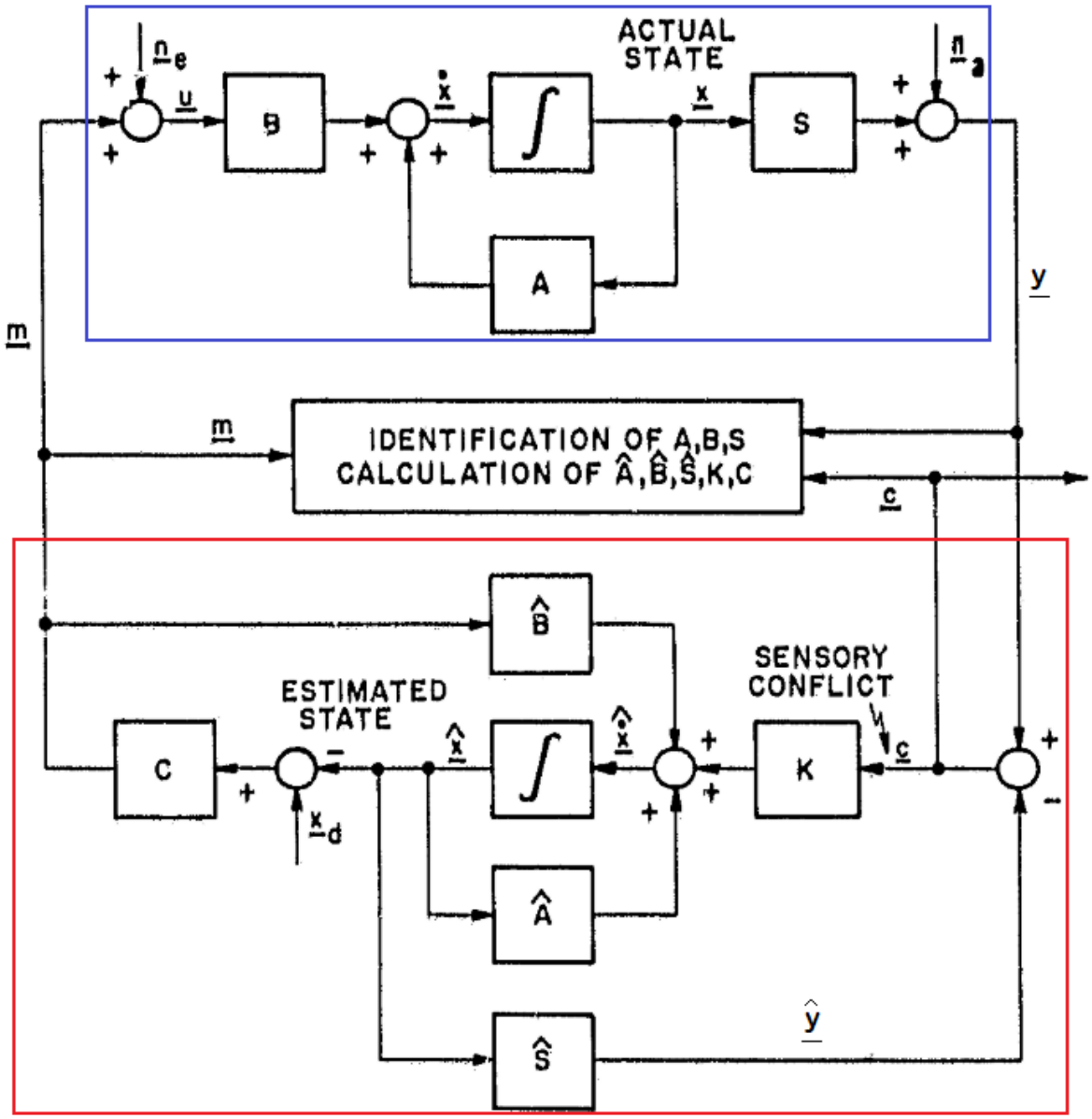

Figure 4.2: Adaptive movement control. Reprinted from [9].

Part two of the model can be found in Fig. 4.3. The function $h(t)$ is a scalar mathematical parameter that deals with Reason's proposal about the proportional relationship between the mismatch signal, which increases as a function of the conflict in any sensory channel, and the severity of MS:

$$h(t) = \vec{c}(t)^T T \vec{c}(t) \tag{4.8}$$

Here, the matrix T and its coefficients define the sensitivity of the subjects to the several conflict signals. Two linear n^{th} order low-pass filters are defined to represent the conflict averaging dynamics, which are assumed to be approximately constant [9]. Then a threshold is defined with a high threshold value T_0 suggesting that subjects are not experiencing symptoms of MS in a daily life situation even though low levels of conflict may be present. The added bias before the threshold is to take extrinsic factors into account such as anxiety, smell, etc. Finally, the subjective estimation magnitude characteristic is a power-law that is experimentally determined for subjective sensations being disturbed by a variety of external physical stimulus modalities. The output will then be the subjective discomfort [9].

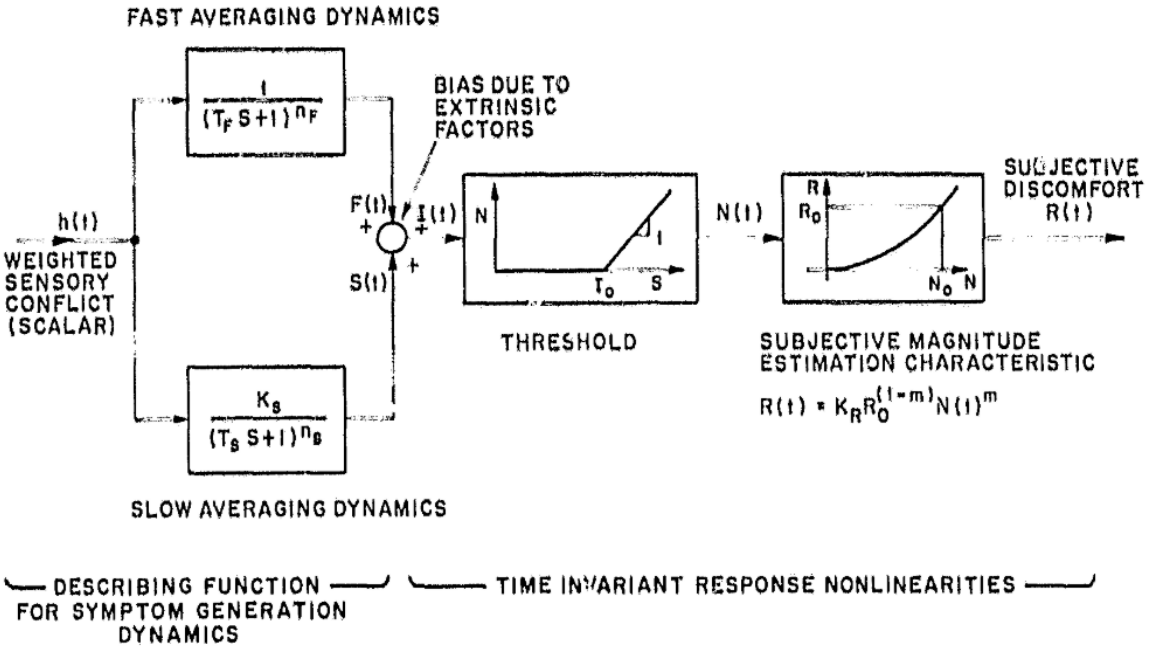

Figure 4.3: Preliminary dynamic model for motion sickness response pathways. Reprinted from [9].

4.1.3. Advances and Limitations

Although this model has a heuristic and conceptual nature, it has some conceptual validity [9]. An internal model is integrated to specify the CNS assumptions on dynamic behavioral characteristics of the body, sense organs and the vehicle under manual control. This is directly related to the suggestion that the CNS needs this internal model since it is unable to measure all important states of body and sensory organs directly, which comes from a control-theoretic perspective. Then, MS should be experienced continuously in daily life, because there are a lot of unanticipated disturbances causing a conflict. But MS is not always experienced since noise processes are present in sensory pathways and imperfect sense organ characteristics. Only when the conflict occurs for a sustained period, symptoms of MS can be detected and changes in $\hat{A}$, $\hat{B}$ and $\hat{S}$ will be employed. This knowledge is also applied in the current model. Besides the adaption part, the difference between susceptibility of MS between passenger and driver is taken into account. Drivers can predict the consequences of their action and this is represented with the internal feedback signal $\hat{B}$. Passengers do not have this information and regard vehicle motion as an external influence that makes the conflict larger. Furthermore, the relation between Reason's neural model can be detected. The $\hat{A}$, $\hat{B}$ and $\hat{S}$ matrices are updated when MS adaption takes place, which can be seen as the "Neural Store" of Reason's model [8] [9].

However, this model has still many limitations. It does not consider the physiology in detail and gives no guidance in how quick the adaptation process evolves including its limits and changes. Furthermore, Oman [9] suggested that there is not an optimal strategy for sensory-motor adaption and that the CNS probably uses multiple sets of internal models and multiple strategies in the appropriate context for the adaptation process. This suggestion is not taken into account in the model. Altogether, this model was not experimentally validated and should be seen as already mentioned before, predominantly heuristic [9]. The conflict hypothesis on which this model is based remains unproven and many physiological mechanisms are only present in an abstract form. However, it extends the qualitative concepts of von Holst [71], Held [70] and Reason [8] and is an advance of the analytically concise statement of a conflict hypothesis.

4.2. A sensory conflict model of spatial orientation

Merfeld came up with his velocity storage model based on experimental data obtained from a squirrel monkey and later of humans [45] [81]. This model is closely related to the heuristic approach of Oman and employs optimal observer theory as well as [45]. First, the one-dimensional model structure will be explained in Section 4.2.1 and thereafter its multidimensional extension in Section 4.2.2. Several other researchers extended this model to overcome some of its limitations and some of these will be given in Section 4.2.3.

4.2.1. One-Dimensional velocity storage model

In 1993, D. M. Merfeld came up with his one-dimensional velocity storage model based on the CNS of the squirrel monkey for the slow phase of the angular vestibule-ocular reflex (VOR), which is a mechanism that makes sure that an unblurred vision is realized during head rotations. He started with a one-dimensional ”velocity storage” model for upright yaw rotation without otolith inputs. The velocity storage and/or acceleration storage are here described as the central estimates made by the CNS on gravity, acceleration and angular velocity. Furthermore, the body dynamics are neglected, the SCC are modeled as first-order high-pass filters for both the sensory dynamics as the internal model, passive motion is assumed and the afferent signal conflict vector is weighted with a single free parameter. It was shown that Merfeld’s model prediction corresponded to the slow phase velocity of the VOR quite well [46] [45].

4.2.2. Multidimensional sensory conflict model

Merfeld extended his model to three dimensions, which can be seen in Fig. 4.5. Now all scalars have become vectors. Some assumptions of this model are [45]:

- SCC are mutually orthogonal to keep the parameters easily identified and to avoid mathematical cross-coupling
- The internal model ($\hat{OTO}, \hat{SCC}$) has the same sensory and body dynamics as the actual dynamics.
- A right-handed coordinate system was assumed, which means that the x-axis is aligned with the naso-occipital axis, the y-axis with the interaural axis and the z-axis is cranial.

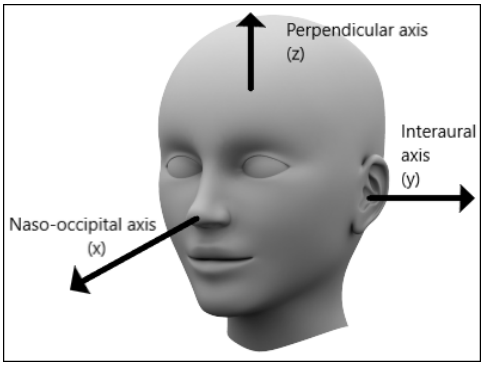

Figure 4.4: Human head reference frame

The third assumption listed above influences the orientation of the gravitational force, since this orientation changes due to the three-dimensional rotations that are made by the body. The following equation is used to rotate the central estimate of gravity based on angular velocity information:

$$\frac{d\vec{g}}{dt} = \vec{\omega} \times \vec{g} \tag{4.9}$$

But since we have the coordinate system as described above, the z-axis points upward and on the contrary, the gravitational force points downwards. This has been taken into account by initializing the gravitational vector as [0 0 -1] and by changing the formula of above:

$$\frac{d\vec{g}}{dt} = -\vec{\omega} \times \vec{g} \tag{4.10}$$

The minus in this equation is essential for the appropriate rotation in the used reference frame. A method to rotate the central estimate of gravity based on angular velocity information was also implemented within the internal model to keep it similar to the true dynamics.

Three error calculations are made within this model, e_ω, e_a and e_f. The first error is the difference between the actual and expected SCC signals and is weighted by the feedback gain k_ω, which determines how much the SCC error (e_ω) influences the central estimate of the angular velocity. Then k_a has a similar function as k_ω for the linear acceleration error e_a. The next error, which is the GIF rotation error ($\vec{e}_f$), requires a more elaborate explanation. Merfeld postulates that the CNS adjusts its estimate of gravity based on the difference between the actual sensed and expected otolith input [45]. The GIF rotation error, a rotation with a magnitude and direction, is required to align the otolith measurement of the gravito-inertial force ($\vec{y}_f$) with the centrally estimated measurement of gravito-inertial force ($\hat{\vec{y}}_f$). To calculate the direction of this rotation a cross-product is used to obtain a unit vector perpendicular to the plane ($\vec{y}_f$) and ($\hat{\vec{y}}_f$) and a dot product is used to determine the magnitude of the rotation [45]:

$$\frac{\vec{e}_f}{|\vec{e}_f|} = \frac{\vec{y}_f \times \hat{\vec{y}}_f}{|\hat{\vec{y}}_f \times \vec{y}_f|} \tag{4.11}$$

$$|\vec{e}_f| = \cos^{-1}\left(\frac{\vec{y}_f}{|\vec{y}_f|} \cdot \frac{\hat{\vec{y}}_f}{|\hat{\vec{y}}_f|}\right) \tag{4.12}$$

The GIF feedback gain k_f influences the effect of the GIF rotation error on the internal sense of gravity to align with the otolith measured GIF. This gain does not induce a change of the central estimate of angular velocity. The gain that does change this latter central estimate is the remaining feedback gain $k_{f\omega}$. When the GIF rotation error increases, an estimate of self-rotation will arise that tends to align the central estimate of gravity with the output of the otoliths ($\vec{y}_f$). With the given information about the different parameters in this model from Merfeld, this model was able to predict several responses to several motion stimuli such as post-rotational tilt and Off-Vertical Axis Rotation (OVAR) [45].

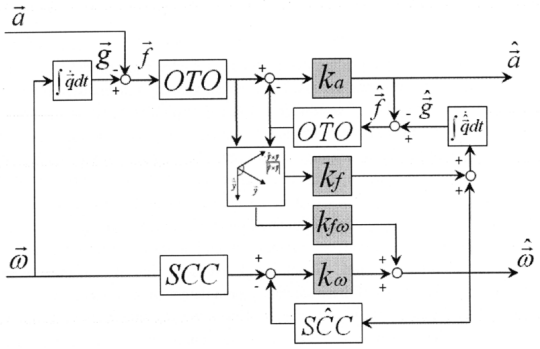

Figure 4.5: Merfeld 1993 Spatial Orientation Model. Reprinted from [46].

4.2.3. Extensions

Glasauer (1992)
Another approach by Glasauer [82] has been proposed to model SCC and otolith interactions for human spatial orientation and to discriminate between translational and gravitational linear acceleration. This model, which can be found in Fig. 4.6, had the main focus on human spatial orientation relative to gravity based on psychophysical measurements of the visual vertical. It shares similar conceptual ideas to Merfeld's model [45], such as a cybernetic approach in conjunction with estimation theory, cartesian coordinate system and the use of mostly linear elements. Furthermore, this model uses an internal model as well to estimate external variables (gravity, acceleration, angular velocity, etc.) by mimicking the physical relationship between these variables and the physical system sensitive to these variables [43]. Glasauer also used Eq. (4.9) to explain the physical relationship between gravitational acceleration and the angular velocity of the body. The "NL" block is used to switches off implausible canal signals by comparing them to the GIF acceleration error vector. Thereby it provides an estimate of angular velocity that is more veridical. The error vector, $\vec{\epsilon}$ is eventually the same in both the Merfeld and Glasauer model [43].

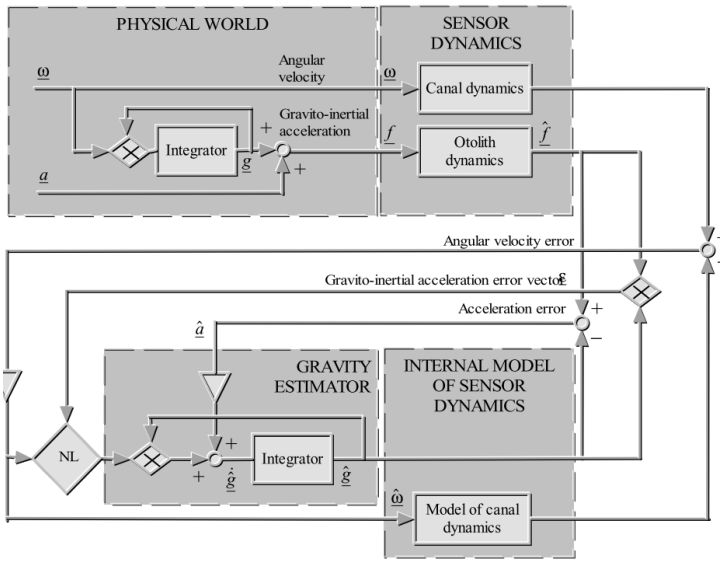

Figure 4.6: Outline of the three-dimensional model of Glasauer. Reprinted from [43]

.

Halswanter (2000)
Haslwanter [83] used a model to describe three-dimensional eye-movement responses to off-vertical axis rotations (OVAR) in humans. This model is based on the studies from Merfeld ([45], [84] since his approach has been used successfully to explain eye movement characteristics after post-rotatory tilts. The basic structure of Haslwanter's model was based on the one suggested by Merfeld [83] as can been seen in Fig. 4.7. The model did, however, not fit the experimental data considering the vertical and torsional eye-velocity modulation components found during OVAR at large tilt angles and was therefore adapted, which can be seen from the shadowed blocks. A constant external force was added to the otolith transfer functions S_{oto} to keep these organs in equilibrium when the head is in an upright position. This can be seen as compensation for the gravitational pull exerted by the 30 degrees nose-up angle of the utricle plane and the angle of the saccular striola relative to the horizontal plane during normal head-upright position. Furthermore, a high-pass filter was added to the linear velocity response path to reproduce the results of other responses during OVAR, such as rotation out on the arm of a centrifuge, post-rotatory tilt, and pitching while rotating.

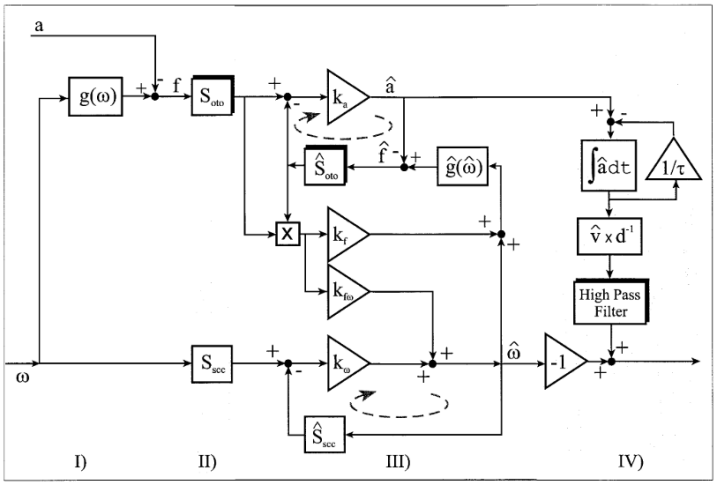

Figure 4.7: Model of otolith-canal interaction, adapted from Merfeld (1995). Elements that have been changed with respect to the original model have a black shadow. From left to right, the panels represent: movement in space (I), transduction by otoliths and canals (II), internal processing (III), vestibulo-ocular reflex (IV): $S_{scc} = \frac{\tau_d S}{\tau_d S+1}\frac{\tau_a S}{\tau_a S+1}$; $\hat{S}_{scc} = \frac{\tau_d S}{\tau_d S+1}$. Reprinted from [83]

.

Merfeld and Zupan (2002)

Merfeld's model was again adapted in 2002 by Merfeld and Zupan [81]. It is altered such that it matches human responses instead of that from the squirrel monkey. First, the parameters k_a, $k_{f\omega}$, k_f and k_ω were changed by trial and error. Furthermore, this model used a 2^{nd} order transfer function to model the human SCC:

$$\omega^i(s) = \frac{\tau_a \tau_d s^2}{(\tau_a s+1)(\tau_d s+1)}\omega^i \quad (i = x, y, z) \tag{4.13}$$

with τ_d as the dominant time constant representing and τ_a as the adaptation time constant with a value of respectively 5 and 80 seconds. The internal sensory dynamics were simplified to:

$$\hat{\omega}^i(s) = \frac{\tau_d s}{(\tau_d s+1)}\tilde{\omega}^i \quad (i = x, y, z) \tag{4.14}$$

, which is a first-order transfer function that contains only the dominant time constant. Adding the adaption time constant here has little influence on the modeling responses [81] [85].

4.3. Subjective Vertical Conflict model

Oman [9] described a conflict vector consisting of all individual sensor discrepancies that can be related to MS. However, this model has some flaws as already mentioned by Oman himself [9]. On the other hand, Section 3.3 explained that there is just one relevant conflict vector: the discrepancy between the gravitational vertical, as sensed by an individual from afferent signals, and a subjective vertical as expected based on previous experience. First,Section 4.3.1 will elaborate on the implementation of this conflict vector into a model to predict MS. This model employs observer theory as well and Section 4.3.2 explains why an internal model is important here as well. Thereafter, Section 4.3.3 gives a detailed explanation of the visual-vestibular interaction model. Finally, the output of this model, which is the motion sickness incidence (MSI), will be described in Section 4.3.4

4.3.1. Only one conflict

According to Bos and Bles [41], the model of Oman nicely explains the mathematical basis of the conflict **c**, but it does not present any quantitative data [41]. Furthermore, it lacks a good description of the MS characteristics as they are observed, so it was adapted by [67] and [11]. The model that is based on the SVC-theory of Bles and Bos [67] can be found in Fig. 4.8. Oman's way of determining the conflict based on sensory conflict is located within the dotted lines. Bles and Bos made an "adaptation" to this model, which is represented by the thick lines. Block B represents Oman's model state space representation

as given by the blue box in Fig. 4.2 without the S block, since this one is given in Fig. 4.8 separately. Block V in the model constructs $\vec{g}_{sens}$ based on incoming sensory information and the same holds for block $\hat{V}$ within the internal model that constructs $\vec{g}_{subj}$. The SVC-model uses the vector $\vec{d}$ instead of $\vec{c}$ as the conflict that generates MS, which is represented by the difference between the sensed vertical $\vec{g}_{sens}$ and the expected or subjective vertical $\vec{g}_{subj}$. Then this vector $\vec{d}$ is used to update $\vec{g}_{subj}$. Again, Eq. (2.3) is used to mathematically solve Einstein's Equivalence principle of GIF resolution problem within the model (Block V).

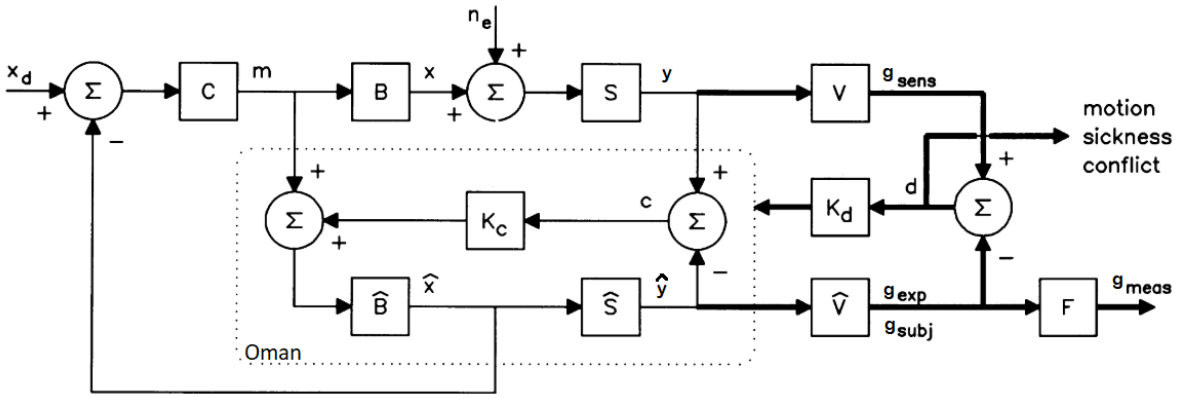

Figure 4.8: The SVC MS model as described by Oman [33], extended with the modules that are necessary for the computation of the subjective vertical (thick lines). The vector d is considered to be the conflict vector for generating MS. Reprinted from [67].

4.3.2. The need for an internal model

First, our CNS model can not be explained using simple servo theory where the feedback signal is perfect without any delays. Our CNS contains neural delays and suffers from an imperfect assessment of linear accelerations due to motion (e.g. somatogravic effect). These imperfections can easily lead to instabilities, so the CNS employs a different solution to control body movements. Adding an internal model generates an additional error generated by a predicted body output instead of the imperfect primary sensory afferents signals. This has two advantages [41]: the predicted output of the body dynamics ($\hat{\vec{x}}$) in Fig. 4.8 lacks the delay of the sensory system resulting in a fast and accurate control of body motion. Secondly, the imperfection during the assessment of body motion is duplicated in the internal model. So when a new environment is encountered, a process of habituation will load this new data into the internal model and update the model subsequently (vestibular adaption). Similarly, Oman [9] uses optimal estimation theory, the principle of efference copies and the classic Luenburger observer in his model (see Section 4.1).

As explained in Section 4.2, Merfeld (1993) [45] used the same model approach to explain the behavior of physiological responses such as eye movements. Glasauer (1992) [82] used this approach as well to explain the behavior of psychophysiological responses such as the subjective vertical [41]. However, these models are not explaining the interaction between the otoliths and SCC unambiguously. Bos and Bles (2002) tried to give a theoretical and mathematical background about this interaction [41]. They have shown that there is a need for an internal model for control purpose as described above. Also, this internal model may act implicitly as a low-pass filter to solve the GIF problem [41].

4.3.3. Visual-vestibular interaction model

The visual-vestibular interaction model part of Bos and Bles can be found in Fig. 4.9 and is a combination of the blocks S and V or $\hat{S}$ and $\hat{V}$ from Fig. 4.8 . The vestibular part (VES) consists out of the SCC and otolith transfer functions. The SCC canals are here assumed to be a first-order high-pass filter:

$$\vec{\omega}_{SCC} = \frac{\tau_c s}{\tau_c s + 1}\vec{\omega}_h \tag{4.15}$$

with $\tau_c = 10s$ and $\vec{\omega}_h$ as the head angular velocity. The olotiths transfer functions are taken as identity: $\vec{f}_{OTO} = \vec{f}_h$.

The visual part (VIS) processes visual flow as explained in Section 2.1.1. Processing the visual flow and the images in our visual system is a complex process. First, the image is projected on our retina in which chemical process generate action potentials that are transported by nerves to our visual centers. These visual centers are located in our brain and make sure that a meaningful output is generated. But all these processes are quite slow due to their complexity and neural delays. For example, the visual system has to deal with the so called flash-lag effect. This effect is described as following: suppose a flashed stimulus that is presented physically aligned with a continuously moving object, then the flash is visually perceived as lagging behind the moving object [86]. Furthermore, the human visual system is sensitive to velocity and position, but not to acceleration. Although, an individual can see differences or changes in velocities [87]. In this model, linear vection is assumed in combination with the fact that vection increases gradually. Therefore a first-order low-pass filter is used to describe this effect:

$$\vec{v}_{vis} = \frac{1}{\tau_v s + 1}\vec{v}_e \tag{4.16}$$

with $\vec{v}_e$ representing the velocity with respect to earth and $\tau_v = 1$. Besides velocity, the eyes can perceive rotatory motions. These motions can also induce vection generally referred to as circular vection, which is reached after several second of motion. Again a low-pass filter is employed, because it is observed that the sense of angular velocity is just given by the complement of the vestibular angular velocity (for which a high-pass filter is employed, see Eq. (4.15)) [87]

$$\vec{\omega}_{vis} = \frac{1}{\tau_c s + 1}\vec{\omega}_h \tag{4.17}$$

with $\tau_c = 10s$ similar to the time constant of the high-pass filter used for the vestibular system.

Finally, the visual system can ”see” the direction of gravity, but not its magnitude. This system uses houses and trees to see what is upright referred to as orientation information (polarity). Furthermore, perpendicular lines from structures around us are used as frame information. Taking this into account with the fact that the horizontal is always horizontal and that this is a relatively fast process, a first-order low pass filter can be used for the approximation of this system as well [87]:

$$\vec{g}_{vis} = \frac{1}{\tau_v s + 1}\vec{g}_e \tag{4.18}$$

with $\tau_v = 1s$. Altogether, the human visual system perceives the vertical from three sources: rotational optical flow, linear optic flow and frame-information [87].

The last part of the model as presented in Fig. 4.9 is the idiotropic vector. People show the tendency to align their subjective vertical towards their longitudinal body axis [88]. The vector has a relatively small magnitude and is added to the total subjective vertical such that the sense of verticality tends to align with the main body axis.

There are different levels of visual-vestibular interactions within this model. First, the angular velocity information from both the visual system and vestibular system in combination with the specific force is used to solve Eq. (2.3). The block $RLPR^{-1}$ can be replaced by this equation to obtain the vertical $\vec{g}$. Subtracting this latter signal from the original otolith outputs give the linear acceleration $\vec{a}$ due to motion. The visual system is not able to detect this acceleration as explained before and visual

information will therefore only enter the path of motion perception after vestibular signals have been integrated temporally. This is also due to Newton's second law, which states that acceleration and force are linearly dependent. Furthermore, force perception does not depend on vision either [87]. Normally, the human sense of acceleration vanishes after some time and this is modeled through a high pass filter included in the otolith part of Eq. (2.3). However, there would still be a perception of velocity when simply integrating the acceleration to velocity. Therefore, an additional high-pass filter is added to drive the vestibular velocity percept towards zero [89]. The integration of acceleration to velocity can then be formulated as follows:

$$\vec{v} = \frac{1}{s}\frac{vs}{vs+1}\vec{a} = \frac{v}{vs+1}\vec{a} \tag{4.19}$$

and this final result can be regarded as a low-pass filtered acceleration with v = 5 s. The visual velocity and vestibular velocity output are linear weighted using a linear weighted addition as done by Howard [90]:

$$\vec{y} = \frac{w_1\vec{u}_1 + w_1\vec{u}_1 + \ldots + w_n\vec{u}_n}{w_1 + w_2 + \ldots w_n}, \tag{4.20}$$

with $\vec{y}$ as output vector and $\vec{u}$ as the input vector. The weights for the vestibular information is taken as w_a = 0.2 and for the visual system as w_v = 0.8, because the visual information is supposed to be dominant [89] [91]. Circular vection, the perception of rotational motions induced by only the visual surroundings, behaves contrary to the vestibular angular velocity motion perception. When both sense systems are available, the outputs can be simply added and it is even suggested that the sense of self motion is perfect in this case:

$$\vec{\omega} = \frac{\tau_c s}{\tau_c s + 1}\vec{\omega}_h + \frac{1}{\tau_c s + 1}\vec{\omega}_h, \tag{4.21}$$

because now the low-pass filtered part and high-pass filtered part are added such that the original signal becomes the result. This calculation step is represented at the summation sign at the left part of Fig. 4.9 where the two ω's are summed. Finally, the attitude or vertical consists out of the visual, the vestibular and the idiotropic part. These should be added differently, because the idiotropic and visual vector only contain orientation information and the vestibular vector contains both orientation and magnitude information. So, Bos and Bles decided to give the idiotropic, vestibular and visual vectors only attitude information and an arbitrary length, which means that the magnitude of the vectors are the same indicating their mutual weight. Thereafter, the are added together using Eq. (4.20). The eventual vertical has the magnitude of the vestibular system only [89]. MS is related to the difference between the gravity vector as sensed and the gravity vector as expected by the internal model and therefore it needs a magnitude to explain MS. The weighting factors that are used have the following values: w_f = 0.75 (visual), w_i = 0.05 (idiotropic) and w_g = 0.2 (vestibular). When there is no source of visual information, then the parameters are chosen as: w_f = 0.95, w_i = 0.05 and w_g = 0.0 [89] [91].

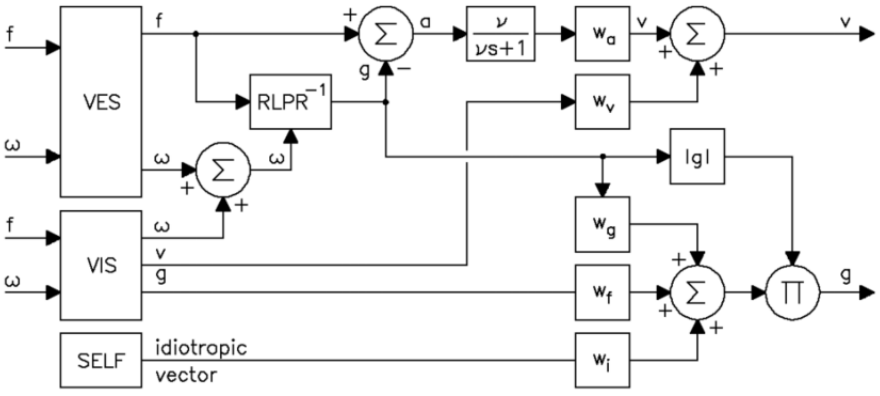

Figure 4.9: Resolving linear acceleration ($\vec{a}$) and velocity ($\vec{v}$), angular velocity ($\vec{\omega}$), and attitude ($\vec{g}$) by means of integrated visual (VIS) and vestibular (VES) inputs ($\vec{f}$ and $\vec{\omega}$), together with the idiotropic vector. Reprinted from [87].

4.3.4. SVC-Model output

From here, the model in Fig. 4.8 is considered again and the output of this SVC-model is the motion sickness incidence (MSI), which is the percentage of vomiting subjects [11]. The MSI has as advantage that it is an observable marker of behavior [17]. Two blocks are required to determine the MSI, see Fig. 4.10. When using the MSI it should be taken into account that people can not become sicker than sick, so this maximum is reached asymptotically. On the other hand, small conflicts can be transformed exponentially. As the conflict vector, $\vec{d}$ can become very large and besides, it can become both positive and negative, a Hill-type function is used that transform the conflict according to these needs [41]:

$$h = \frac{(||\vec{d}||/b)^n}{1 + (||\vec{d}||/b)^n} \tag{4.22}$$

The parameter n accounts for the steepness of the function. And when it is chosen even, the conflict will always be positive as desired. For $n = 2$ the function is logarithmic for larger conflicts and the function is exponentially increasing for smaller conflicts. Parameter b can be chosen such that is fits the experimental data best [11].

Then, a leaky integrator is introduced to account for the cumulative behavior of MS and to get the MS severity. Small disturbances or short temporal fluctuations in the conflict vector should normally not be provocative to induce MS. Therefore a second-order filter is chosen to ignore the slightly different cumulations at different acceleration levels. This leaky integrator also makes sure that the sickness severity does not return to zero after cessation of the conflict [41] [11].

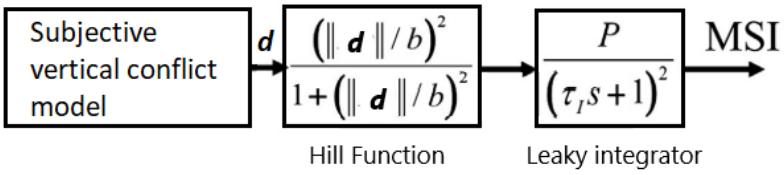

Figure 4.10: Processing the conflict vector **d** to acquire the MSI.

4.4. 6DOF-SVC model

Kamiji [12] extended the 1DOF SVC-model into a vestibular based 6 DOF SVC-model as can be seen in Fig. 4.11. The inputs of the model are the acceleration vector and angular velocity vector in a head reference frame. In this head reference frame, the x-axis is aligned with the naso-occipital axis, the y-axis is aligned with interaural axis and the z-axis is oriented perpendicular to the x-y plane where forward, to the left and up are the positive directions as been showed in Fig. 4.4. The ”G” block is used to rotate the gravity vector according to the head’s rotation and the output will be the direction of the gravity vector seen from the head reference frame. It is assumed that gravity is constant. The specific force can be calculated by adding the inertial acceleration and gravitational acceleration, which are both in the head reference frame. This specific force is sensed by the otoliths, which is assumed as a unit matrix if the inputs are below the 1 Hz [45] [41]. The angular velocities are sensed by the SCC and the dynamics that describe the transduction properties are:

$$\omega^i(s) = \frac{\tau_a \tau_d s^2}{(\tau_a s + 1)(\tau_d s + 1)} \omega^i \quad (i = x, y, z) \tag{4.23}$$

where τ_a and τ_d are the adaptive and the dominant time constant respectively. To distinguish between the inertial acceleration from the senses and the subjective vertical, Kamiji [12] applied the solution of the GIF-resolution problem in block LP (low-pass) as done by Bos and Bles (1998) [11] (see Eq. (2.3)). The final afferent outputs, or the incoming sensory information, consists out of $\hat{\vec{a}}$, $\hat{\vec{\omega}}$ and $\hat{\vec{v}}$ (taken in this thesis as $\vec{g}$), which are the linear translational acceleration, rotational angular velocity and the sensation of the vertical direction ($\vec{g}_{sens}$ in this thesis).

The lower part of the model represents the internal model where the transfer function for the internal model otoliths $O\bar{T}O$ is also a unity matrix. On the other hand, the transfer function for the internal model of the SCC ($S\bar{C}C$) differs:

$$\hat{\omega}^i(s) = \frac{\tau_d s}{(\tau_d s + 1)} \tilde{\omega}^i \quad (i = x, y, z) \tag{4.24}$$

where $\hat{\omega}$ is the estimated angular velocity from the internal model and $\tilde{\omega}$ is the estimated angular velocity of the head obtained from somatic sensation including joint angles. It is assumed that the human roughly estimates body kinematics such as angular velocity, but also acceleration ([12] [14]). The gains K_ω and K_a represent the estimation errors of the mentioned body kinematics. Furthermore, the block $\bar{LP}$ is considered to be identical to block LP, but the output of $\bar{LP}$ will be the expected/subjective vertical $\vec{v}_{subj}$ ($\vec{g}_{exp}$ in this thesis). The afferent signals are compared with the estimated outputs of the internal model to generate the error vectors $\delta\vec{a}$, $\delta\vec{g}_{exp}$ and $\delta\vec{\omega}$, which are fed back into the system. An integrator with gains is used to reduce these errors, which can be seen as the learning process of the human. Again, a Hill function and a leaky integrator are used to calculate the MSI.

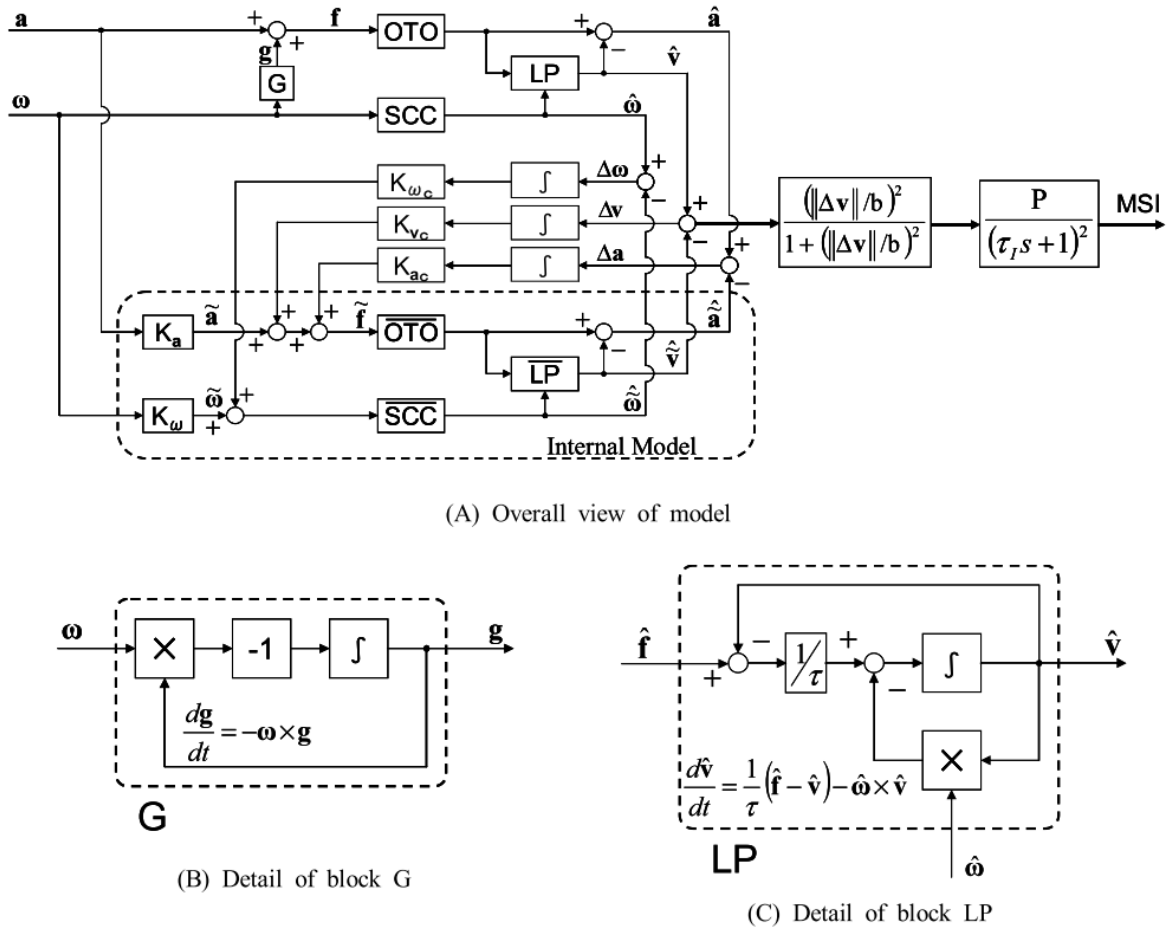

Figure 4.11: 6DOF-SVC (three-dimensional subjective vertical conflict) model. Reprinted from [12]

4.5. A multisensory observer model for human spatial orientation perception

The basis of Newman's model [46] is the multi-dimensional sensory conflict model from Merfeld and Zupan [81]. This basic structure is extended and modified according to Fig. 4.12. The black boxes indicate the differences with Merfeld's model. **A.** refers to a transformation from head to limbic frame of reference which is done using quaternion representations. The limbic frame of reference is defined by

a quaternion vector $\vec{\hat{q}}$ that is based on the gravitation state $\vec{\hat{g}}$. **B.** shows a leaky integrator that is used to integrate acceleration to velocity as been done by Vingerhoets [92] with an individual time constant for motion about each limbic coordinate axes ($\vec{\tau} = [16.66 \quad 16.66 \quad 1.0]^T$). Normally, the initial veridical head rotation perception decays gradually to zero and on the other hand, a circular head translation occurs against the actual direction. The leaky integrator is used to correctly predict the magnitude of this illusory translation during OVAR [92]. According to Newman these time constant values capture the qualitative characteristics of the large physical scale of integrated self-motion. The time constants for motion within the horizontal plane are quite different from the one in the vertical plane as humans make large estimation and phase estimation errors when integrating inertial acceleration cues along a gravitational vertical axis. These errors are modeled by shortening the leaky integration time constant substantially. A standard integrator in block **C.** is used to get from velocity to position to ensure that static visual position input will result in a dynamic response without a steady-state error [46]. Furthermore, there are some additional parameters added to the model. $K_{\omega f}$ is employed to influence the angular velocity on the rate of change of gravity by the user and is nominally set to 1.0. It is mainly used to simulate tilt-gain and tilt-translation illusions, which are experienced by astronauts during their return to earth after being exposed to prolonged duration of weightlessness. Finally, k_1 is a function of the angular velocity residual weighting parameter:

$$k_1 = \frac{k_\omega + 1}{k_\omega} \tag{4.25}$$

and is used to make the loop gain 1.0. In Merfeld's model ([45], [81]) the loop gain was found to be 0.75 to mimic 70 % angular VOR response for eye movement data, but this is inconsistent with perceptual responses for simple experiments such as static tilt and constant velocity yaw rotation. Here the initial response to sudden head movements is more veridical.

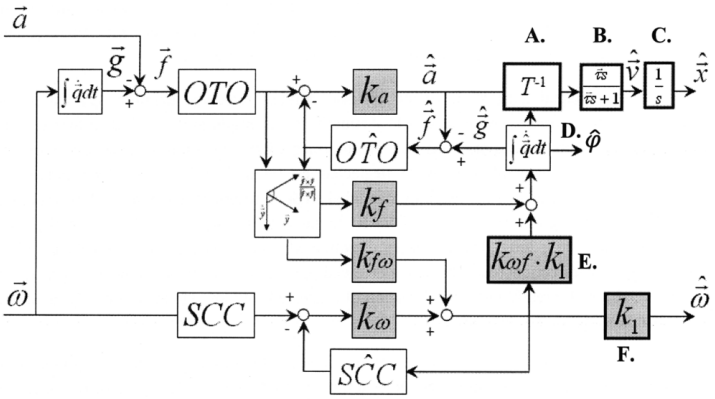

Figure 4.12: Basic structure of Newman's multisensory observer model for human spatial orientation perception. Reprinted from [46].

The basic model structure from Fig. 4.12 is extended with the visual system and the full model structure can be found in Appendix B. All separate visual paths are added as done in Fig. 4.13. The visual system is sensitive to position $\vec{x}$, gravity $\vec{g}$, velocity $\vec{v}$ and angular velocity $\vec{\omega}$ where the first two are the static visual cues and the last two are the dynamic visual cues. Their dynamics are over-simplified and approximated as unity to allow a baseline assessment of the usefulness and practicality of observer theory for modeling multi-sensory interaction [46]. This results in a 3x3 identity matrix to represent the visual sensors where the dynamic visual cues account for the fact that motion is sensed in the opposite direction of the visual field (e.g. vection). Therefore, these dynamic sensors are modeled as negative 3x3 matrices:

$$VIS_x = \begin{bmatrix} 1 & 0 & 0 \\ 0 & 1 & 0 \\ 0 & 0 & 1 \end{bmatrix} \quad VIS_g = \begin{bmatrix} 1 & 0 & 0 \\ 0 & 1 & 0 \\ 0 & 0 & 1 \end{bmatrix} \quad VIS_{\dot{x}} = \begin{bmatrix} -1 & 0 & 0 \\ 0 & -1 & 0 \\ 0 & 0 & -1 \end{bmatrix} \quad VIS_\omega = \begin{bmatrix} -1 & 0 & 0 \\ 0 & -1 & 0 \\ 0 & 0 & -1 \end{bmatrix}$$

The internal dynamics can be represented by identity matrices similar to the equation above, but since the CNS already accounts for the proper direction of the visual estimate, all identity matrices are positive. The visual estimate or afferent signals, for example, $\vec{\alpha}_{Vv}$, will be compared to an expected visual sensory estimate ($\hat{\vec{\alpha}}_{Vv}$) from the internal model of the visual sensor ($V\hat{I}S_V$). The difference or sensory conflict error $\vec{e}_{Vv}$ is weighted by a residual weighting parameter (K_V) and added to the rate of change of the estimated state ($\hat{\dot{\vec{V}}}_v$). The visual model additions are consistent with the structure of a classic Luenberger Observer as mentioned before [21] [46].

The coordinate frame used within this model is a right-handed, orthogonal, world-fixed frame of reference. Before the cues are processed by the sensors, gravity orientation as perceived by the visual system and angular velocity are transformed to the head-fixed coordinate axes and visual position and velocity are transformed to the perceived limbic frame using quaternion calculation. Finally, a gravitational error based on visual information is calculated and requires both a magnitude and direction, which is similar to the implementation within Merfeld's model [45]. Obtaining this error can be done as explained in Section 4.2.2 with as final result the following equation:

$$\frac{\vec{e}_f}{|\vec{e}_f|} = \frac{\vec{y}_f \times \hat{\vec{y}}_f}{|\hat{\vec{y}}_f \times \vec{y}_f|}, \quad |\vec{e}_f| = cos^{-1}\left(\frac{\vec{y}_f}{|\vec{y}_f|} \cdot \frac{\hat{\vec{y}}_f}{|\hat{\vec{y}}_f|}\right) \tag{4.26}$$

The errors due to the difference between the actual and expected visual position, velocity and angular velocity are calculated through vector subtraction [46].

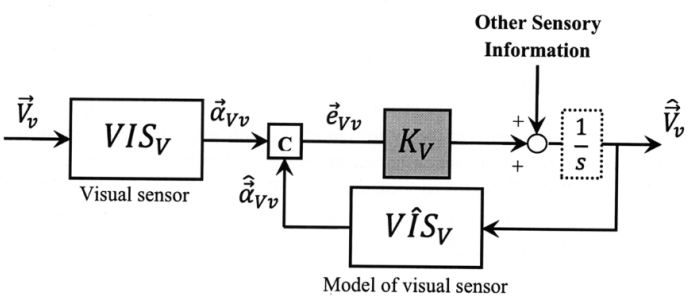

Figure 4.13: General visual pathway. Reprinted from [46].

4.6. Model comparison

This model comparison is used as the first step towards the first iteration of a SS prediction model. Section 4.6.1 will explain the requirement for such an SS predictions model, which will be used to compare the models from the previous sections in Section 4.6.2. Finally, some limitations should be taken into account when employing perception models as discussed in Section 4.6.3.

4.6.1. Model requirements

Eventually, some parts of the models discussed will be used to develop the new SS prediction model. To understand which parts are useful, some requirements for this new model need to be stated to make it verifiable:

- The main goal of the model is to predict SS and therefore a part that involves the sickness or production of symptoms is crucial.
- SS can be mainly described by VIMS, so the interactions between the visual and vestibular system are of vital importance to get a proper representation. Therefore the visual system should be included.
- Experimental data are required to on the one hand see if the perception model part can estimate certain vestibular motion paradigms, visual sensory paradigms and visual-vestibular paradigms available in literature correctly. On the other hand, the model outputs or SS predictions should be compared with experimentally obtained MS and SS data.

- The experiment to be conducted will involve a multiple DOF motion, which means that 3 dimensions and possibly 6 DOF need to be taken into account by the model. So the model must be verified and validated for multi-dimensional cases.

4.6.2. Comparison

The models discussed in the previous sections can now be compared using the requirements described above to capture their potential for the to be developed model. This comparison is shown in Table 4.1 and will be elaborated below. Oman's model included the sensory conflict theory and tried to give a quantitative model approach to predict MS, which was not done by Reason [9]. So it incorporates tools to assess the symptom development of MS. Besides, it is designed as a multi-dimensional model. The limitation of this model is that it is designed with only the vestibular dynamics involved and it is not experimentally validated for any form of data. That is also why the heuristic term is used here. Secondly, Merfeld came up with his velocity storage model and based it first on experimental data obtained from a squirrel monkey and later on human data [45] [81]. This model is capable of simulating some motion paradigms such as constant velocity-earth rotation, off-vertical axis rotation, and post-rotary tilt. Furthermore, Merfeld extended his model to a multidimensional case. The limitations are that it is not related to sickness, it does not take the visual system into account and it is not validated for the remaining desired motion and sensory paradigms. The next model from Bos and Bles takes into account both the visual and vestibular system and it is validated for experimentally obtained MS data and some motion and sensory paradigms. However, this last part is quite limited, that is why the star-shaped symbols (*) can be found for these locations in the table. Finally, it is only validated for an one degree of freedom case. But Kamiji and Wada extended the model from Bos and Bles to a 6-DOF model to assesses MS with a particular focus on head-movements [12]. This model was validated for some MS data. Limitations are again a lack of the visual system and one of the contributors to the model, prof. Wada already suggested to implement the visual system himself [26]. Furthermore, there is limited validation data available that verifies the ability of the model to accurately simulate certain motion or sensory paradigms. Finally, Newman's model has the same advantages as Merfeld's model, but the main advantage of this model is that the visual system has been implemented. This model can be validated against a large set of classic vestibular motion, visual sensory and visual-vestibular sensory paradigms [46]. Unfortunately, this model has not been related to MS or other sickness data. Furthermore, Nooij used this model for evaluation of heading perception and it turned out that the model output was not in line with experimental results. Besides, the visual dynamics are assumed to be unity. So vection delays and dynamics of visual perception are not considered.

	1. MS assessment	2. Incorporates vestibular and visual system	3. Vestibular motion paradigms	4. Visual sensory paradigms	5. Visual-vestibular sensory paradigms	6. Validated against MS experimental data	7. Multi-dimensional
A Heuristic Mathematical MS Model (1982)	X						X
A Sensory Conflict model (1993)			X				X
SVC-model (2001)	X	X	*	*	*	X	
6DOF-SVC model (2007)	X					X	X
Multi-sensory observer model (2009)		X	X	X	X		X

Table 4.1: Model Comparison

It can be concluded that there is not yet a suitable model that satisfies all requirements. Newman's model and Bos and Bles model have the most potential and the last of these two can be extended to multiple dimensions as done by Kamiji and Wada [12]. But in this case the model is still limited to the vestibular system.

4.6.3. Limitations perception models

Finally, some limitations of perception modeling should be taken into account. Perceptual data are mainly limited to subjective descriptions of possible presented stimuli as given by the subject during the experiments [46]. The current models mainly consider passive motions [21]. The models do not take adaptation to MS or SS into account. In other words, the expectations that we have based on previous experience or future information such as preview is circumvented [17]. Finally, our actual brain is much more complex, because it probably uses multiple internal models and strategies to predict the output and corrections for the given dynamic environment [9].

4.7. Discussion

Several perception models and models to describe MS are presented in this chapter. These models have also been implemented in Matlab Simulink to verify their results as presented in the articles, see Appendix C, D, E and F. A key factor for this chapter is to describe how the visual system could be included. Bos and Bles implemented the visual system with appropriate dynamics taking into account vection delay. Newman implemented the visual system as identity matrix without taking into account the dynamics. Besides the need for a visual system, other requirements could be stated to assess the potential of the available MS models to be a part of the to be proposed SS prediction model based on the theory as explained in the previous chapters. And when looking to the model comparison, it can be concluded that the most potential models are the ones from Bos and Bles [11] combined with the extension of Kamiji [12]. The next step is to develop a SS prediction model based on the two potentially useful models and the requirements as described in this chapter.

5

Simulator Sickness Prediction Model

The results of the model comparison of Section 4.6 are used to develop a SS prediction model, which will be explained in Section 5.1. This proposed model will be verified by comparing its results to MS data and motion and sensory stimuli data to show that a suitable first iteration is developed (Section 5.2). The performance of the model will be discussed together with its limitations and potential improvements in Section 5.3.

5.1. Simulator Sickness Prediction Model

The first iteration of a Simulator Sickness Prediction Model consists of model parts from the SVC-model by Bos and Bles (see Section 4.4) and its extension as done by Kamiji (see Section 4.5). The model structure can be found in Fig. 5.1 and the different parts will be explained below. The input selection and kinematics are selecting the required inputs to be used by our senses and calculate the orientation of the gravitational force vector with respect to the body as done by block G in Fig. 4.11, see Appendix G. Our senses include the visual-vestibular interaction model (light green box) as described in Section 4.3.3. The difference is that the dynamics for the SCC are employed as done by Kamiji and Wada (see Section 4.5) [12] [14]. After the human senses, the angular velocity, acceleration and sensed gravity vector will enter the observer part. Here, the conflict is determined between the expected afferent signals coming from the internal observer and the actual sensed signals. The feedback gains are tuned such that the output of the model matches the data of McCauley [10]. This procedure will be explained in the next section. Furthermore, the MSI is employed as output as done by Bos and Bles (Section 4.3.4, which is as explained before as the number of people that will experience maximum sickness, so vomiting, in terms of percentage during a specific motion or sensory stimuli. Finally, this model is multidimensional and takes the visual system into account. A limitation, however, remains the possibility to properly verify the model against verification data available on which will be elaborated in the next section as well.

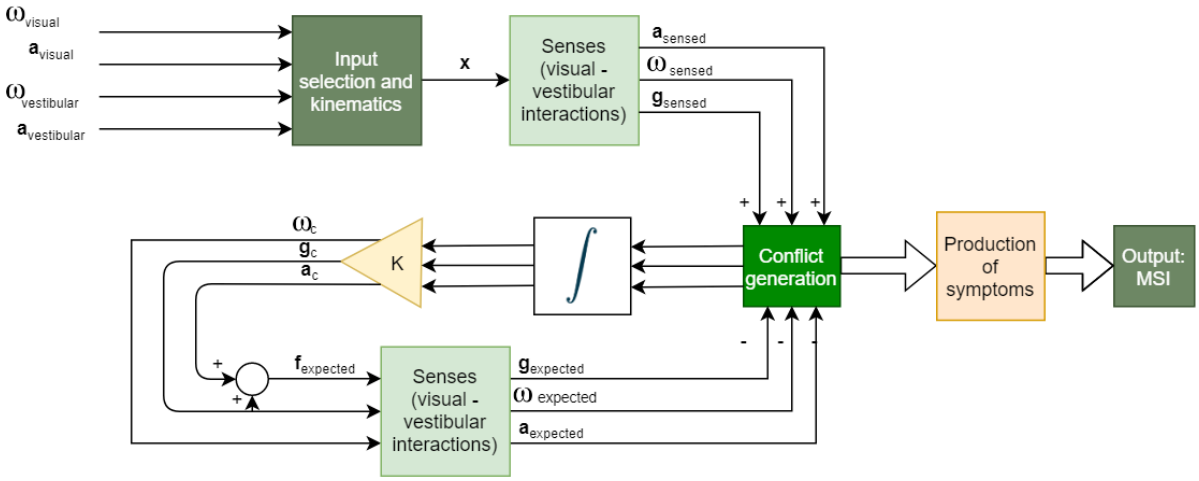

Figure 5.1: Mathematical SS prediction model structure.

5.2. Model results

The model results section is subdivided into the following subsections. First, the parameters tuning is explained in Section 5.2.1 that is used to be able to predict McCauley's experimental data as accurately as possible. Secondly, the capability results of predicting the right outputs for some motion and sensory paradigms are given in Section 5.2.2. Finally, some simulation results will be presented that can be used to formulate some first hypotheses for the experiment to be conducted.

5.2.1. Generate the right MS data

To see if the model is capable of generating the right MSI data it can be compared to experimentally obtained MS data from McCauley [10]. McCauley subjected participants to vertical sinusoidal motions in a ship-motion simulator and the results of the experiment can be found in Fig. 5.2 together with their fitted data. The mathematical function that is used to fit the experimentally obtained data is calculated as following [10] [17]:

$$MSI = 100 \cdot \phi(z_a) \cdot \phi(z_t'), \tag{5.1}$$

Where $\phi(z)$ is a normal distribution function of z and this function is formulated as:

$$\phi z = \frac{1}{2\pi} \int_{-\infty}^{z} e^{-\frac{1}{2}x^2} dx, \tag{5.2}$$

with variables z_a and z_t' as:

$$z_a = 2.128 log_{10}(a) - 9.277 log_{10}(f) - 5.809 log_{10}^2(f) - 1.851; \tag{5.3}$$

$$z_t' = 1.13 z_a + 1.989 log_{10}(t) - 2.904 \tag{5.4}$$

where a is the RMS of the vertical acceleration component in g's, f is the frequency of the vertical acceleration component in Hz and t is the time of exposure to the acceleration in minutes. When comparing the experimentally obtained data and the mathematical obtained data fit, then the root mean square error (RMSE) is 6.1%. However, Fig. 5.3 shows a large deviation (RMSE = 32.49%) between the data produced by the first iteration of the SS prediction model and McCauley's data. But, McCauley's model lacks a vestibular base and predicts only the MSI for vertical sinusoidal motions [11]. Hence, the currently used parameters in the model are the ones from Kamiji and Wada (2007) [12] [14]. A sensitivity analysis was done to see which parameters had a positive effect on attenuating this error. For this linear motion case, so vertical accelerations in the z-axis, the parameters K_{ac}, K_{vc} and b were tuned such that the RMSE was as low as possible. To get this lowest RMSE, an optimization algorithm in Matlab was employed. This optimization function is called the "fminsearch" function and is a multidimensional unconstrained nonlinear minimization that makes use of the Nelder-Mead method. The cost function

used within this algorithm is the SS prediction Matlab Simulink model in which the changing parameters were K_{ac}, K_{vc} and b. After performing the optimization algorithm on the parameters K_{ac}, K_{vc} and b, an RMSE of 14.3217% has been achieved when comparing the results to the original data of McCauley together with Fig. 5.4. The RMSE deviation between the experimentally obtained data and McCauley's model data is only 6.1%, which is still better than the RMSE deviation of the SS sickness model. The 1-DOF SVC model of Bos and Bles has an RMSE deviation of 22.25%. Furthermore, the 6-DOF SVC model of Kamiji and Wada shows an RMSE deviation of 21.42%, which is a bit better. In the end, the developed and tuned SS prediction model presents the best results.

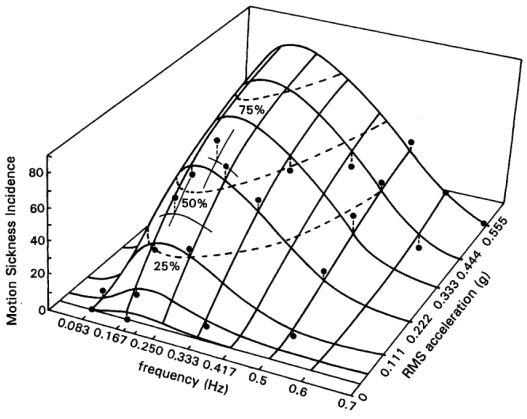

Figure 5.2: Experimentally obtained results of MSI's for different accelerations and frequencies. Reprinted from [10]

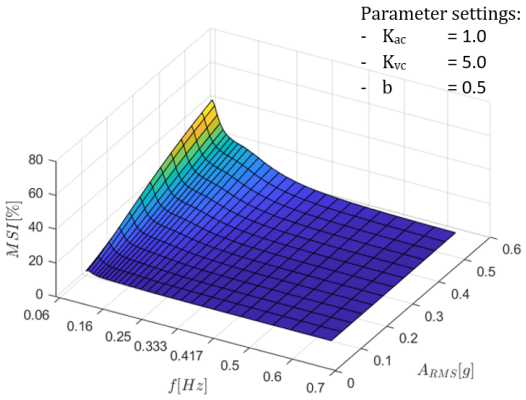

Figure 5.3: MSI results from SS prediction model before parameter tuning.

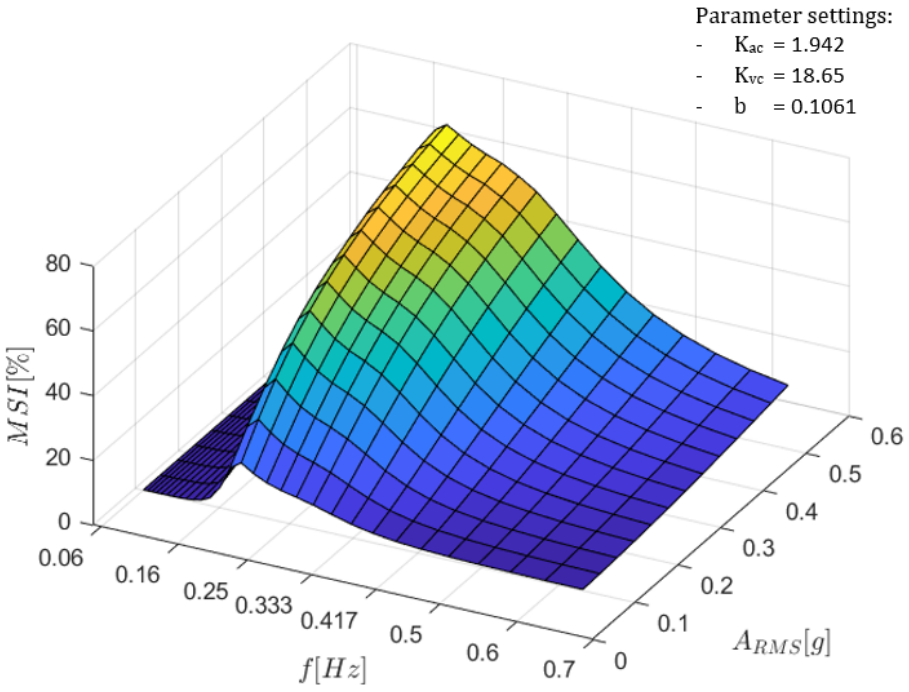

Figure 5.4: MSI results from SS prediction model after parameter tuning.

The change of MSI over time for one specific frequency of 0.25 Hz and three different acceleration according to McCauley's data is displayed in Fig. 5.5. On the right of this figure, the results for the SS prediction model can be found with the belonging parameter settings. They are now quite similar, so the prediction of the model is more accurate already. All parameters of the model are given in Table 5.1.

	Value	Unit
K_{ac}	1.942	[-]
K_{vc}	18.65	[-]
$K_{\omega c}$	5.0	[-]
τ_a	190.0	[s]
τ_d	7.0	[s]
τ	5.0	[s]
τ_c	10.0	[s]

	Value	Unit
τ_v	1.0	[s]
σ	5.0	[s]
υ	5.0	[s]
g_0	9.80665	[m/s]
b	0.1061	[-]
μ	12	[min]
P	85.0	[%}

Weights	Light	Dark	No motion
w_a	0.2	1.0	0.0
w_v	0.8	0.0	1.0
w_g	0.2	0.95	0.0
w_f	0.75	0.0	0.95
w_i	0.05	0.05	0.05

Table 5.1: Parameters and weights SS prediction model according to [12] [91] [89] and the parameter tuning as discussed.

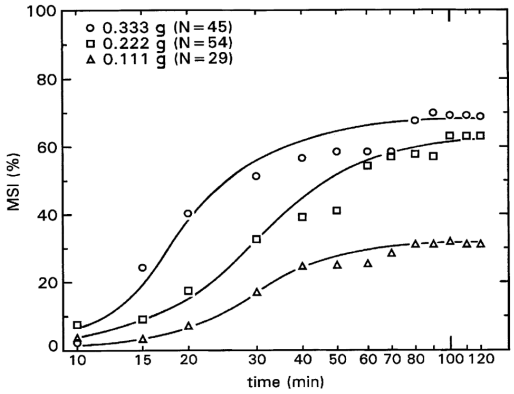

Figure 5.5: Experimentally obtained results of MSI's overtime for one specific frequency (0.25 Hz) and three different acceleration conditions. Reprinted from [10]

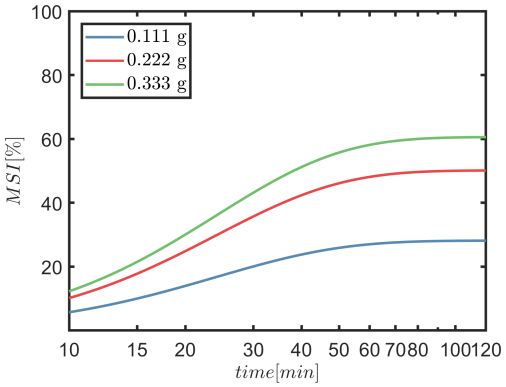

Figure 5.6: SS model predictions MSI over time for 0.25 Hz and three different acceleration conditions.

5.2.2. Verification motion and sensory paradigms

This subsection will discuss the capability of the model to produce the expected motion by a human when considering different motions and sensory paradigms as done by Newman and Merfeld [46] [45].

Constant Velocity Rotation about an Earth Vertical Axis

Fig. 5.7 shows the results of Newman's model predictions for a constant velocity rotation around an earth vertical axis as reported in [46] together with model predictions of the SS prediction model. A participant is sitting upright in a rotation chair while being rotated in light and dark conditions with an angular velocity of 0.26 rad/s for 30 seconds. A second case is where the visual surroundings are rotated in light conditions with the same angular velocity around participant (circular vection). The third case considers dark conditions and the results are similar to the results from Merfeld [45], because now the visual information is not available. When comparing these results to the results of the proposed SS prediction model, then it can be seen that the behavior is almost the same, but the values deviate. However, it still shows proper behavior in different conditions. For example, a sustained sensation of rotational motion that decays towards a value that is near the actual input stimuli ($\omega_{z_{input}}$). It also properly predicts circular vection when just the visual field rotates around the participant in the absence of motion. The difference with Newman's results can be found when considering the fast-rising component followed by a slow rising component because it is harder to distinguish between these components for the SS prediction model results. However, the model takes into account the delay of the circular vection, which is typical for human participants [46] and this part lacks in the model of Newman. This motion paradigm is of particular importance since this research will focus mainly on strong yaw motions during a corner in urban environments.

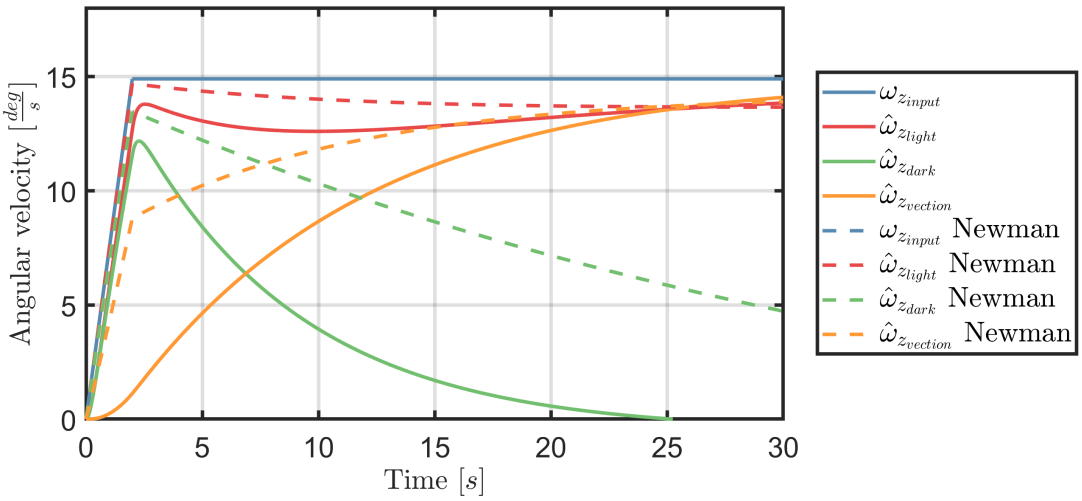

Figure 5.7: SS model predictions for constant velocity rotation about an Earth vertical axis compared to the model outputs of Newman for the same motion paradigm.

Post-Rotary Tilt

The post-rotary tilt is simulated with an initial constant yaw rotation of 100 deg/s about an earth-vertical axis. After 50 seconds, the SCC responses should have decayed to zero and the simulated subject is decelerated to 0 deg/s in one second. After stopping, an immediate angular roll velocity is applied with 45 deg/s for 2 seconds such that the participant is rolled 45 degrees to the right. This can be seen in the upper figure of Fig. 5.8. Here the results of the SS prediction model show quite some deviations. First, for the expected angular velocity a y-component is missing after the roll rotation. This component is induced due to the strong post rotary tilt sensation that causes the SCC afferent signal $\vec{\omega}$ to be not aligned with gravity anymore. Furthermore, the expected acceleration and gravity deviate as well around to the roll-rotation point. A strong oscillation is visible that should not be there when comparing these results to Merfeld's model outputs. However, the end values correspond again.

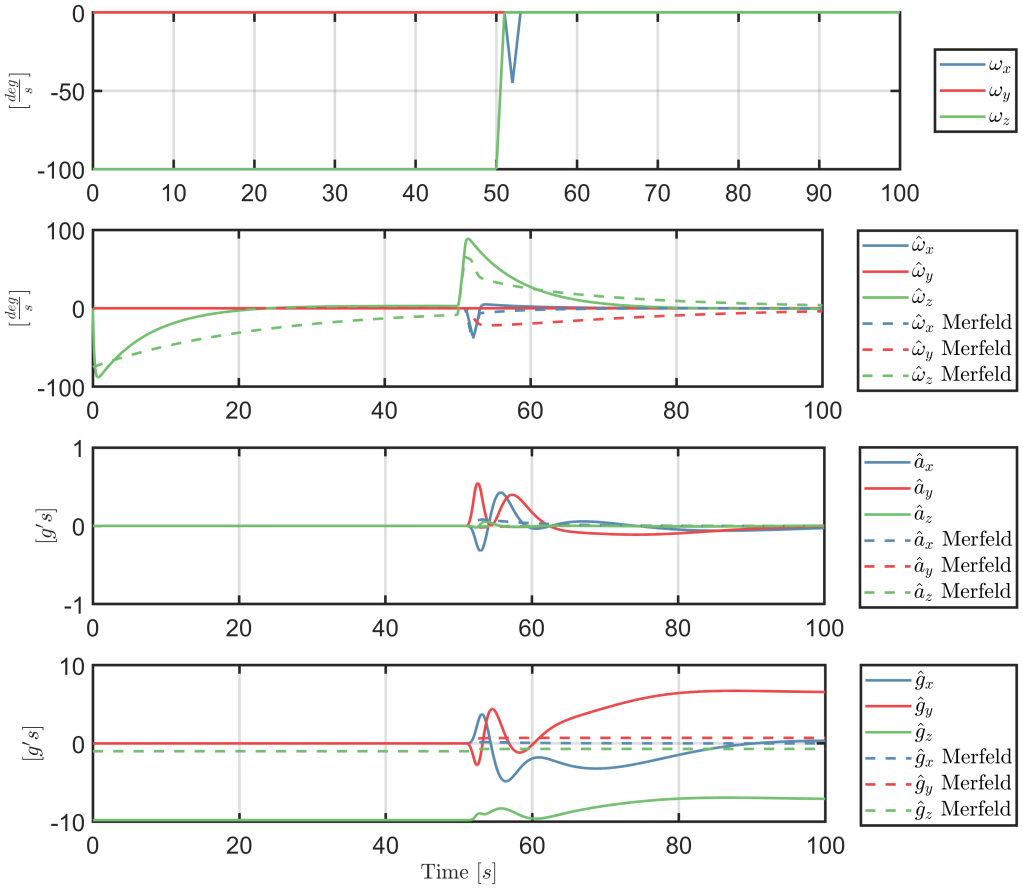

Figure 5.8: Results SS prediction model for the Postrotatory tilt motion paradigm in Matlab Simulink versus the results from Merfeld's velocity storage model for the same motion paradigm.

Off-Vertical Axis Rotation

The OVAR is simulated by rotating the human participant 45 degrees from the vertical. In this position, the subject is rotated with 100 deg/s around the body z-axis. According to Merfeld, it should be taken into consideration that many of the estimated state vectors become fixed in magnitude and direction with respect to inertial space [45]. The oscillatory behavior of the x and y components in Fig. 5.9 are a result of the rotation from the human about these fixed vectors. Furthermore, the otoliths are not activated, so its afferent signals are fixed, because it physically tracks the real gravity vector. When comparing Merfeld's results to the SS prediction model results, then the first remarkable thing is the missing oscillation for the x and y component of the angular velocity. The behavior of the estimated acceleration and gravity components seems quite similar. Although, the frequency of the oscillation and amplitude do deviate from Merfeld's results. Finally, the simulation for the SS prediction models starts with the 45 degrees tilt instead of just simulating the rotation around the human's z-axis where the tilt is already established.

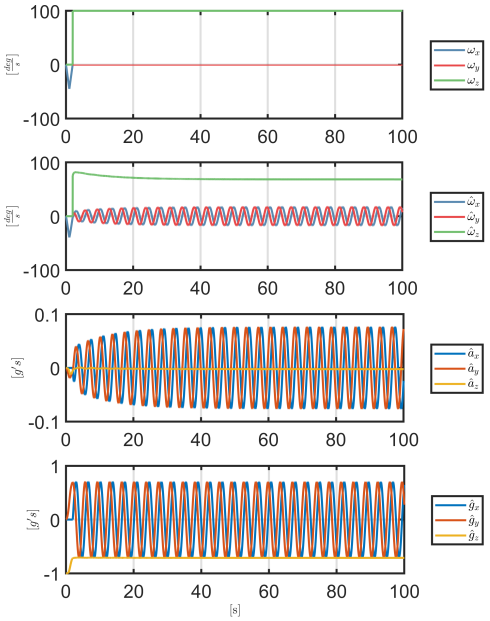

Figure 5.9: ”OVAR”-model predictions of Merfeld’s model. Panel A shows the yaw velocity trapezoid (ω_z) that is applied about an axis tilted 45 degrees from the vertical. Panel B shows predicted central estimates of angular velocity, Panel C shows the predicted central estimates of linear acceleration. D shows the central estimates of gravity.

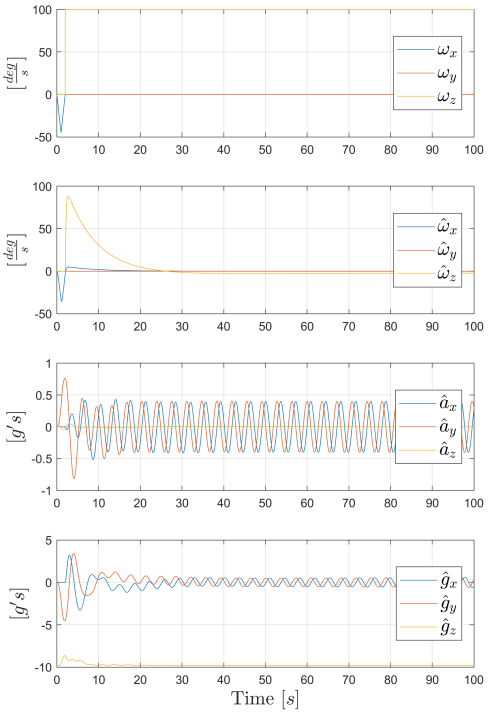

Figure 5.10: OVAR results from generated three-dimensional velocity storage model in Matlab Simulink.

Somatogravic Illusion

The Somatogravic Illusion can be described as the development of a pitch up movement sensation when being forward accelerated at a constant rate on a sled. Again, the results of both Newman’s model and the SS prediction model for this visual-vestibular sensory paradigm can be found in Fig. 5.11 and Fig. 5.16. The observer model of Newman displays similar results as the actual visual-vestibular interaction mechanism responsible [46]. On the other hand, the results from the SS prediction model are displaying a deviation. At the start of the simulation, the rise time of the linear acceleration and pitch angle is slower than Newman’s model. Furthermore, the rise time of the light condition is slower than the dark condition, which means there is a difference that is not visible in Newman’s model. However, the behavior at the end is again quite similar. In light conditions, there will be a constant sensation of acceleration due to the addition of the visual and vestibular input suppressing the somatogravic illusion.

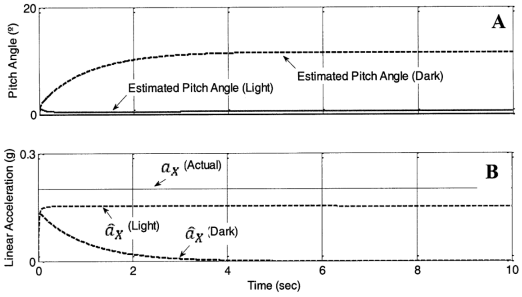

Figure 5.11: Newman's model predictions for a forward linear acceleration on a sled (Somatogravic Illusion). Reprinted from [46].

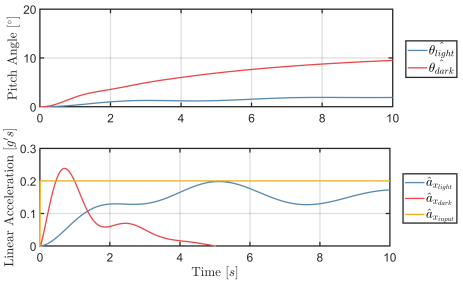

Figure 5.12: SS model predictions for a forward linear acceleration on a sled (Somatogravic Illusion)

Forward Linear Vection

For this visual sensory paradigm, a human participant is seated upright and subjected to a 15 cm/s step visual linear velocity input. The CNS gradually accepts the visual input resulting in vection, an illusory sensation of linear motion [46]. Fig. 5.13 and Fig. 5.14 present the results of a forward linear vection stimulus from Newman's model and the SS sickness model. Newman's model fails to predict the vection onset delay as seen with the constant velocity rotation around an earth vertical axis in contrary to the SS prediction model. There is also a slight overshoot visible from the SS prediction model results that differ from Newman's model predictions.

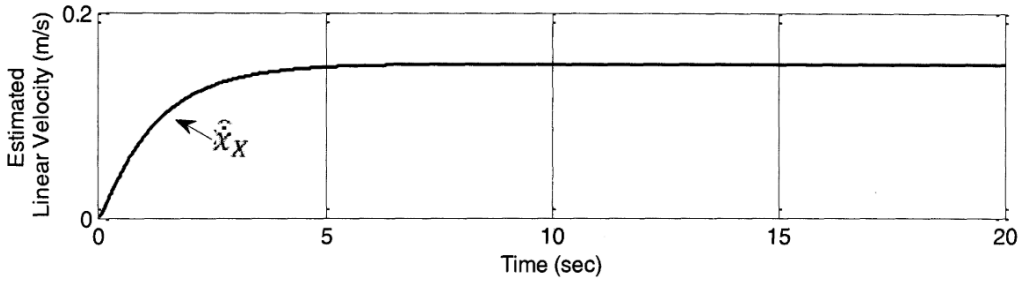

Figure 5.13: Newman's model predictions of a forward linear vection stimulus. Reprinted from [46].

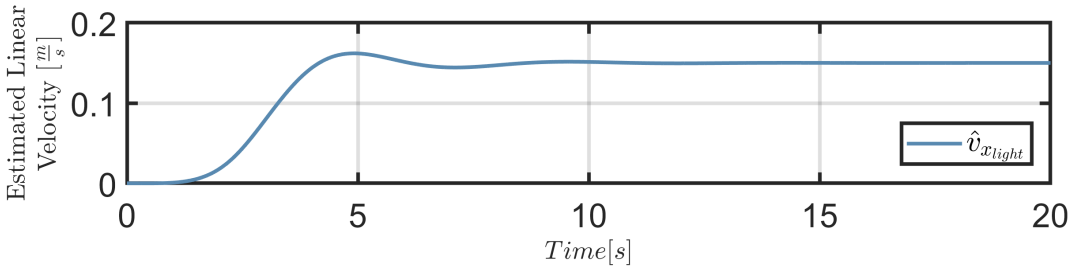

Figure 5.14: SS model predictions of a forward linear vection stimulus.

5.2.3. Results simulation data

The second main objective of this research is to see if motion attenuates SS when human participants are being driven around within an urban environment. The developed SS prediction should be able to predict MSI such that hypotheses can be formed for the research question. Participants will be driven around in an eight shaped form for 45 minutes. More about the experimental design can be found in Chapter 6. The tracks have already been driven and the data are saved, so it can be used as input for the new SS prediction model. Furthermore, the model is capable of presenting the results for the case with motion and without motion. These results can be found in Fig. 5.15. The results for the motion and without motion case are presented in the top figure and the 6 DOF vehicle output data is presented in the two lower figures. Both an eight-shaped track and a simple curve to the left was used as input data. The figures show that less people get sick when motion is available for both motion profiles. Finally, the eight-shaped track shows more people getting sick than the curve to the left.

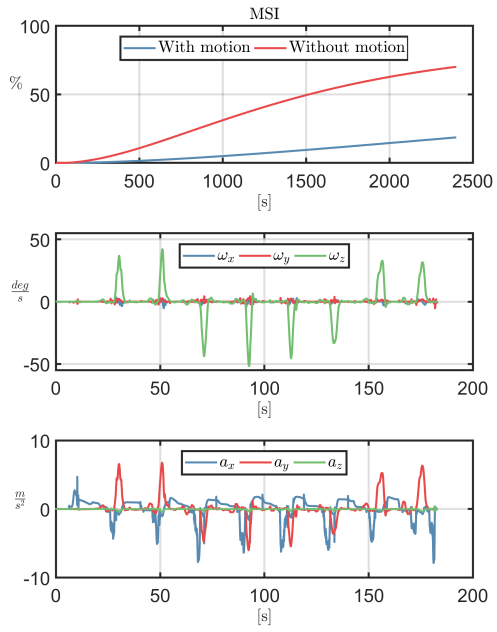

Figure 5.15: SS model prediction using simulation data acquired within BMW as input for a motion and no motion condition.

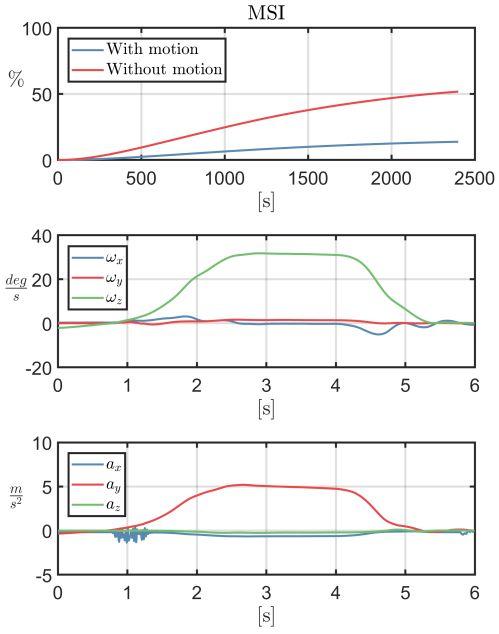

Figure 5.16: SS model predictions for a forward linear acceleration on a sled (Somatogravic Illusion)

5.3. Discussion

Initially, the model is verified for experimentally obtained MS data. Altogether, it can be stated that the first iteration of the SS prediction model is relatively good compared to other models. However, the amount of data to verify the model for its effectiveness of correctly predicting sickness are less and should be elaborated on.

Secondly, the perception part of the model was assessed by comparing the model output data to some motion and sensory paradigms to see if the data matches the earlier performed research in this area. The model output is already similar to the data considering the different kinds of motion and sensory paradigms. For the constant velocity rotation about an earth vertical axis case it is clear that values do not match the exact results of Newman. On the one hand, the difference can be explained by the implementation of different transfer functions to describe the dynamics of the SCC, which highly affects the decay of the angular velocity rotation in the dark situation. On the other hand, the SS prediction model uses parameters to determine the vection delay. These values could be revised to get more similar results to Newman. There is not a clear difference between the fast-rising component and slow rising as described by Newman as well. More research to this part is required to get similar behavior. Both the post-rotary tilt and OVAR results are not sufficient, because the values and behavior deviate from the to be expected outcomes. A possibility to overcome this problem is to use the velocity storage mechanism as employed by Merfeld instead of the subjective vertical conflict as a way to steer the observer towards reality. The somatogravic illusion and forward linear vection results of the SS prediction model are deviating, but the behavior is decent. Changing the parameters and delay components could be a way of producing more equal absolute value compared to Newman's results. And an advantage of the SS prediction compared to Newman's model is that it takes into account vection delays. The visual part of the model must behave sufficiently since VIMS is of main interest during simulator studies and so for this thesis. There are still some paradigms that need to be verified using the new model. Besides the paradigms, the focus should be more on taking into account the characteristics and factors that influence the perception of path, rotation and heading during strong yaw motions as stated by [44]. Subsequently, the SS prediction model can be verified for the experimental data obtained by Nooij [44].

Finally, the SS prediction model can predict SS in light and dark environments and with or without motion. Some vehicle simulation data from BMW are used as input and the results show that people get less sick when motion is available. This conclusion is however based on the fact that the real motion is added. In a simulator, this is not possible and aspects as motion range should be taken into account. Applying limited motion to the simulation requires an adaptation of the weight values as stated in Table 5.1. An extra case should be added, where some motion is available with suitable weight factors. However, based on the results in this chapter, it can be hypothesized that adding motion attenuates SS.

6

Experiment design

This chapter will concern the experimental design of the driving simulation study that will be conducted at the BMW Group, München, as part of this MSc research. The purpose is to study the effect of simulator motion on simulator sickness in a driving simulation environment and this purpose is elaborated on in section 6.1. Then, Section 6.2 goes into more detail about the participants. For this experiment, a 9 degree of freedom (DOF) simulator will be made available by the driving simulation department of the BMW Group, which is discussed in Section 6.3. The experimental conditions and the measurements that will be made can be found in Sections 6.4 and 6.5 respectively. The procedure to be followed for each participant is given in Section 6.6. Finally, the data needs to be analyzed and this analysis is explained in Section 6.7.

6.1. Purpose and Research question

As explained before, experience has shown that urban driving environments are associated with an increased occurrence of simulator sickness (SS) [27] [23]. Curvy roads within cities that bring strong visual flow and changing textures to the human sensory eyes are associated with more SS. When human participants are driving a simulator without or limited vestibular cues, the subjective vertical conflict (SVC) theory tells us that a difference between the sensed vertical and expected vertical will arise causing SS symptoms [67]. Besides the theory, the results of the generated SS prediction model also point out that the motion sickness incidence (MSI) will decrease motion that is congruent with the simulated vehicle motion is provided. Part of the research objective is to attenuate SS during urban driving scenarios with a particular focus on strong yaw motions by adding yaw motion or the vestibular reproduction of the vehicle's yaw motion limited by the simulator capabilities and to verify the results of the proposed SS prediction model. Hence, the following research question was given in Chapter 1:

> What is the effect of adding motion on simulator sickness, when passively driving in urban scenarios containing several sharp turns?

The output of the experiment whose variation is being studied or the dependent variable is simulator sickness. The simulator sickness questionnaire (SSQ) and the misery scale (MISC) are commonly used to get an indication of strength of SS occurrence and will also be employed in this study. On the other hand, motion is the independent variable and represents the input or reason that will be controlled and systematically varied during the experiment. Now, the hypotheses need to be stated to convert the research question into a falsifiable statement. Based on the results of the simulations and literature in the previous chapters, the following hypotheses are formulated and will be tested by the experiment:

- *H1*: If motion is added to a static simulator, then SSQ and MISC scores will be reduced.
- *H2*: If purely yaw motion is added to the static simulator, then SSQ and MISCscores will be reduced compared to the no motion case.
- *H3*: If the limited multi-DOF vestibular reproduction of the vehicle's yaw motion is added to the static simulator, then SSQ and MISC scores will be reduced more than adding just yaw motion.

6.2. Sample description

Participants will be recruited by Spiegel Institute, a contractor contracted by BMW Group. They need to possess a valid driving license. Since the susceptibility of MS is different between people from different ages and genders, the people will be equally divided among the groups by these characteristics. Two other characteristics will be taken into account: the experience with simulators and the experience with MS. For the last one, the motion sickness history questionnaire (MSHQ) needs to be filled in. Based on these results the participants will be divided equally among the three scenarios. A one-factorial between-subjects design will be employed because an adaptation or learning factor cannot be ruled out for this experiment. And since MS depends on adaptation and more specifically can be reduced due to adaptation, this approach is desirable.

The study is approved by the Ethics Commission of the Technical University of Delft and participant should give informed consent before they participate in the experiment. Around 60 to 65 participants will be recruited and they will be compensated for their participation. A total of four weeks will be used to prepare and conduct the experiment.

6.3. Apparatus

The VI-Grade ”DiM Platform” will be used as a driving simulator in the experiment to present the visual and vestibular motion, see also Fig. 6.1. This platform has 9 degrees of freedom and consists out of a Hexapod and Tripod assembly. The hexapod is capable of cueing high-frequency movements ($\pm 0 - 30Hz$) and the tripod is capable of cueing the low-frequency movements ($\pm 0 - 5Hz$). Below a table can be found that summarizes the simulator performance of the combined hexapod and tripod structure.

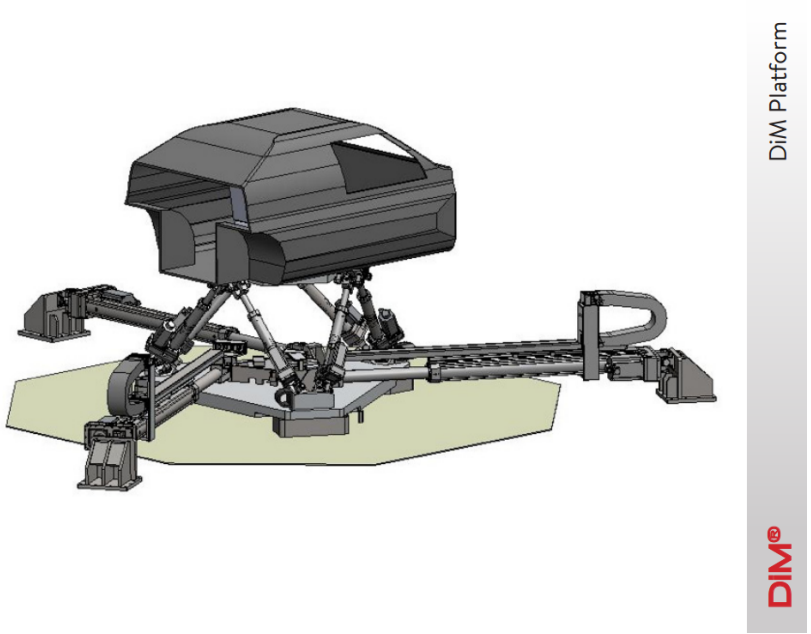

Figure 6.1: DiM Platform. Reprinted from [1].

The climate within the mock-up of the simulator can be controlled by the participants. Sound on the other hand is available in the form of road, motor, and other environmental noises. The projectors that displays the visuals has a field-of-view of 230 degrees, an 8 meter diameter and a height of 3.5 meters.

	Stroke	Max. Velocity	Max. Acceleration
X	±1.08 m	3.7 m/s	37 m/s^2
Y	±1.00 m	3.2 m/s	35 m/s^2
z	±0.22 m	1.6 m/s	35 m/s^2
Roll	±20 °	135 °/s	2500 $°/s^2$
Pitch	±20 °	130 °/s	1000 $°/s^2$
Yaw	±45 °	300 °/s	3900 $°/s^2$

Table 6.1: DiM Platform characteristics.

6.4. Experimental conditions

The variable to change or the independent variables ”motion” consists of three scenarios. Participants will be driven passively around an eight shaped track as can be seen in Fig. 6.2. An urban environment will be simulated with a number of sharp 90 degree turns, passengers and large city buildings. Thus, the scenery can be characterized as eliciting a rather strong optic flow. The first scenario will be without movement, so subjects will be driven the track with purely visual inputs. Secondly, participants will sense purely yaw motions, which will be presented almost one to one taking into account the limitations of the simulator (Table 6.1). The third scenario will present the output of a wash-out based motion cueing algorithm that will be tuned to have the best possible cueing.

Figure 6.2: Driving track

6.5. Measurements

Participants will start by filling in the MSHQ. It contains a brief instruction and some initial questions about the personal details such as age and gender. Then twelve questions will be asked about the experience with MS while traveling in different forms of transport. Subjects are also asked to give a self-rating of their susceptibility to MS compared to other people and there will also be two questions about their present and past health [93].

A specific tool to measure simulator sickness is the SSQ by Kennedy, Lane, Berbaum, and Lilienthal [29]. As explained in the literature review, SS differs somewhat from MS and this questionnaire takes these variations into account. This questionnaire is seen as the single most important questionnaire regarding simulator, cyber or virtual reality sickness [94]. There are 16 items on the SSQ that will be rated by the participant on a 4-point Likert-scale. These items are divided over three sub-scales [29] [94] and eventually a total SSQ score and scores for every sub-scale can be calculated. The three sub-scales are:

- Disorientation (e.g., vertigo, concentration issues);
- Nausea (e.g., general discomfort, nausea);
- Oculomotor Issues (e.g., eyestrain, focusing issues).

Secondly, the misery scale (MISC) will be employed, which is 10-point Likert-scale. This subjective measurement scale has the advantage that people may feel sick without ever reaching emesis. It gives a more sensitive measure of sickness than for example the MSI, which is desirable for when studying a small group of participants as will be done in the present experiment [28]. This scale will be used as a verbal rating scale, which will be monitored every minute during the stimulus. Subjects are only requested to give a number, which takes only a couple of seconds, as soon as they are familiar with the rating scale. The misery scale according to [28] can be found in Table 6.2.

Symptom		Score
No problems		0
Uneasiness (no typical symptoms)		1
Dizziness, warmth, headache, stomach awareness, sweating, ...	vague	2
	slight	3
	fairly	4
	severe	5
Nausea	Slight	6
	fairly	7
	severe	8
	(near) retching	9
Vomiting		10

Table 6.2: Misery Scale (MISC)

A maximum of 6 to 7 on the misery scale will be allowed during the experiment, which means people will only suffer from minor nausea effects. If people do get sick, the simulation will be stopped immediately. There will be vomit bags available for the worst-case scenario. Furthermore, there will be some sweets that can counteract the nausea feeling.

6.6. Procedure

An overview of the procedure can be found in Table 6.3. Participants will start filling out the informed consent followed by some instructions about the questionnaires and experiment. They will fill in the required questionnaires and get a safety briefing before starting the simulation. In total, participants will be driven for 45 minutes from which 5 minutes are familiarization and this data can be neglected in data analysis. After the experiment, the SSQ will be filled in again and there will be some time for questions and answers. Furthermore, a buffer of 15 minutes is taken into account between participants for technical failures or time issues such as subjects having a delay before the start of the time slot.

Step	Duration (min)	Notes
Pick-up and welcome	10	
Instructions at desk	3	Includes informed consent
Pre-test Interview	10	Fill in SSQ/MSHQ
Instructions in simulator	2	Incl. Safety instructions
Familiarization	5	Familiarization
Experiment	45	
BUFFER	15	
Post-test Interview	5	Fill in SSQ
Q&A	2	Question and Answers
Departure	2	
Sum	75	

Table 6.3: Experimental procedure

6.7. Data analysis

The MISC data can be categorized as ordinal data meaning that a non-parametric test need to be selected. First, the amount of drop-outs will be determined based on the amount of MISC scores above 6 or two times 6 and indicated with a zero (completed experiment) or one (dropped out). Subsequently, a Pearson Chi-square test will be performed on the data because it is categorical and a between-subject design is employed. This statistical test will investigate the effect of the three motion cases (case 1 vs. case 2 vs. case 3) on the amount of drop-outs and is used to test the effect of just motion on the amount of drop-outs (case 1 vs. case 2 + case 3). Secondly, the MISC scores will be ordered per case and the MISC end values will be used to test if there is a difference in MISC scores between the three cases by using a Pearson Chi-square test as well.

The SSQ results will be continuous data. A one-way ANOVA test will be performed, since the independent variable (motion) is categorical, more than two predictors (case 1, 2 and 3) are involved and a between-subjects design is employed. However, it requires all data sets to be normally distributed.

Finally, the experimental data will be based on the MISC, with a maximum value of 7. This means that the percentage of people that got sick, can be calculated with 7 to be defined as sick. However, the MSI is the percentage of people that get sick with a value of 10 on the MISC. So, to see if the model output data is similar to the experimentally obtained data, a correlation parameter will be employed.

7

Conclusion

The aim of this research is to better understand SS by developing a mathematical model that can predict SS when driving in urban environments and to understand the effects of adding motion to a fixed-based simulator. As first step, this preliminary thesis presents the results of an initial SS prediction model and the theory that substantiates the model. The first main question (MQ1) is *"Which state-of-the-art theories on MS, perceptual-based MS models and knowledge about SS would identify and verify a SS prediction model that includes visual system?"*, which can already be answered partly.

The theory that substantiates the model consists of an explanation of MS, the theories that try to describe its etiology and existing mathematical MS models. From the first part of the theory, that is related to sub-question 1.1 (SQ1.1), it can be concluded that the MS and SS remain phenomena that are hardly understood within the literature. Furthermore, since this research focuses particularly on SS in urban environments where the visual system is essential, knowledge of VIMS should be used. Furthermore, the human sensation of motion or human spatial perception plays an important role in understanding SS and MS. There are multiple theories that try to describe the etiology of MS (SQ1.2), but the sensory conflict theory is the most accepted theory within the literature. This theory can describe many cases that induce MS, but it is still not an established theory yet since it cannot be falsified. The SVC-theory is a simplification of the sensory conflict theory and focuses just on one conflict. This theory is also implemented mathematically and seems suitable, but it does not account for circular vection related sickness and does not give a clear cut answer to the etiology of MS as well. To answer SQ1.3, a reference can be made to Table 4.1. These models are all observer-based and incorporate a mechanism to solve the GIF resolution problem. The visual system can be implemented (SQ1.4) by using linear weighting addition techniques or by adding visual pathways as done by Newman. So, a new SS prediction model requires (SQ1.5) an assessment of sickness, an implementation of the vestibular and visual system, it should be verified for multiple motion paradigms, sensory paradigms and experimentally obtained MS data and it should employ multiple dimensions. It can be concluded that the SVC-model has the most potential when extended to multiple DOF and keeping the visual system incorporated. To make SS measurable, it should be quantified. This can be done in two ways (SQ1.6): using the MSI by Bos and Bles [11] or a subjective discomfort scale as done by Oman [9]. This knowledge resulted in the first iteration of a SS prediction model that is based on the model by Bos and Bles [89] and Kamiji [12] and Wada [14]. The model takes into account all the requirements. It can predict SS for vertical ship motions quite accurately. Furthermore, the perception part shows promising results, but some adaptations are required. The next stage of this research should focus on validating the model for more experimentally obtained data, such as the data that will be generated by the experiment, but also by using the data and model implementation suggestions from Nooij [44]. It will remain the first step towards a SS prediction model because factors such as adaptation, the intra-laboratory effect, and individual differences are not considered in this model yet. Besides these factors, the limitations of human perception modeling such as the inability to model the complexity of the human brain and the lack of perceptual data should be taken into account.

Secondly, to better understand the effects of adding motion to a fixed-based simulator, a second main question (MQ2) is: *"What is the effect of adding motion on SS, when driving in urban scenarios containing several sharp turns?"*, will be answered after the experiment has been executed. The first hypothesis, based on the sensory conflict theory and the first iteration of the SS prediction model, is that adding motion to a fixed-based simulator attenuates the number of people that get sick. An experiment in a 9-DOF simulator at the BMW group will be executed in which 64 participants will be driven around in an urban environment for 45 minutes. SS will be assessed online using the MISC scale. Offline, the SSQ will be filled in by the participants before and after the drive. The results of the experiment will be used to update the SS prediction model by validating the model for the experimentally obtained data.

Urban environments are provocative environments to induce SS and this scenario is used as a research case to investigate the effects of adding motion to a fixed-based simulator on SS. With this research, another step is taken towards a better understanding of SS in particular.

Bibliography

[1] VI-Grade, . Technical Manual Dynamic Servo DiM Platform. Technical report.

[2] Hock, P., Kraus, J., Babel, F., Walch, M., Rukzio, E., and Baumann, M. How to Design Valid Simulator Studies for Investigating User Experience in Automated Driving. In *Proceedings of the 10th International Conference on Automotive User Interfaces and Interactive Vehicular Applications - AutomotiveUI '18*, pages 105–117, 2018.

[3] Brooks, J. O., Goodenough, R. R., Crisler, M. C., Klein, N. D., Alley, R. L., Koon, B. L., Logan, W. C., Ogle, J. H., Tyrrell, R. A., and Wills, R. F. Simulator sickness during driving simulation studies. *Accident Analysis & Prevention*, 42(3):788–796, 2010.

[4] Kay, P. Feasibility of Virtual Environments to Develop Future Driving Cycles. In *International Powertrains, Fuels & Lubricants Meeting*, sep 2018.

[5] De Winter, J., Happee, R., and Leeuwen, van P. Advantages and disadvantages of driving simulators: a discussion. *Proceedings of Measuring Behavior*, (January):47–50, 2012.

[6] Birren, J. Motion sickness: its psychophysiological aspects. A survey report on human factors in undersea warfare. Technical report, Committee on Undersea Warfare, National Research Council, Washington, D.C., 1949.

[7] Dobie, T. G. Motion Sickness: A Motion Adaptation Syndrome, 2019.

[8] Reason, J. T. Motion sickness adaptation: a neural mismatch model. *Journal of the Royal Society of Medicine*, 71(11):819–29, 1978.

[9] Oman, C. M. A Heuristic Mathematical Model for the Dynamics of Sensory Conflict and Motion Sickness. *Acta Oto-Laryngologica*, 94(SUP 392):4–44, 1982.

[10] McCauley, M. E., Royal, J. W., Wylie, C. D., O'Hanlon, J. F., and Mackie, R. R. Motion sickness incidence: exploratory studies of habituation, pitch and roll, and the refinement of a mathematical model. Technical report, 1976.

[11] Bos, J. E. and Bles, W. Modelling motion sickness and subjective vertical mismatch detailed for vertical motions. *Brain Research Bulletin*, 47(5):537–542, 1998.

[12] Kamiji, N., Kurata, Y., Wada, T., and Doi, S. Modeling and validation of carsickness mechanism. In *SICE Annual Conference 2007*, pages 1138–1143, 2007.

[13] Groen, E. L. and Bos, J. E. Simulator Sickness Depends on Frequency of the Simulator Motion Mismatch: An Observation. *Presence: Teleoperators and Virtual Environments*, 17(6):584–593, oct 2008.

[14] Wada, T., Fujisawa, S., Imaizumi, K., Kamiji, N., and Doi, S. Effect of Driver's Head Tilt Strategy on Motion Sickness Incidence. *IFAC Proceedings Volumes*, 43(13):192–197, 2010.

[15] Nooij, S. A., Pretto, P., Oberfeld, D., Hecht, H., and Bülthoff, H. H. Vection is the main contributor to motion sickness induced by visual yaw rotation: Implications for conflict and eye movement theories. *PLoS ONE*, 12(4):1–19, 2017.

[16] Keshavarz, B., Philipp-Muller, A. E., Hemmerich, W., Riecke, B. E., and Campos, J. L. The effect of visual motion stimulus characteristics on vection and visually induced motion sickness. *Displays*, 2018.

[17] Lewkowicz, R. Modeling Motion Sickness. *The Polish Journal of Aviation Medicine, Bioengineering and Psychology*, 22(3):32–42, 2017.

[18] Johnson, D. M. *Introduction to and review of simulator sickness research*. Number Approved for public release; distribution is unlimited. Rotary-Wing Aviation Research Unit, U.S. Army Research Institute for the Behavioral and Social Sciences, Fort Rucker, AL, 2005.

[19] Benson, A. J. Motion sickness. *G. Dhenin & J. Ernsting (Eds.), Aviation Medicine*, pages 468–493, 1978.

[20] Reason, J. T. and Brand, J. J. *Motion sickness.* Academic Press, London, 1975.

[21] Clark, T. K., Newman, M. C., Karmali, F., Oman, C. M., and Merfeld, D. M. Mathematical models for dynamic, multisensory spatial orientation perception. *Progress in Brain Research*, pages 65–90, 2019.

[22] Sharkey, T. and Mccauley, M. E. Does a motion base prevent simulator sickness? *Flight Simulation Technologies Conference*, 1992.

[23] Klüver, M., Herrigel, C., Preuß, S., Schöner, H.-P., and Hecht, H. Comparing the Incidence of Simulator Sickness in Five Different Driving Simulators. *Driving Simulation Conference 2015*, pages 16–18, 2015.

[24] Blana, E. Driving simulator validation studies: A literature review. Technical report, Institute of Transport Studies, University of Leeds, Leeds, 1996.

[25] Stoner, H., Fisher, D., and Mollenhauer, M. Simulator and Scenario Factors Influencing Simulator Sickness. *Handbook of Driving Simulation for Engineering, Medicine, and Psychology*, 2011.

[26] Wada, T., Fujisawa, S., and Doi, S. Analysis of driver's head tilt using a mathematical model of motion sickness. *International Journal of Industrial Ergonomics*, 63:89–97, 2018.

[27] Mourant, R. R., Rengarajan, P., Cox, D., Lin, Y., and Jaeger, B. K. The Effect of Driving Environments on Simulator Sickness. *Proceedings of the Human Factors and Ergonomics Society Annual Meeting*, 51(18):1232–1236, 2007.

[28] Bos, J. E., MacKinnon, S. N., and Patterson, A. Motion sickness symptoms in a ship motion simulator: effects of inside, outside, and no view. *Aviation, space, and environmental medicine*, 76(12):1111–8, 2005.

[29] Kennedy, R. S., Lane, N. E., Berbaum, K. S., and Lilienthal, M. G. Simulator Sickness Questionnaire: An Enhanced Method for Quantifying Simulator Sickness. *The International Journal of Aviation Psychology*, 3(3):203–220, 1993.

[30] Stoffregen, T. and Riccio, G. *An Ecological Critique of the Sensory Conflict Theory of Motion Sickness*, volume 3. sep 1991.

[31] Cleij, D., Venrooij, J., Pretto, P., Pool, D. M., Mulder, M., and Bülthoff, H. H. Continuous subjective rating of perceived motion incongruence during driving simulation. *IEEE Transactions on Human-Machine Systems*, 48(1):17–29, 2018.

[32] Rolnick, A. and Lubow, R. *Why is the driver rarely motion sick—the Role of controllability in motion sickness*, volume 34. aug 1991.

[33] Kuiper, O. X., Bos, J. E., Schmidt, E. A., Diels, C., and Wolter, S. Knowing What's Coming: Unpredictable Motion Causes More Motion Sickness. *Human Factors: The Journal of the Human Factors and Ergonomics Society*, page 001872081987613, 2019.

[34] Steen, van der F. *Self-Motion Perception*. PhD thesis, Delft Universtity of Technology, 1998.

[35] Correia Grácio, B. J. *The Effects of Specific Force on Self-Motion Perception in a Simulation Environment*. PhD thesis, Technical University of Delft, 2013.

[36] Gibson, J. J. *The perception of the visual world.* Houghton Mifflin, Oxford, England, 1950.

[37] Howard, I. P. and Childerson, L. The Contribution of Motion, the Visual Frame, and Visual Polarity to Sensations of Body Tilt. *Perception*, 23(7):753–762, jul 1994.

[38] Goldberg, J. M. and Fernández, C. Vestibular Mechanisms. *Annual Review of Physiology*, 37(1):129–162, mar 1975.

[39] Raphan, T., Matsuo, V., and Cohen, B. Velocity storage in the vestibulo-ocular reflex arc (VOR). *Experimental Brain Research*, 35(2):229–248, 1979.

[40] Berger, D. R. *Sensor Fusion in the Perception of Self-Motion*. PhD thesis, Universitat Ulm, 2006.

[41] Bos, J. E. and Bles, W. Theoretical considerations on canal-otolith interaction and an observer model. *Biological Cybernetics*, 86(3):191–207, 2002.

[42] Mayne, R. *A Systems Concept of the Vestibular Organs*. feb 1974.

[43] Glasauer, S. and M. Merfeld, D. *Modelling Three Dimensional Vestibular Responses During Complex Motion Stimulation*. 1997.

[44] Nooij, S. A., Nesti, A., Bülthoff, H. H., and Pretto, P. Perception of rotation, path, and heading in circular trajectories. *Experimental Brain Research*, 234(8):2323–2337, 2016.

[45] Merfeld, D. M., Young, L. R., Oman, C. M., and Shelhamer, M. J. A multidimensional model of the effect of gravity on the spatial orientation of the monkey. *Journal of Vestibular Research*, 3(2):141–161, 1993.

[46] Newman, M. C., Oman, C. M., and Darmofal, D. L. *A multisensory observer model for human spatial orientation perception*. PhD thesis, Massachusetts Institute of Technology, 2009.

[47] Bertin, R. and Berthoz, A. Visuo-vestibular interaction in the reconstruction of travelled trajectories. *Experimental brain research. Experimentelle Hirnforschung. Expérimentation cérébrale*, 154:11–21, feb 2004.

[48] Huppert, D., Benson, J., and Brandt, T. A Historical View of Motion Sickness-A Plague at Sea and on Land, Also with Military Impact. *Frontiers in neurology*, 8:114, apr 2017.

[49] Steele, J. E. The symptomatology of motion sickness. In *Fourth symposium on the role of the vestibular organs in space exploration*, Pensacola, Florida, 1968. Naval Aerospace Medical Institute, NASA SP-187.

[50] Pausch, R., Crea, T., and Conway, M. A Literature Survey for Virtual Environments: Military Flight Simulator Visual Systems and Simulator Sickness. *Presence: Teleoperators and Virtual Environments*, 1(3):344–363, jan 1992.

[51] Irwin, J. A. THE PATHOLOGY OF SEA-SICKNESS. *The Lancet*, 118(3039):907–909, 1881.

[52] Bos, J. E., Bles, W., and Groen, E. L. A theory on visually induced motion sickness. *Displays*, 29(2):47–57, 2008.

[53] Matas, N. A., Nettelbeck, T., and Burns, N. R. Dropout during a driving simulator study: A survival analysis. *Journal of Safety Research*, 55:159–169, 2015.

[54] Cheung, B. and E Money, K. *The influence of age on susceptibility to motion sickness in monkeys*, volume 2. 1992.

[55] Schwab, R. S. CHRONIC SEASICKNESS*. *Annals of Internal Medicine*, 19(1):28–35, jul 1943.

[56] McGuinness, J., Bouwman, J. H., and Forbes, J. M. Simulator sickness occurrences in the 2E6 Air Combat Maneuvering Simulator (ACMS). Technical report, FL: Naval Training Equipment Center, Orlando, 1981.

[57] Mooij, H. *Motion Cues in Flight Simulation and Simulator Induced Sickness*. Number 433. 1988.

[58] Seay, A. F., Krum, D. M., Hodges, L., and Ribarsky, W. Simulator sickness and presence in a high FOV virtual environment. In *Proceedings IEEE Virtual Reality 2001*, pages 299–300, 2001.

[59] Keshavarz, B., Hecht, H., and Zschutschke, L. Intra-visual conflict in visually induced motion sickness. *Displays*, 32(4):181–188, 2011.

[60] Nooij, S. A., Pretto, P., and Bülthoff, H. H. More vection means more velocity storage activity: a factor in visually induced motion sickness? *Experimental Brain Research*, 236(11):3031–3041, 2018.

[61] Keshavarz, B., Riecke, B. E., Hettinger, L. J., and Campos, J. L. Vection and visually induced motion sickness: how are they related? *Frontiers in Psychology*, 6(472), 2015.

[62] Wood, R. W. The 'Haunted Swing' illusion. *Psychological Review*, 2(3):277–278, 1895.

[63] Steen, van der F. and Kamphuis, H. H. The environment provides the reference frame for self-motion perception. In *Conference on human decision making and manual control*, page 65, Delft, 1995. Delft University of Technology.

[64] Bonato, F., Bubka, A., Palmisano, S., Phillip, D., and Moreno, G. *Vection Change Exacerbates Simulator Sickness in Virtual Environments*, volume 17. jun 2008.

[65] Hosman, R., Cardullo, F., and Bos, J. *Visual-Vestibular interaction in motion perception*. aug 2011.

[66] Konno, H., Fujisawa, S., Imaizumi, K., Wada, T., Kamiji, N., and Doi, S. *Analysis of Driver's Head Movement by Motion Sickness Model*. mar 2019.

[67] Bles, W., Bos, J. E., De Graaf, B., Groen, E., and Wertheim, A. H. Motion sickness: Only one provocative conflict? *Brain Research Bulletin*, 47(5):481–487, 1998.

[68] Wada, T., Kamij, N., Doi, S. S. S., Kamiji, N., and Doi, S. S. S. *A Mathematical Model of Motion Sickness in 6DOF Motion and Its Application to Vehicle Passengers*. jan 2013.

[69] Oman, C. M. Sensory conflict theory and space sickness: our changing perspective. *Journal of Vestibular research*, 8(I):51–56, 1998.

[70] Held, R. Exposure-History as a Factor in Maintaining Stability of Perception and Coordination. *The Journal of Nervous and Mental Disease*, 132(1):26–32, 1961.

[71] Holst, von E. Relations between the Central Nervous System and the peripheral organs. *The British Journal of Animal Behaviour*, 2(3):89–94, 1954.

[72] Treisman, M. *Motion sickness: An evolutionary hypothesis*, volume 197. aug 1977.

[73] Riccio, G. E. and Stoffregen, T. A. An ecological Theory of Motion Sickness and Postural Instability. *Ecological Psychology*, 3(3):195–240, sep 1991.

[74] Dennison, M. S. and D'Zmura, M. Cybersickness without the wobble: Experimental results speak against postural instability theory. *Applied Ergonomics*, 58:215–223, 2017.

[75] Warwick-Evans, L. A., Symons, N., Fitch, T., and Burrows, L. Evaluating sensory conflict and postural instability. theories of motion sickness. *Brain Research Bulletin*, 47(5):465–469, 1998.

[76] Von Holst, E. and Mittelstaedt, H. The Principle of Reafference: Interactions Between the Central Nervous System and the Peripheral Organs. *Perceptual Processing: Stimulus Equivalence and Pattern Recognition*, (1950):41–72, 1950.

[77] Ji, J. T. T., So, R. H. Y., and Cheung, R. T. F. Isolating the Effects of Vection and Optokinetic Nystagmus on Optokinetic Rotation-Induced Motion Sickness. *Human Factors*, 51(5):739–751, oct 2009.

[78] Bles, W. Coriolis effects and motion sickness modelling. *Brain Research Bulletin*, 47(5):543–549, 1998.

[79] Kalman, R. E. and Bucy, R. S. New Results in Linear Filtering and Prediction Theory. *Journal of Basic Engineering*, 83(1):95–108, 1961.

[80] Wonham, W. On the Separation Theorem of Stochastic Control. *SIAM J. Control*, 6, 1971.

[81] Merfeld, D. M. and Zupan, L. H. Neural Processing of Gravitoinertial Cues in Humans. III. Modeling Tilt and Translation Responses. *Journal of Neurophysiology*, 87(2):819–833, 2002.

[82] Glasauer, S. *Interaction of Semicircular Canals and Otoliths in the Processing Structure of the Subjective Zenith*, volume 656. 1992.

[83] Haslwanter, T., Jaeger, R., Mayr, S., and Fetter, M. Three-dimensional eye-movement responses to off-vertical axis rotations in humans. *Experimental Brain Research*, 134(1):96–106, 2000.

[84] Merfeld, D. M. and Young, L. R. The vestibulo-ocular reflex of the squirrel monkey during eccentric rotation and roll tilt. *Experimental Brain Research*, 106(1):111–122, 1995.

[85] M. Merfeld, D. *Modeling Human Vestibular Responses during Eccentric Rotation and Off Vertical Axis Rotation*, volume 520 Pt 2. feb 1995.

[86] Nijhawan, R. Neural delays, visual motion and the flash-lag effect. *Trends in Cognitive Sciences*, 6(9):387–393, 2002.

[87] Bos, J. E., Bles, W., and Hosman, R. J. A. W. Modeling human spatial orientation and motion perception. In *AIAA Modeling and Simulation Technologies Conference and Exhibit*, 2001.

[88] Mittelstaedt, H. A new solution to the problem of the subjective vertical. *Naturwissenschaften*, 70(6):272–281, 1983.

[89] Bos, J. E., Hosman, R. J. A. W., and Bles, W. Visual-vestibular interactions and spatial (dis)orientation in flight and flight simulation. Technical report, TNO, 2002.

[90] Howard, I. P. Interactions Within and Between the Spatial Senses. *Journal of Vestibular Research*, 7(4):311–345, 1997.

[91] Groen, E. L., Jenkin, H. L., and Howard, I. P. Perception of self-tilt in a true and illusory vertical plane. *Perception*, 31(12):1477–1490, 2002.

[92] Vingerhoets, R., Van Gisbergen, J., and Medendorp, W. P. Verticality Perception During Off-Vertical Axis Rotation. *Journal of Neurophysiology*, 97(5):3256–3268, 2007.

[93] Griffin, M. and Howard, H. Motion Sickness History Questionnaire. *ISVR Technical Report*, (No. 283), 2000.

[94] Keshavarz, B. and Hecht, H. Validating an efficient method to quantify motion sickness. *Human Factors*, 53(4):415–426, 2011.

III

Preliminary Research Report Appendices

This part has already been graded under AE4020

Understanding and Attenuating Simulator Sickness when driving in Urban Environments

M. Hogerbrug

A

Derivation of the GIF-resolution equation

From Equation 2.5, the following equation can be derived:

$$\frac{d\vec{g_{sens_e}}}{dt} = \frac{1}{\tau}(\vec{f_e} - \vec{g_{sens_e}}) \tag{A.1}$$

with the subscript ”e” to denote an earth-fixed reference scheme. To rotate the estimate of gravity from an earth fixed reference frame to a head reference frame, a inverse rotation can be used: $\vec{g_{sens_h}} = \vec{R^{-1}}\vec{g_{sens_e}}$. From this equation it follows that $\vec{g_{sens_e}} = \mathbf{R}\vec{g_{sens_h}}$ and this gives:

$$\frac{d\mathbf{R}\vec{g_{sens_h}}}{dt} = \frac{1}{\tau}(\mathbf{R}\vec{f_h} - \mathbf{R}\vec{g_{sens_h}}) \tag{A.2}$$

From here the following notation will be used: $\vec{g_{sens_h}}$ = $\vec{g_{sens}}$. And then we get:

$$\frac{d\mathbf{R}\vec{g_{sens}}}{dt} = \frac{1}{\tau}(\mathbf{R}\vec{f} - \mathbf{R}\vec{g_{sens}}) \tag{A.3}$$

On the left part of this equation, the product rule can be applied, which gives

$$\frac{d\mathbf{R}}{dt}\vec{g_{sens}} + \mathbf{R}\frac{d\vec{g_{sens}}}{dt} = \frac{1}{\tau}(\mathbf{R}\vec{f} - \vec{g_{sens}}) \tag{A.4}$$

Now apply $\mathbf{R}^{-1}$ to both sides of the equation and bringing $\frac{d\mathbf{R}}{dt}\vec{g_{sens}}$ to the right side of the equation results in:

$$\frac{d\vec{g_{sens}}}{dt} = \frac{1}{\tau}(\vec{f} - \vec{g_{sens}}) - \mathbf{R}^{-1}\frac{d\mathbf{R}}{dt}\vec{g_{sens}} \tag{A.5}$$

When you rotate a vector $\vec{x}$ to get a new vector $\vec{y}$, you can use $\vec{y}$ = $\mathbf{R}$ $\vec{x}$. When differentiating this equation and focusing just on the rotation you get:

$$\frac{d\vec{y}}{dt} = \frac{d\mathbf{R}}{dt}\vec{x} \tag{A.6}$$

Another way of obtaining $\frac{d\vec{y}}{dt}$ is by using the cross product of the angular velocity and the vector $\vec{y}$ (both in same frame): $\frac{d\vec{y}}{dt} = \vec{\omega} \times \vec{y}$, which results in:

$$\frac{d\mathbf{R}}{dt}\vec{x} = \vec{\omega} \times \vec{y} \tag{A.7}$$

Now $\vec{x}$ was an example, so if we take $\vec{g_{sens}}$ as this vector we get $\vec{y} = \mathbf{R}\vec{g_{sens}}$ giving:

$$\frac{d\mathbf{R}}{dt}\vec{g_{sens}} = \mathbf{R}\vec{\omega} \times \mathbf{R}\vec{g_{sens}} = \mathbf{R}(\vec{\omega} \times \vec{g_{sens}}) \tag{A.8}$$

Hence, also $\vec{\omega}$ should then be rotated since it was in the same frame as $\vec{y}$. Now, when applying $\mathbf{R}^{-1}$ to both sides of the above equation it can replace the last term of equation (5) giving the final results:

$$\frac{d\vec{g_{sens}}}{dt} = \frac{1}{\tau}(\vec{f} - \vec{g_{sens}}) - \vec{\omega} \times \vec{g_{sens}} \tag{A.9}$$

B

Full Newman Model for human spatial orientation perception

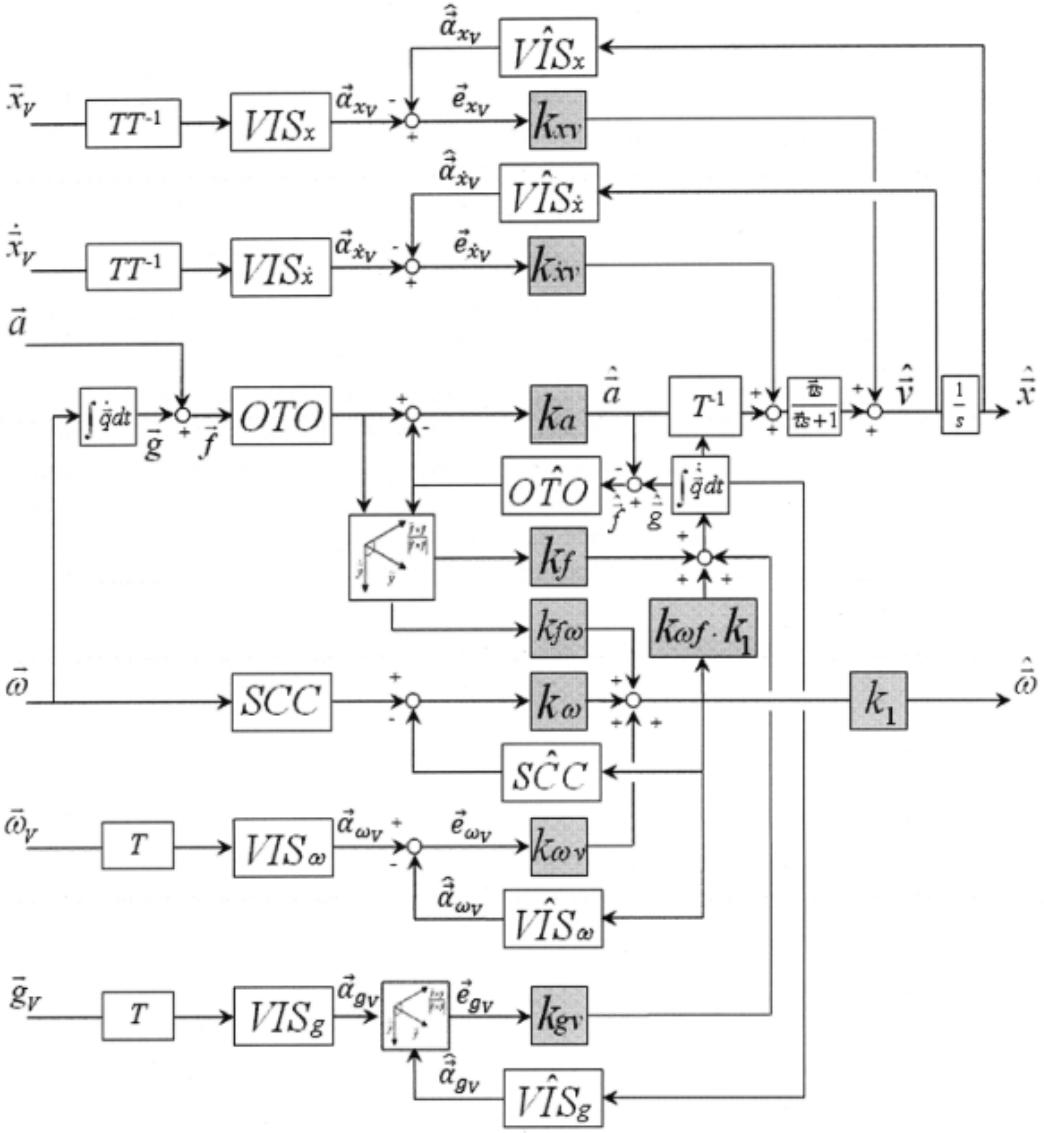

Figure B.1: Newman's model for human spatial orientation perception. Reprinted from [46].

C

One-D Velocity Storage model

The One-D Velocity Storage model of Merfeld can be found below (Figure C.1) and $K_w = 3.0$ is taken from [45]. The results of Merfeld's model for different τ settings are shown in Figure C.2 and compared to the Matlab Simulink implementation results given in Figure C.3.

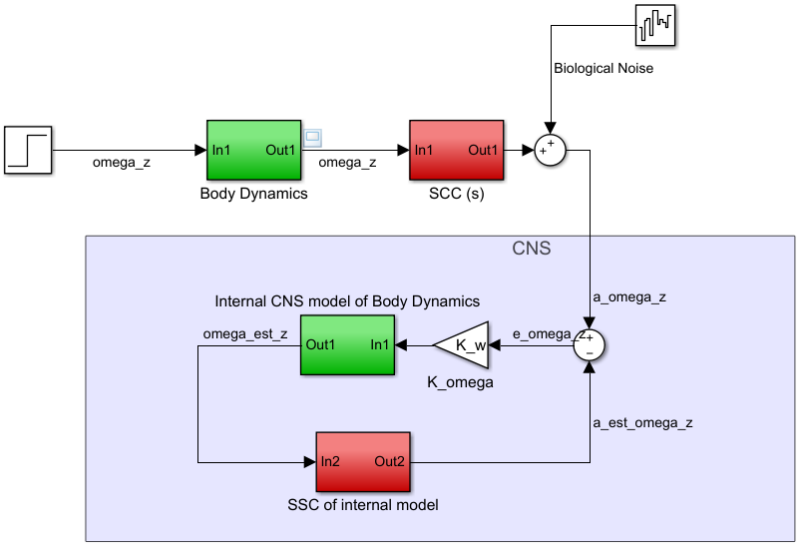

Figure C.1: One-dimensional "Velocity Storage" model of Merfeld [45].

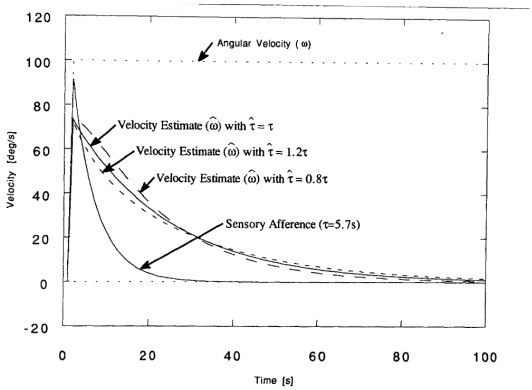

Figure C.2: "Velocity Storage" model predictions. Plot shows the SCC afference ($\tau = 5.7$) predicted to occur due to the constant velocity trapzoid ω. The time course of the central estimate of angular velocity is shown with model time constant equal to the time constant of the SCC ($\hat{\tau} = \tau = 5.7s$), with the model time constant 20 percent less than the SCC time constant ($\hat{\tau} = 0.8\tau = 4.56s$), and with the internal model time constant 20 percent greater than the SCC canal time constant ($\hat{\tau} = 1.2\tau = 6.84s$). Feedback gain ($k_{omega}$) was fixed at 3.0 for all simulations. Reprinted from [45].

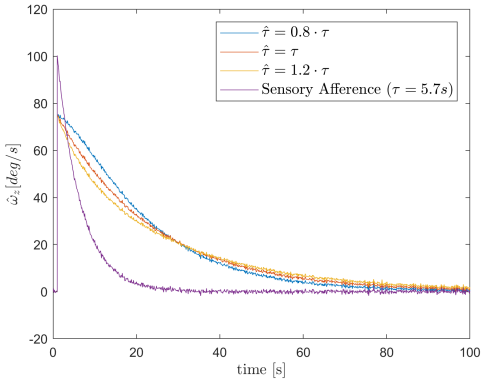

Figure C.3: Results from generated one-dimensional velocity storage model in Matlab Simulink with same parameters as the previous figure.

D

Multidimensional Sensory Conflict Model

The results of Merfeld's sensory conflict model and the comparison to the Matlab Simulink implementation can be found in Figure D.1 till Figure D.4. The sensory conflict model structured is implemented in the Matlab Simulink software is shown in (Figure D.5). A first order transfer function has been chosen by Merfeld to represent the SCC dynamics with the parameter τ_d chosen as 5.7 seconds [45]. The remaining parameters can be found in Table D.1.

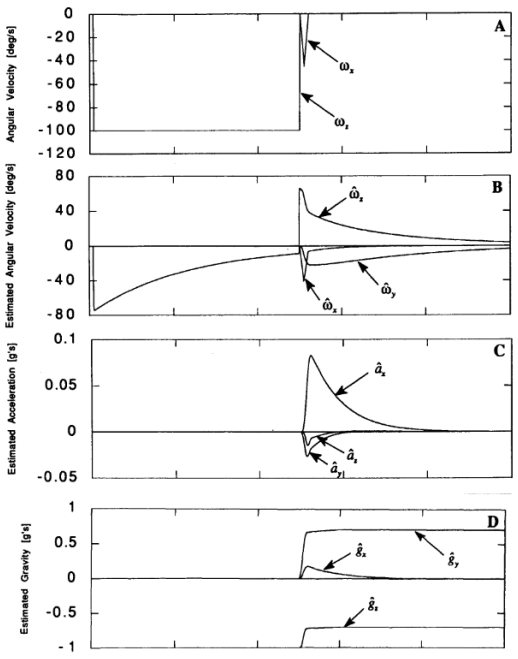

Figure D.1: "Postrotatory tilt"-model predictions. Panel A shows the yaw velocity trapezoid (ω_z), followed by a roll (ω_x), which results in a 45 degree tilt to the left. Panel B shows predicted central estimates of angular velocity, Panel C shows the predicted central estimates of linear acceleration. D shows the central estimates of gravity. Reprinted from [45].

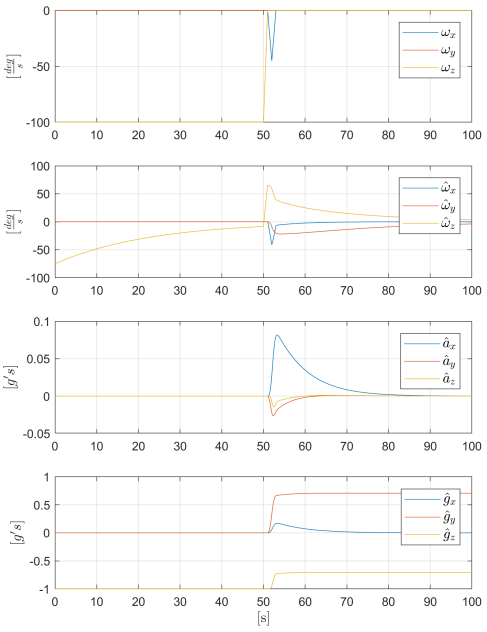

Figure D.2: Results from generated three-dimensional velocity storage model in Matlab Simulink.

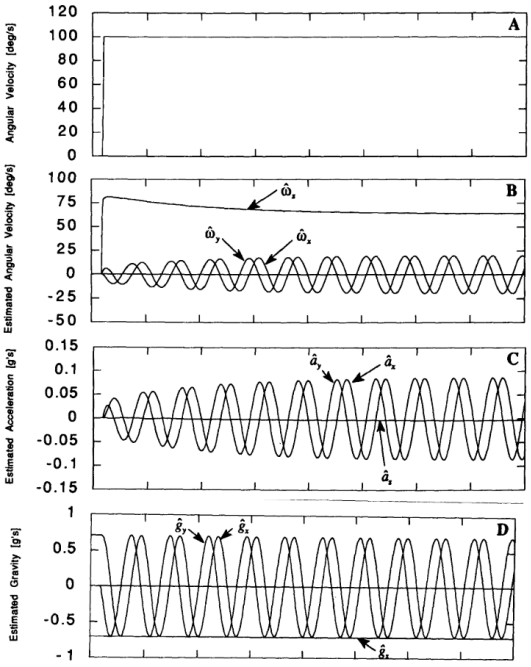

Figure D.3: "OVAR"-model predictions. Panel A shows the yaw velocity trapezoid (ω_z) that is applied about an axis tilted 45 degrees from the vertical. Panel B shows predicted central estimates of angular velocity, Panel C shows the predicted central estimates of linear acceleration. D shows the central estimates of gravity. Reprinted from [45].

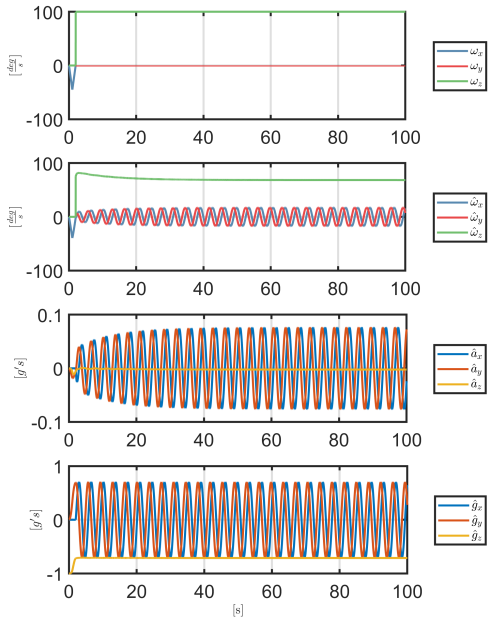

Figure D.4: Results from generated three-dimensional velocity storage model in Matlab Simulink.

Parameter	Value	Unit
k_ω	3.0	-
k_a	-0.9	-
k_f	2.0	-
$k_{f\omega}$	20.0	-

Table D.1: Parameters sensory conflict model Merfeld.

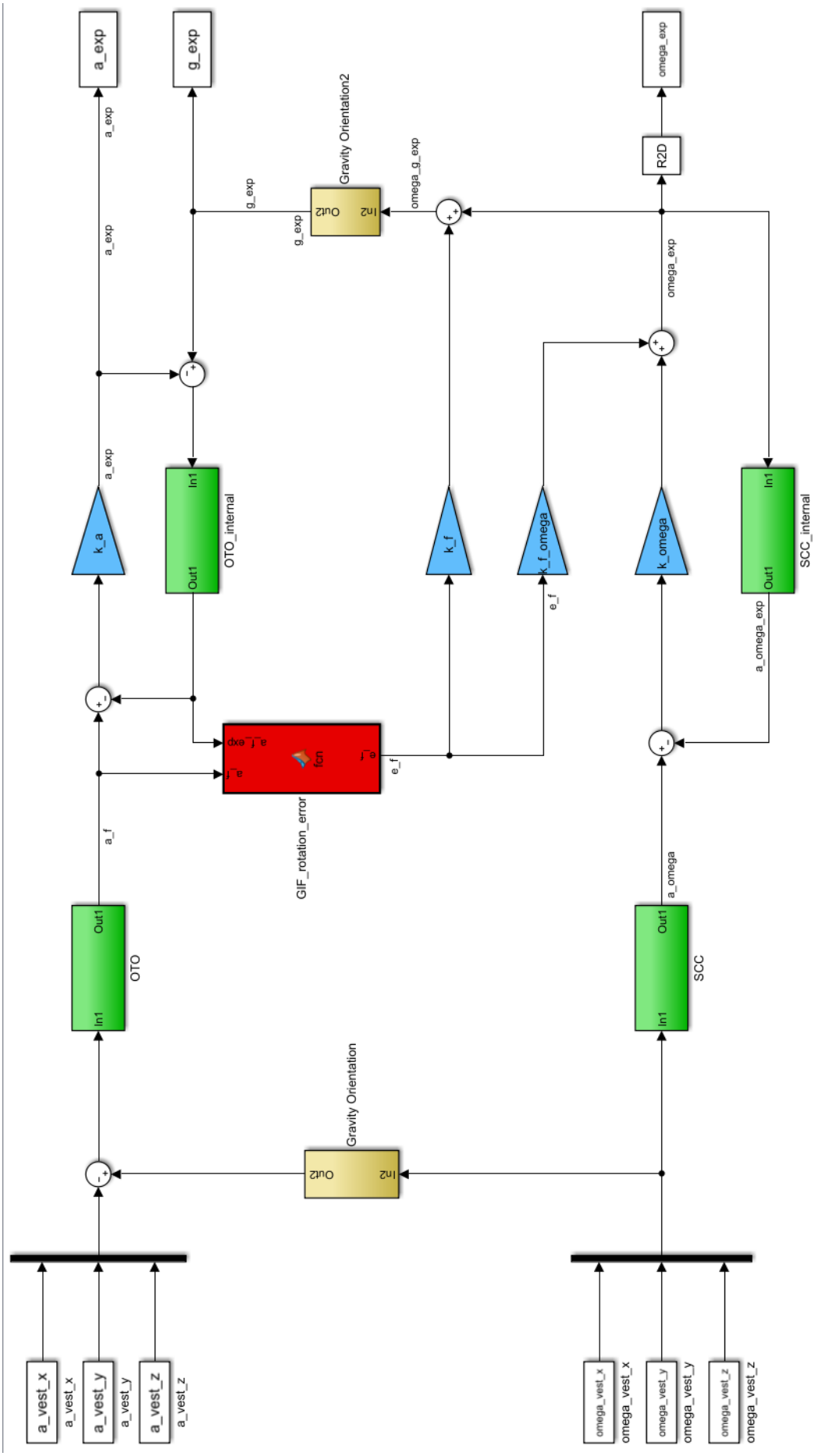

Figure D.5: Matlab Simulink implementation of Merfeld's multidimensioanl sensory conflict model.

E

Visual-vestibular interaction model Bos and Bles

The model results of the visual-vestibular interaction model of Bos and Bles and the results of the Matlab Simulink implementation can be found in Figure E.1 and Figure E.2. The parameters that are used for the visual dynamics, the vestibular dynamics and the velocity wash-out can be found in Table D.1. Furthermore, the values used for the different weighting constant are shown in Table E.2. Finally, Figure E.3 presents the model structure as implemented in Matlab Simulink.

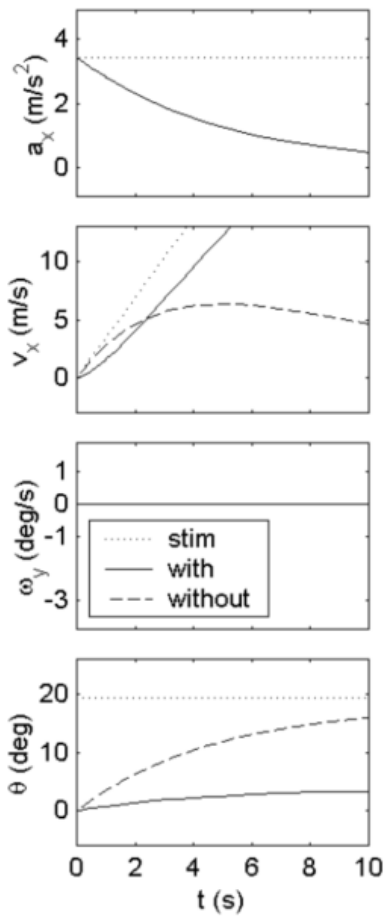

Figure E.1: Model predictions regarding a moderate take-off. Results of a real take-off [89]

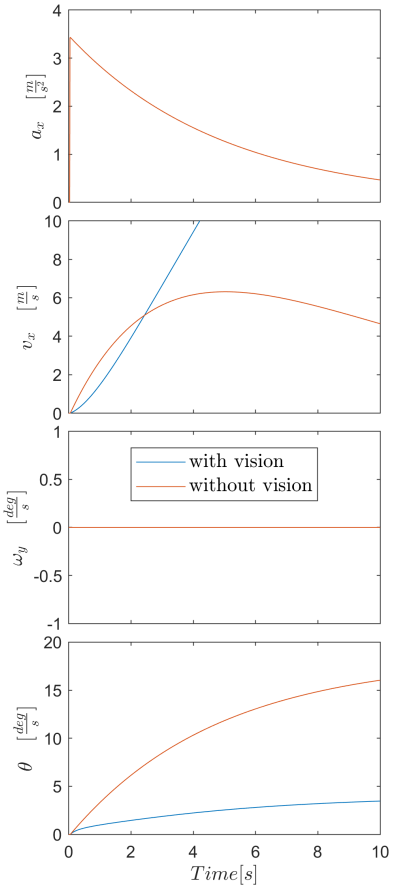

Figure E.2: Model predictions regarding a moderate take-off. Results of a real take-off from the implemented Matlab Simulink model

Parameter	Value	Unit
τ_d	10.0	s
τ	5.0	s
τ_c	10.0	s
τ_v	1.0	s
υ	5.0	s

Table E.1: Parameters for vestibular dynamics, visual dynamics and velocity wash-out.

	w_a	w_v	w_g	w_f	w_i
Light	0.2	0.8	0.2	0.75	0.05
Dark	1.0	0.0	0.95	0.0	0.05

Table E.2: Values of the weighting constants.

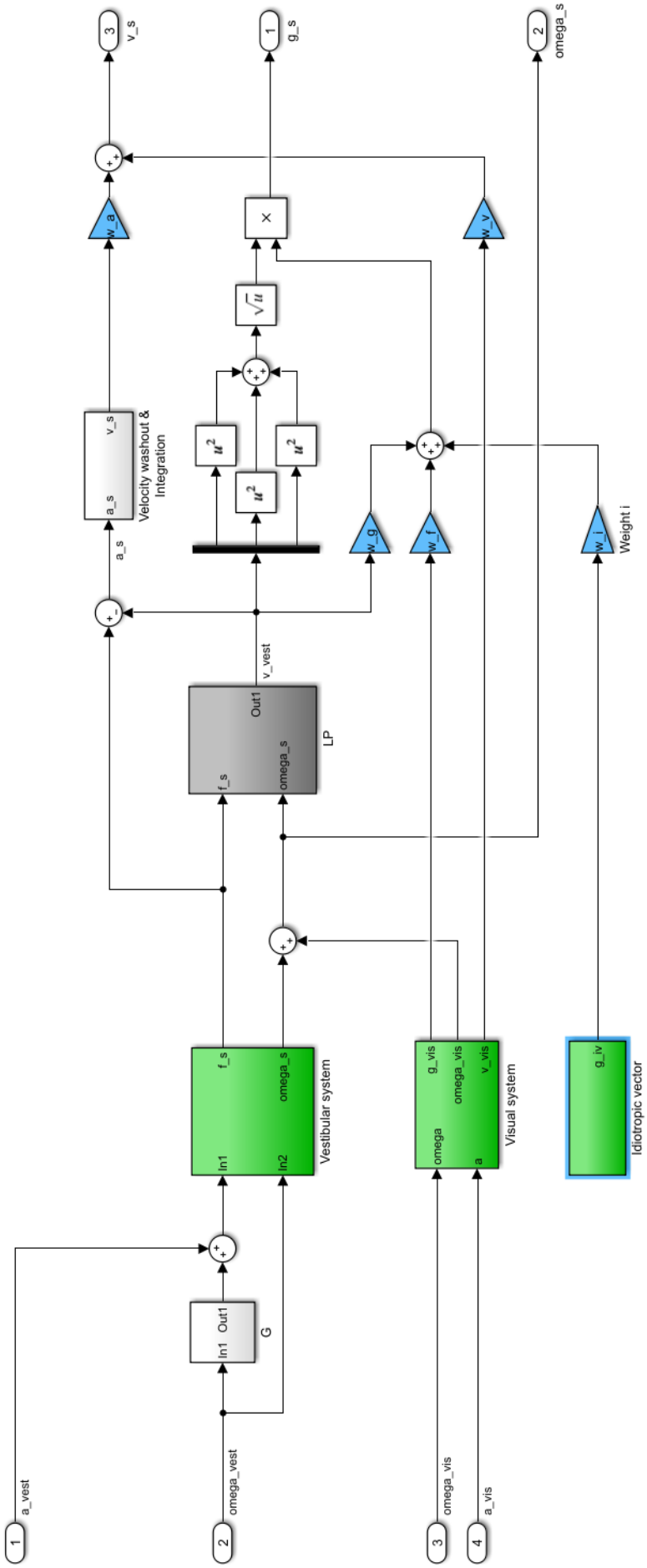

Figure E.3: Matlab Simulink implementation of visual-vestibular interaction model by Bos and Bles.

F

6DOF-SVC model results

The model results of the 6DOF-SVC model of Kamiji and Wada and the esults of the Matlab Simulink implementation can be found in Figure F.1 and Figure F.2. The belonging parameters to generate this results are shown in Table F.1 and the full model structure as used in Matlab Simulink is presented in Figure F.3.

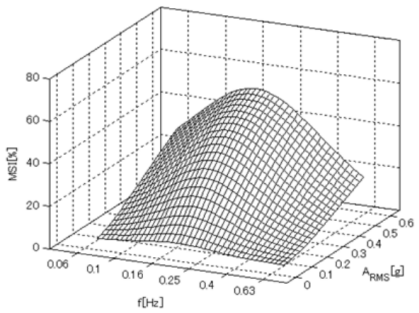

Fig.2 Predicted MSI from horizontal and vertical[10] oscillation

Figure F.1: Predicted MSI for horizontal and vertical linear acceleration oscillation inputs using Kamiji's model. Reprintend from [12].

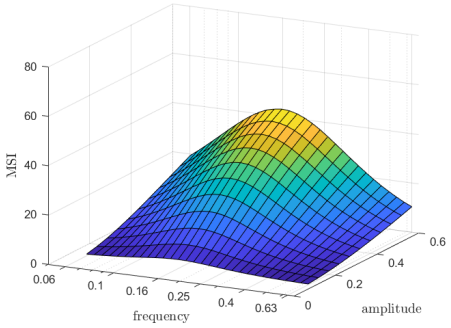

Figure F.2: Matlab Simulink implementation model predictions for horizontal and vertical linear acceleration oscillation inputs.

Parameters	K_a	K_ω	$K_{\omega c}$	K_{vc}	K_{ac}	τ_a	τ_d
values	0.1	0.8	5.0	5.0	1.0	190.0	7.0
Parameters	τ	g	g_0	b	μ	P	
values	5.0	9.80665	[0 0 -g]	0.5	720.0	85.0	

Table F.1: Parameters Kamiji and Wada model as used in the Matlab Simulink implementation

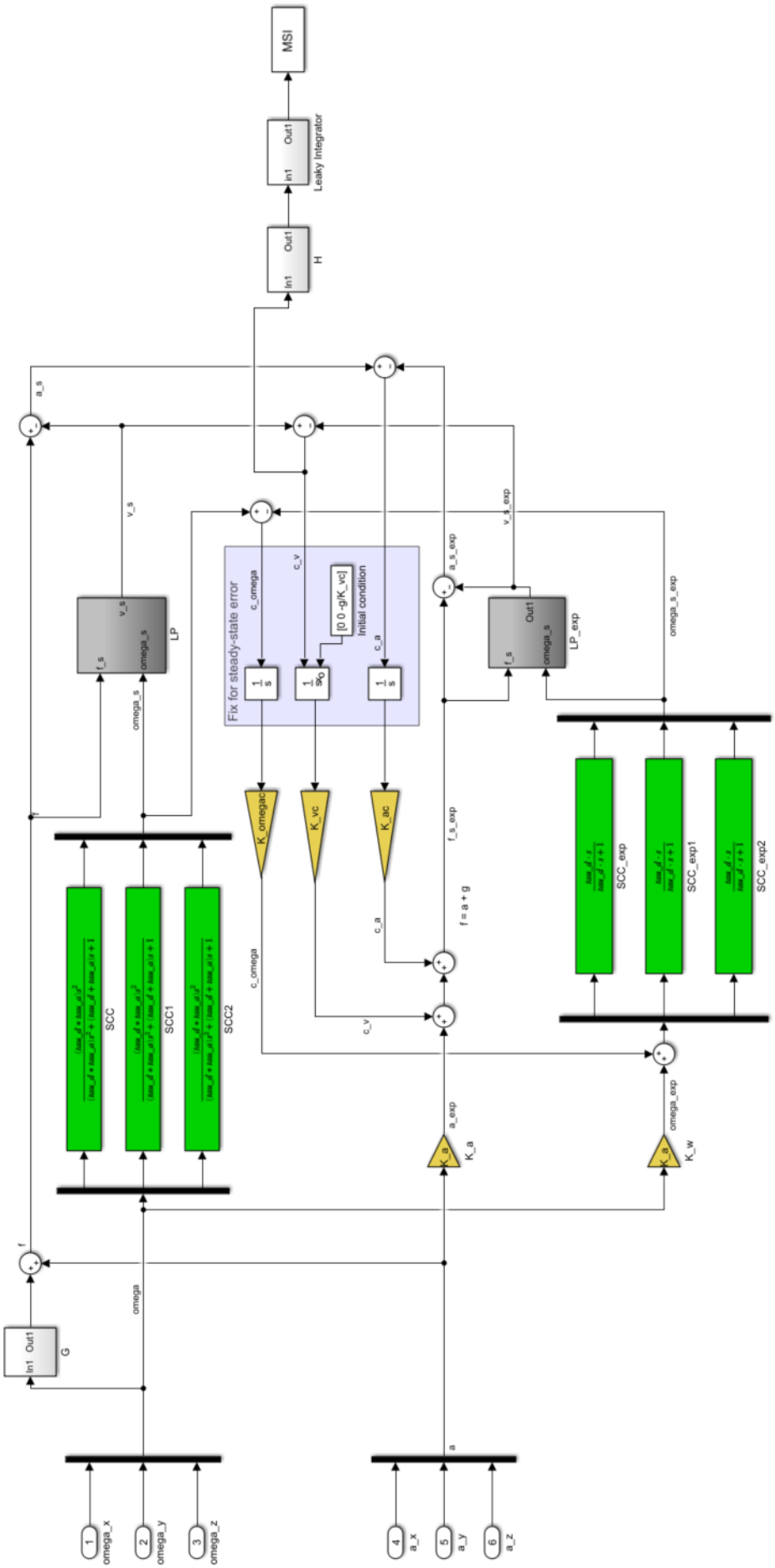

Figure F.3: Matlab Simulink implementation of 6DOF-SVC model Kamiji.

G

SS prediction model input selection

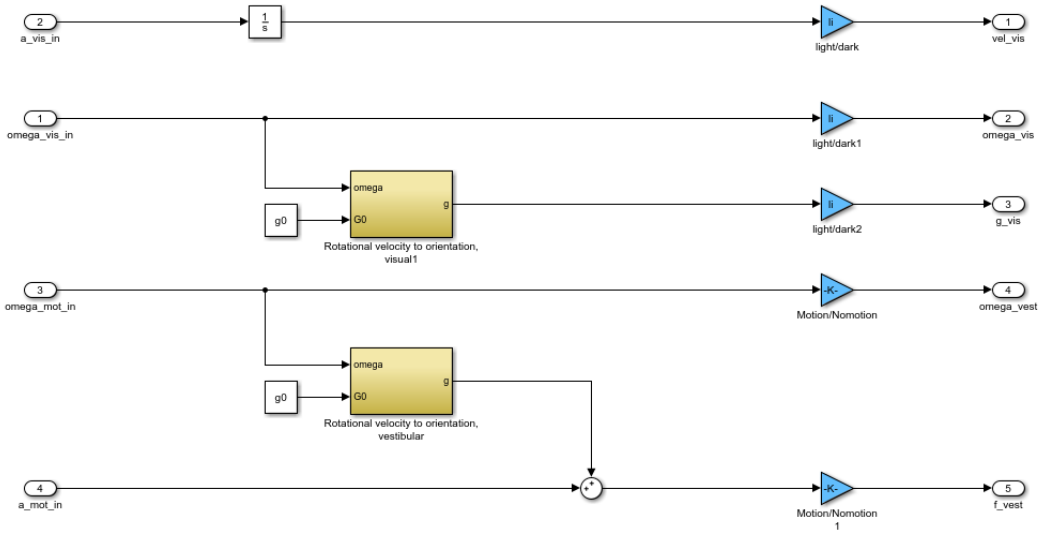

Figure G.1: Input selection for the senses block. Calculation of the gravity orientation with respect to the body. The gains are used to select a dark or light case and to select a motion or without motion case.

IV

Final thesis Appendices

To be graded as part of AE5310 - Thesis Control and Operations

Understanding and Attenuating Simulator Sickness when driving in Urban Environments

M. Hogerbrug

H

Participants overview

Table H.1: Participants overview part 1

	Age	Gender	MS susceptibility	Case	End MISC score	Dropped out	Excluded from Analysis
Participant 1	33	Female	3	3	4	No	No
Participant 2	26	Male	1	2	1	No	No
Participant 3	42	Female	2	1	2	No	No
Participant 4	39	Female	1	2	3	No	No
Participant 5	57	Female	2	1	7	Yes	No
Participant 6	57	Male	1	3	0	No	No
Participant 7	52	Male	1	2	2	No	No
Participant 8	34	Female	2	2	4	No	No
Participant 9	41	Male	1	1	6	Yes	No
Participant 10	32	Male	1	3	0	No	No
Participant 11	23	Male	1	1	1	No	No
Participant 12	57	Female	1	3	2	No	No
Participant 13	21	Female	1	1	0	No	No
Participant 14	26	Male	2	3	1	No	No
Participant 15	28	Female			Did not show up		
Participant 16	60	Male	3	2	6	No	No
Participant 17	19	Female	1	2	2	No	No
Participant 18	46	Female	4	2	0	No	No
Participant 19	45	Male	1	3	0	No	No
Participant 20	28	Female	1	3	0	No	No
Participant 21	41	Female	1	1	6	Yes	No
Participant 22	42	Female	1	3	4	No	No
Participant 23	54	Female	1	1	1	No	No
Participant 24	60	Female	3	1	1	No	No
Participant 25	57	Female	1	3	0	No	Yes
Participant 26	48	Male	1	2	0	No	No
Participant 27	57	Male	3	1	4	No	No
Participant 28	42	Female	1	3	0	No	No
Participant 29	53	Male	1	2	0	No	No
Participant 30	35	Female	1	1	0	No	No
Participant 31	38	Male	2	1	2	No	No

Table H.2: Participants overview part 2

	Age	Gender	MS susceptibility	Case	End MISC score	Dropped out	Excluded from Analysis
Participant 32	23	Male	2	3	4	No	No
Participant 33	29	Male	1	1	2	No	No
Participant 34	42	Female	1	2	7	Yes	No
Participant 35	44	Male	1	2	0	No	No
Participant 36	49	Male	2	3	3	No	No
Participant 37	38	Female	1	1	4	No	No
Participant 38	39	Male	2	2	0	No	No
Participant 39	42	Male	1	1	7	Yes	No
Participant 40	45	Female	1	3	0	No	No
Participant 41	57	Female	1	2	0	No	No
Participant 42	57	Female	1	3	0	No	Yes
Participant 43	32	Female	1	2	0	No	No
Participant 44	59	Male	1	1	0	No	No
Participant 45	31	Female	1	3	5	No	No
Participant 46	59	Male	1	2	0	No	No
Participant 47	42	Male	1	1	7	Yes	No
Participant 48	45	Male	4	3	0	No	No
Participant 49	29	Male	1	2	0	No	No
Participant 50	30	Male	3	3	0	No	No
Participant 51	31	Male	1	1	0	No	No
Participant 52	26	Female	1	3	1	No	No
Participant 53	45	Female	1	2	6	Yes	No
Participant 54	29	Female	1	1	0	No	No
Participant 55	24	Female	1	3	3	No	Yes
Participant 56	51	Female	1	2	2	No	No
Participant 57	19	Male	1	1	0	No	No
Participant 58	42	Female	2	2	3	No	No
Participant 59	35	Male	3	3	3	No	No
Participant 60	49	Male	1	1	0	No	No
Participant 61	32	Female	1	3	0	No	Yes
Participant 62	44	Female	1	2	0	No	Yes
Participant 63	35	Male	1	2	0	No	No
Participant 64	44	Male	1	3	7	Yes	No

Additional MISC results

As mentioned in the Preliminary Research Report, it is not the age that influences the severity or susceptibility of MS directly, but it is the experience of the individual that often comes with age. For the experimental results, 58 participants were used in the analysis with a mean age of 40.5 years. The participants were dived into two groups based on the mean age, see Figure I.1. As we can see here, the median of the younger group (19-40 years) is lower than the median of the older group (41-60). A Pearson Chi-Square has been employed to determine of this difference is significant. However, a significance difference could not been found between the two groups, □(2) = 11.01, $p > 0.05$.

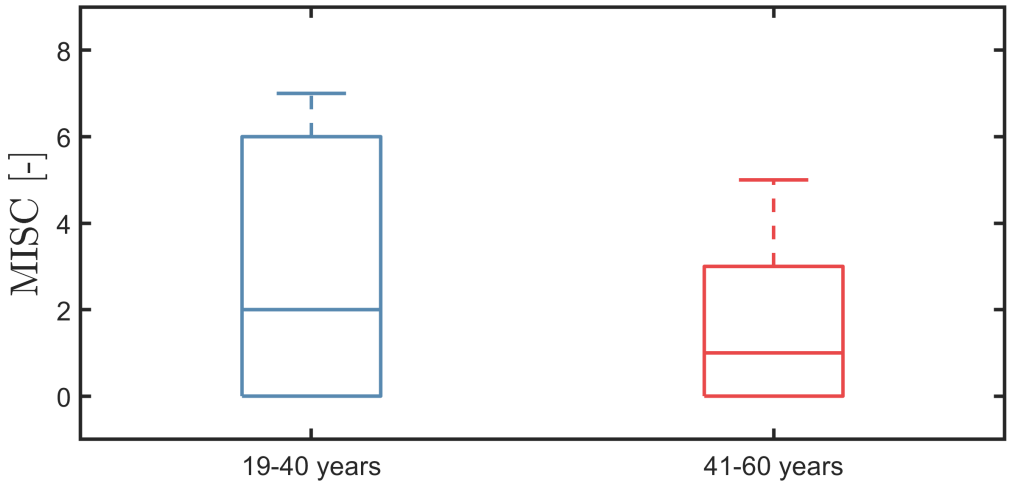

Figure I.1: Boxplot of the MISC end values for the group with ages between 19-40 and 41-60.

J

Additional results PMI

In the article the results of the mean maximum PMI per corner is compared between the dropped-out participants and the participants that finished the whole simulation trial. Here there participants are divided over two groups based on their final MISC score. This means that the groups sick and non-sick are defined based on the MISC score threshold value. First, the results are given for the group with participants that had a MISC score larger than five and the group with participants that had a MISC score equal to or lower than five in Figures J.1 and J.2.

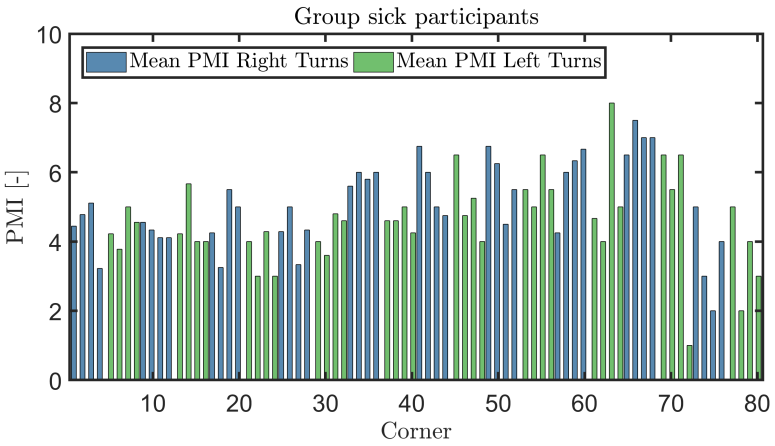

Figure J.1: Mean maximum PMI of average participants that that had a MISC score larger than five per corner for left and right turns.

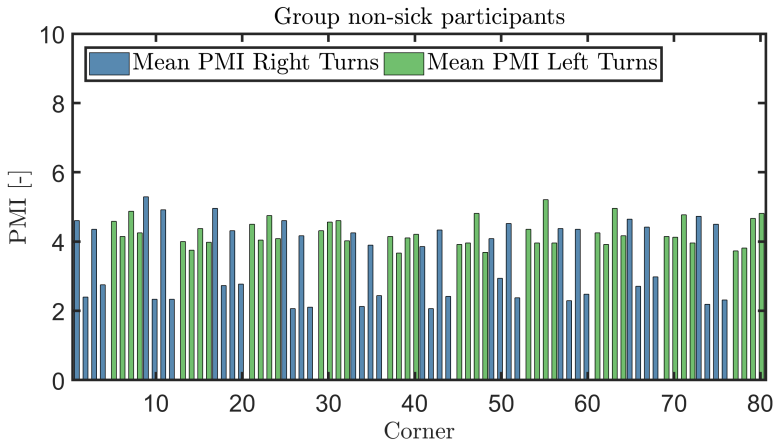

Figure J.2: Mean maximum PMI of average participants that that had a MISC score equal or lower than five per corner for left and right turns.

Secondly, the results are given for the group with participants that had a MISC score larger than three and the groupt with participants that had a MISC score equal to or lower than three in Figures J.3 and J.4.

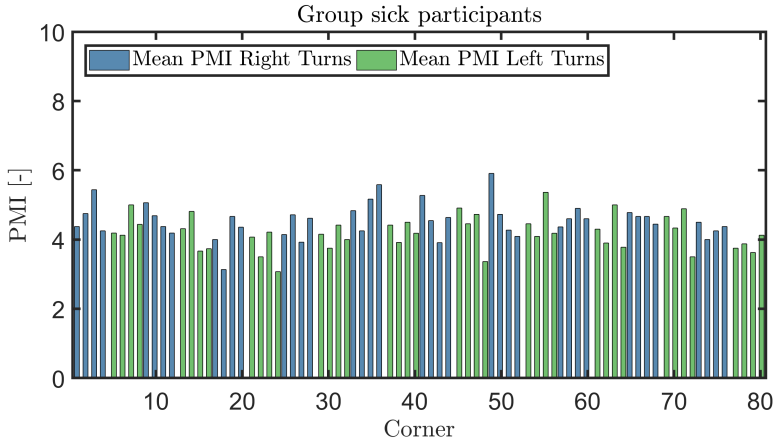

Figure J.3: Mean maximum PMI of average participants that that had a MISC score larger than three per corner for left and right turns.

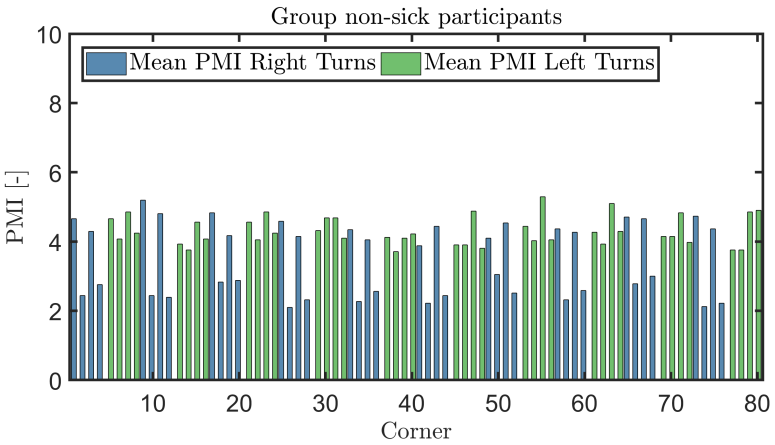

Figure J.4: Mean maximum PMI of average participants that that had a MISC score equal or lower than three per corner for left and right turns.

Finally, the results are given for the group with participants that had a MISC score larger than one and the group with participants that had a MISC score equal to or lower than one in Figures J.5 and J.6.

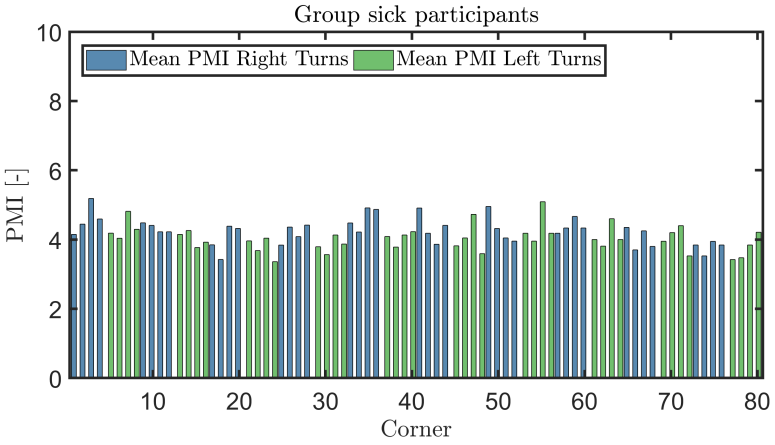

Figure J.5: Mean maximum PMI of average participants that that had a MISC score larger than one per corner for left and right turns.

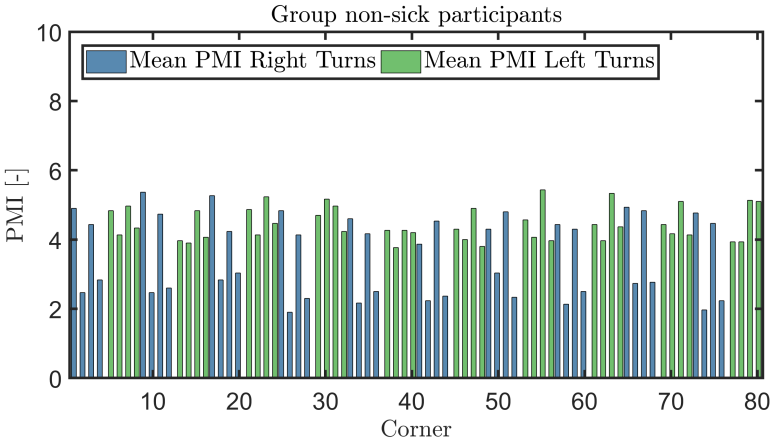

Figure J.6: Mean maximum PMI of average participants that that had a MISC score equal or lower than one per corner for left and right turns.

In general, the mean maximum PMI of the right corners are rated lower that the mean maximum PMI of the left corners. Furthermore, the mean maximum PMI of all corners together are larger on average for the sick group than the non-sick group.

K

Additional head data results

The cumulative head yaw rate scores for the human participants in the group with MISC scores larger than 3 ($\mathrm{MISC} > 3$) and in a group with MISC scores smaller or equal to 3 ($\mathrm{MISC} \leq 3$) were given in the article. First, this appendix shows the cumulative head yaw rate scores for the human participants in the group with MISC scores larger than five ($\mathrm{MISC} > 5$) and in a group with MISC scores smaller or equal to five ($\mathrm{MISC} \leq 5$) in Figure K.1.

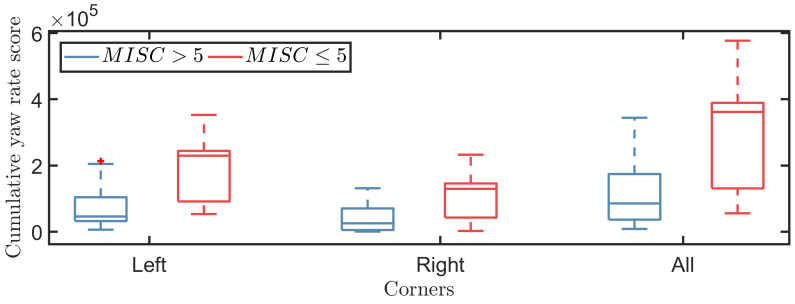

Figure K.1: Boxplot of the cumulative yaw rate scores between human participants in group with MISC scores larger than five ($\mathrm{MISC} > 5$) and in a group with MISC scores smaller or equal to five ($\mathrm{MISC} \leq 5$).

Secondly, the cumulative head yaw rate scores for the human participants in the group with MISC scores larger than one ($\mathrm{MISC} > 1$) and in a group with MISC scores smaller or equal to one ($\mathrm{MISC} \leq 1$) in Figure K.2.

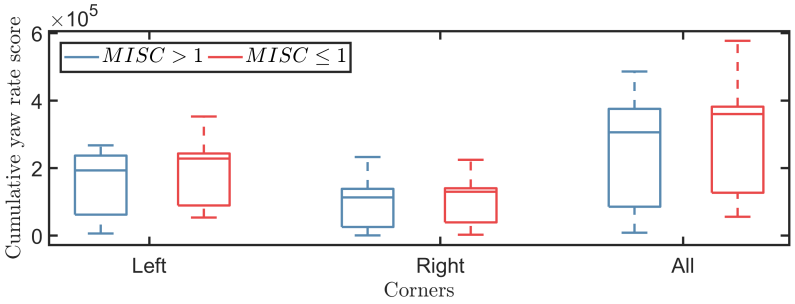

Figure K.2: Boxplot of the cumulative yaw rate scores between human participants in group with MISC scores larger than one ($\mathrm{MISC} > 1$) and in a group with MISC scores smaller or equal to one ($\mathrm{MISC} \leq 1$).

Experiment documents

This Appendix incorporates the following document that were employed during the experiment at the BMW Group, Munich (all documents are in German):

1. The experiment instructions
2. The Motion Sickness History Questionnaire
3. The Simulator Sickness Questionnaire

Ansprechpartner:
Marc Hogerbrug
Telefon: *0031615613896*

Stadtfahrt mit Abbiegemanövern

Herzlich willkommen zu unserer Studie „Stadtfahrt mit Abbiegemanövern“! Wir danken Ihnen für Ihr Interesse an dieser Studie.

Allgemeine Information für Teilnehmende

In der heutigen Studie wird es um Ihr persönliches Wohlbefinden gehen. Ihre Aufgabe als **Mitfahre**r wird die Bewertung der Abweichung zwischen erwarteter Bewegung eines realen Fahrzeuges und der dargestellten Bewegung sein. Die Bewertung wird während einer Stadtfahrt stattfinden. Wir möchten währenddessen Ihr persönliches Wohlbefinden messen, indem wir Sie in regelmäßigen Zeitabständen mündlich befragen.

Aufgabe und Messungen während der Fahrt

Kontinuierliche Bewertung

Während der Fahrt sollen Sie mit Hilfe eines Drehknopfes kontinuierlich die Abweichung zwischen erwarteter Bewegung aus einer realen Autofahrt und dargestellter Bewegung im Simulator bewerten. Diese Abweichungen können in verschiedenen Formen auftreten. Einerseits können Bewegungen ganz fehlen, das heißt es ist zu wenig Bewegung bei einem spezifischen Fahrmanöver spürbar. Andererseits können auch entgegengesetzte Bewegungen zur visuellen Fahrt wahrgenommen werden. Diese Abweichungen sollen nach eigenem Empfinden bewertet werden.
Die Eingabe erfolgt kontinuierlich über einen Drehknopf auf der Mittelkonsole. Die Skala reicht von 0 bis 10, wobei 0 keine Abweichung zu einer realen Fahrt und 10 eine sehr große Abweichung zur Realfahrt repräsentiert. Der aktuelle Skalenwert wird durch einen Balken in der Fahrszene angezeigt. Wir bitten Sie darum, die komplette Skala zu verwenden, um eine Vergleichbarkeit gewährleisten zu können.

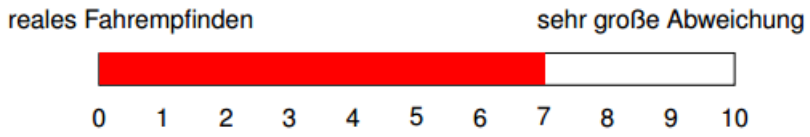

Bitte bewerten Sie ausschließlich die Bewegung des Simulators. In die Bewertung **NICHT** mit einfließen sollen:

- Visualisierungsfehler, bspw. Verpixelungen, Ende der Projektionswand.
- Fehlende Straßenbeschaffenheiten, bspw. Schlaglöcher, Abwasserdeckel.
- Soundeffekte, bspw. Motorsound, Fahrtwind.

- Störgeräusche vom Simulator, bspw. von Elektromotoren.
- Unmittelbarer Beginn und Ende der Fahrt. Der Simulator fährt in die neutrale Position, dies ist nicht Bestandteil der Messfahrt ist.
- Unrealistische Gegebenheiten im Fahrerraum, bspw. Lenkrad und Fußpedale bewegen sich nicht.
- Gerüche.

Mündliche Befragung

Neben der kontinuierlichen Bewertung, möchten wir Ihr persönliches Wohlbefinden messen, indem wir Sie in regelmäßigen Zeitabständen mündlich befragen. Dazu billet der Versuchsleiter etwa jede Minute nach einer Bewertung ihres Wohlbefindens. Dafür wird diese Skala genutzt:

Geben Sie, sobald der Versuchsleiter Sie dazu auffordert, bitte die Zahl an, die Ihr Wohlbefinden am besten beschreibt. Falls Sie während der Fahrt Symptome von Übelkeit verspüren (Bewertung 6 oder höher) und die Studie abbrechen wollen, dann können Sie **zu jeder Zeit** dem Versuchsleiter dahingehend informieren geben.

Blickerfassung

Während der Fahrt benutzen wir ein Blickerfassungssystem. Dafür werden Sie während der Fahrt eine Brille (ohne Gläser) tragen. Diese Brille muss vor der Fahrt kurz kalibriert werden. Schauen Sie dazu, sobald der Versuchsleiter Sie dazu auffordert, auf die Karte mit dem schwarzen Kreis (siehe Bild unten) und fixieren Sie diesen Kreis bis die Kalibrierung abgeschlossen ist. Dies dauert in der Regel einigen Sekunden. Es ist wichtig, dass Sie während der Kalibrierung so genau wie möglich auf den Punkt innerhalb des Kreises schauen.


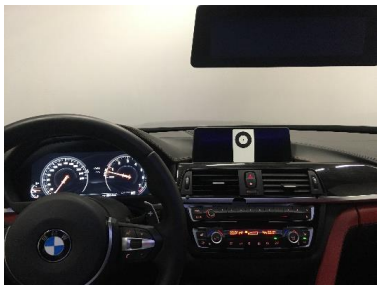
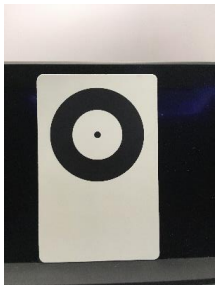

Ablauf der Studie

Das Experiment besteht aus einer 45-minütigen Fahrt. Insgesamt dauert das Experiment etwa 1 Stunde und 15 Minuten. Die Studie wird dabei nach folgendem Ablaufplan durchlaufen:

- Nachdem Sie diese Studieninformation gelesen haben, werden Sie zwei Fragenbögen ausfüllen.
- Danach dürfen Sie in den Simulator einsteigen. Nach dem Sie Platz genommen haben werden Sie eine kurze Einweisung bekommen. Nachdem Sie die Blickerfassungsbrille aufgesetzt haben wird die Blickerfassungsbrille kalibriert
- Um die Bewertungsmethode kennenzulernen und um eine Referenz für der Bewertung zu erhalten, wird eine Testfahrt zu Beginn des Versuchs durchgeführt. Hierbei wird nochmals auf Bewegungsabweichungen für spezifische Manöver hingewiesen und die Bewertung mittels des Drehknopfes geübt. Auch die mündliche Bewertung wird hier geübt.
- Nachdem die Testfahrt abgeschlossen ist und Sie keine weiteren Fragen haben beginnt die Experimentfahrt.
- Während der Messfahrt führen Sie die beschriebenen Aufgaben aus. Bitte teilen Sie dem Versuchsleiter unbedingt mit falls Ihnen unwohl ist. Sie können zu jeder Zeit den Versuch abbrechen.
- Zum Abschluss des Experiments, wenn Sie wieder aus dem Simulator ausgestiegen sind, werden Sie nochmal ein paar Fragebogen ausfüllen. Anschließend ist die Studie beendet.

Wer vor der Fahrt auf die Toilette möchte, hat jetzt die Gelegenheit dazu. Ich bitte Sie außerdem, für die Zeit der Studie Ihr Handy auf lautlos zu stellen und während der Fahrt nicht Ihr Handy zu benutzen. Sollten Sie noch Fragen haben wenden Sie sich bitte an den Versuchsleiter.

Fragebögen

Teil 1: MSHQ. Bitte kreuzen Sie die Skala gemäß dem Ausprägungsgrad der Symptome an.

F1. Wie oft haben Sie im letzten Jahr als Mitfahrer(In) die folgenden Transportmittel benutzt?

	Nie	**1**	**2-3**	**4-15**	**16-63**	**64-255**	**255+**
Auto							
Linienbusse							
Reisebusse							
Kleine Boote							
Schiffe							
Flugzeuge							
Bahn							

F2. Wie oft haben Sie sich im letzten Jahr als MitfahrerIn krank oder schlecht gefühlt während Sie die folgenden Transportmittel nutzten?

	Nie	**1**	**2**	**3**	**4-7**	**8 - 15**	**16+**
Auto							
Linienbusse							
Reisebusse							
Kleine Boote							
Schiffe							
Flugzeuge							
Bahn							

F3. Mussten Sie sich als MitfahrerIn schon einmal übergeben, während dem Sie die folgenden Transportmittel nutzten?

ja unsicher nein

	ja	Unsicher	Nein
Auto			
Linienbusse			
Reisebusse			
Kleine Boote			
Schiffe			
Flugzeuge			
Bahn			

F4. Wenn ja, in welchem Lebensabschnitt haben Sie dies erlebt?

vor dem 16. Lebensjahr	ab dem 16. Lebensjahr	im letzten Jahr

F5. Würden Sie irgendeine der nachfolgenden Transportmöglichkeiten wegen einer Reisekrankheit meiden?

	nie	gelegentlich	häufig	immer
Auto				
Linienbusse				
Reisebusse				
Kleine Boote				
Schiffe				
Flugzeuge				
Bahn				

F6. Welche der folgenden Beschreibungen trifft Ihre Anfälligkeit für Reisekrankheit am besten?

Wesentlich	Weniger als durchschnittlich	Etwas weniger als durchschnittlich	Durchschnittlich	etwas mehr als durchschnittlich	deutlich mehr als durchschnittlich

Teil 2: SSQ.

Diese Fragen sollen erfassen, wie Sie sich in diesem Moment fühlen. Bitte kreuzen Sie die Skala gemäß dem Ausprägungsgrad der Symptome an. Wo notwendig geben Sie bitte auch die Anzahl des Auftretens der Symptome an.

	keine	leicht	mittel	schwer
Allgemeines Unwohlsein				
Ermüdung				
Langeweile				
Konzentrationsschwierigkeiten				
Benommenheit				
Kopfschmerzen				
Kopf ist voll / Kopfdruck				
Verschwommene Sicht				
Schwierigkeiten beim Fokussieren				
Überanstrengung der Augen				
Schwindelgefühl bei geöffneten Augen				
Schwindelgefühl bei geschlossenen Augen				
Gleichgewichtsstörungen				
erhöhter Speichelfluss				

Schwitzen				
Mattigkeit				
bewusstes Atmen				
flau im Magen				
Übelkeit				
Aufstoßen				
Verwirrtheit				
Appetitlosigkeit				
gesteigerter Appetit				
Wunsch auf die Toilette zu gehen				

M

Acceleration transformations

This appendix describes the formula used to transform the accelerations from the vehicle center of gravity, which are available from the vehicle model, to the head. Here, the position vector between the CoG of the car and the human head (h) is taken as: $\bar{h}_{pos} = [x_G\ y_G\ z_G] = [0.1\ 0.5\ 1.0]$, see Figure M.1.

To transform the accelerations from point G to point h, the following steps must be followed. Two reference frames are defined: E_G and E_h. The angular velocity of E_h is:

$$\bar{\omega}_h = [p_G\ q_G\ r_G]\{E_G\} \tag{M.1}$$

The absolute position vector of point h is:

$$\bar{r}_h = \bar{r}_0 + [x_G\ y_G\ z_G]\{E_G\}, \tag{M.2}$$

where r_0 is the initial position of the G. The absolute velocity of point h after differentiation is:

$$\bar{V}_h = \dot{\bar{r}}_0 + [\dot{x}_G\ \dot{y}_G\ \dot{z}_G]\{E_G\} + [x_G\ y_G\ z_G]\{\dot{E}_G\} \tag{M.3}$$

$$\{\dot{E}_H\} = [\Omega_x]\{E_G\} \tag{M.4}$$

$$\bar{V}_h = \dot{\bar{r}}_0 + [\dot{x}_G\ \dot{y}_G\ \dot{z}_G]\{E_G\} + [x_G\ y_G\ z_G][\Omega_x]\{E_G\} \tag{M.5}$$

$[\Omega_x]$ is the rotation operator and is defined as:

$$[\Omega_x] = \begin{bmatrix} 0 & r_G & -q_G \\ -r_G & 0 & p_G \\ q_G & -p_G & 0 \end{bmatrix} \tag{M.6}$$

When differentiating this velocity vector, then it will give the acceleration vector in point h:

$$\bar{a}_h = \ddot{\bar{r}}_0 + [\ddot{x}_G\ \ddot{y}_G\ \ddot{z}_G]\{E_G\} + 2 \cdot [\dot{x}_G\ \dot{y}_G\ \dot{z}_G][\Omega_x]\{E_G\} \tag{M.7}$$

$$+ [x_G\ y_G\ z_G][\dot{\Omega}_x]\{E_G\} + [x_G\ y_G\ z_G][\Omega_x][\Omega_x]\{E_G\} \tag{M.8}$$

where the first term on the right side is the acceleration applied on G due to translation, the second term is the relative acceleration and the fourth term is the acceleration due to rotation. The relative acceleration is zero, because a rigid body is assumed meaning that the position vector h_{pos} remains constant. The third term on the right is the coriolis acceleration and is zero as well for the same reason as the relative acceleration. Finally, the fifth term is defined as the centrifugal acceleration.
The centrifugal acceleration can be written as:

$$\bar{a}_{cf} = [x_G\ y_G\ z_G][\Omega_x][\Omega_x]\{E_G\} = \bar{\omega}_h \times (\bar{\omega}_h \times \bar{r}) \tag{M.9}$$

The acceleration due to rotation, $[x_G\ y_G\ z_G][\Omega_x]$, can be written as:

$$[x_G\ y_G\ z_G][\Omega_x] = \bar{\alpha}_G \times [x_G\ y_G\ z_G] \tag{M.10}$$

where $\bar{\alpha}_G$ is the angular acceleration vector ($[\dot{p}_G\ \dot{q}_G\ \dot{r}_G]$). Finally, we get the following equation for the accelerations in point h:

$$\bar{a}_h = \ddot{\bar{r}}_0 + \bar{\alpha}_G \times \bar{\omega}_G\{E_G\} + \bar{\omega}_G \times (\bar{\omega}_G \times [x_G\ y_G\ z_G])\{E_G\} \tag{M.11}$$

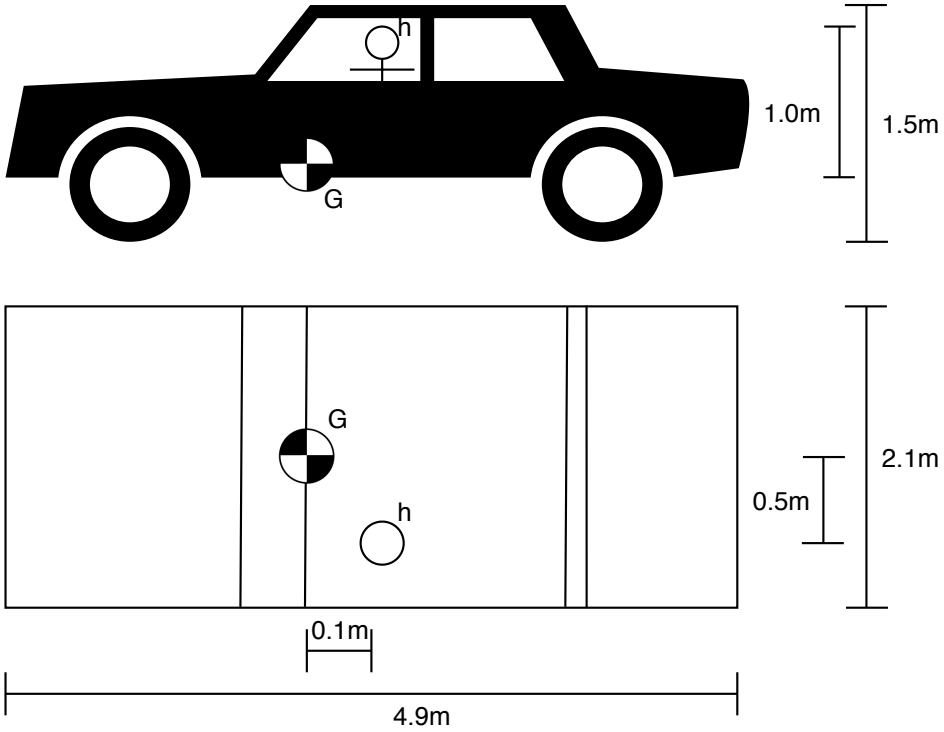

Figure M.1: Reference points: G and h.